ANKARA YILDIRIM BEYAZIT UNIVERSITY

GRADUATE SCHOOL OF NATURAL AND APPLIED SCIENCES



WEIGHT REDUCTION IN AIRCRAFT WITH TOPOLOGY OPTIMIZATION

M. Sc. Thesis by

Hasan Hüseyin ONAY

Department of Aerospace Engineering

June, 2023

ANKARA

WEIGHT REDUCTION IN AIRCRAFT WITH TOPOLOGY OPTIMIZATION

A Thesis Submitted to

The Graduate School of Natural and Applied Sciences of

Ankara Yıldırım Beyazıt University

In Partial Fulfillment of the Requirements for the Degree of Master of Science in Aerospace Engineering, Department of Aerospace Engineering

by

Hasan Hüseyin ONAY

June, 2023

ANKARA

M. Sc. THESIS EXAMINATION RESULT FORM

We have read the thesis entitled **"WEIGHT REDUCTION IN AIRCRAFT WITH TOPOLOGY OPTIMIZATION"** completed by **HASAN HÜSEYIN ONAY** under supervision of **PROF. DR. VELI ÇELİK** and we certify that in our opinion it is fully adequate, in scope and in quality, as a thesis for the degree of Master of Science.

Prof. Dr. Veli ÇELİK

Supervisor

Prof. Dr. Ahmet Salih YİĞİT

Jury Member

Assist. Prof. Dr. Gökhan DURMUŞ

Jury Member

Prof. Dr. Sadettin ORHAN

Director

Graduate School of Natural and Applied Sciences

ETHICAL DECLARATION

I hereby declare that, in this thesis which has been prepared in accordance with the Thesis Writing Manual of Graduate School of Natural and Applied Sciences,

- All data, information and documents are obtained in the framework of academic and ethical rules,
- All information, documents and assessments are presented in accordance with scientific ethics and morals,
- All the materials that have been utilized are fully cited and referenced,
- No change has been made on the utilized materials,
- All the works presented are original,

and in any contrary case of above statements, I accept to renounce all my legal rights.

Date: 14/06/2023 **Signature:**

Name & Surname: Hasan Hüseyin ONAY

ACKNOWLEDGMENTS

First and foremost, I have to thank my tutor and supervisor Prof Dr. Veli ÇELİK, who always helped me in this thesis work. Without his assistance and dedicated involvement in every step throughout the process, this study would have never been accomplished. It has been an honor and a chance for me to work with him.

I would also like to express my gratitude to my colleague Seçkin Uslu from Turkish Aerospace Industries for guiding me with her vast experience.

Finally, I would be negligent by not mentioning my family, especially my parents, my sister. I am grateful to Servet and Orhan ONAY who have stood behind me all my life. I would like to thank my one and only sister, Betül CEYLAN, who is more than an older sister. I would like to express my gratitude to Gizem DOĞAN, who held my hand and walked this path with me all this time. Their belief in me kept my morale and motivation high during this process.

Without you, I wouldn't be here.

2023, 14 June **Hasan Hüseyin ONAY**

WEIGHT REDUCTION IN AIRCRAFT WITH TOPOLOGY OPTIMIZATION

ABSTRACT

One of the most important parameters in airplanes is weight. Aircraft must be light enough to perform the tasks and capabilities expected of them, while at the same time being structurally resistant to the loads they encounter. Historically, different methodologies have been tried to make lighter aircraft designs. Topology optimization has recently become a preferred weight reduction method in the aviation industry. Lighter designs are obtained by removing the material that does not provide sufficient strength to the structure from the structure. In this study, weight reduction was made in the wing area of Cessna 172 aircraft by topology optimization. Before the topology optimization phase of the wing structure, the initial weight and the forces acting on it were calculated analytically. Based on the real-life weight of the wing structure, a finite element model of its pre-optimization state was created, and its structural strength was checked. A valid model was obtained before the topology optimization by making validation analysis of the created finite element model. In topology optimization, two different topology optimizations were applied to 3-dimensional and 2-dimensional structures. In these structures, weight reduction was achieved by determining the design areas and constraints for optimization. The structure obtained from topology optimization was statically evaluated again in order not to fail.

Keywords: Topology optimization, aerospace, weight reduction, Cessna 172, structural analysis.

HAVA TAŞITLARINDA TOPOLOJİ OPTİMİZASYONU İLE AĞIRLIK AZALTIMI

ÖZ

Uçaklarda en önemli parametrelerden birisi ağırlıktır. Uçaklar kendilerinden beklenen görevleri ve kabiliyetleri gerçekleştirebilmesi için yeterince hafif aynı zamanda karşılaştıkları yüklemelere karşı yapısal olarak dayanıklı olmalıdır. Eskiden beri daha hafif uçak tasarımları yapmak için farklı metodolojiler denenmiştir. Topoloji optimizasyonu ise son zamanlarda havacılık sektöründe tercih edilen bir ağırlık azaltımı yöntemi haline gelmiştir. Yapıya dayanım olarak yeteri kadar yarar sağlamayan malzemenin yapıdan çıkarılmasıyla daha hafif tasarımlar elde edilir. Bu çalışmada, Cessna 172 uçağının kanat bölgesinde topoloji optimizasyonu ile ağırlık azaltımı yapılmıştır. Kanat yapısının topoloji optimizasyonu aşamasından önce ilk ağırlığı ve üzerine etki eden kuvvetler analitik olarak hesaplanmıştır. Kanat yapısının gerçek hayattaki ağırlığı esas alınarak, optimizasyon öncesi halinin sonlu elemanlar modeli oluşturularak yapısal açıdan dayanımına kontrol edilmiştir. Oluşturulan sonlu elemanlar modelinin doğrulama analizleri yapılarak topoloji optimizasyonu öncesi geçerli bir model elde edilmiştir. Topoloji optimizasyonunda, 3 boyutlu ve 2 boyutlu yapılara iki farklı topoloji optimizasyonu uygulanmıştır. Bu yapılarda, optimizasyon için tasarım alanları ve kısıtlamalar belirlenerek ağırlık azaltımı sağlanmıştır. Topoloji optimizasyon sonucu elde edilen yapı, kırıma uğramaması için statik açıdan tekrar değerlendirilmiştir.

Anahtar Kelimeler: Topoloji optimizasyonu, havacılık, ağırlık azaltımı, Cessna 172, yapısal analiz.

CONTENTS

M. Sc. THESIS EXAMINATION RESULT FORM ii
ETHICAL DECLARATION iii
ACKNOWLEDGMENTS iv
ABSTRACT v
ÖZ vi
NOMENCLATURE ix
LIST OF TABLES xi
LIST OF FIGURES xii

CHAPTER 1 - INTRODUCTION 1
1.1 Aim and Stages of the Study 1
1.2 Cessna 172 Wing Components 2
1.3 Acting Forces on Wing Component and Initial Weight Calculation 5
1.4 Topology Optimization Methods 13

CHAPTER 2 - FINITE ELEMENT MODEL INPUT 17
2.1 Aircraft Wing Component Weight Computation 17
2.2 Computing Aerodynamic Force on Wing 21
2.2.1 Spanwise Lifting Force Distribution 22
2.2.2 Drag Force and Pitching Moment 25

CHAPTER 3 - FINITE ELEMENT MODELING 31
3.1 Determination of Internal Structures Location 31
3.2 Wing 2D Finite Element Modelling 35
3.3 Finite Element Model Validation 43
3.3.1 Analytical Calculation Check 43
3.3.2 Static Analysis Check 46
3.3.3 Free to Free Modal Analysis Check 47
3.4 Finite Element Model Results 48
3.4.1 Displacement Results 49
3.4.2 Stress Results 49
3.4.3 Buckling Results 54

3.4.4 Fastener Force Results 55
3.4.5 Weight of Wing Structures 59

CHAPTER 4 - TOPOLOGY OPTIMIZATION RESULTS 60
4.1 Rib Topology Optimization 61
4.2 Spar Topology Optimization 64
4.3 Topology Optimization Model Results 66

CHAPTER 5 - CONCLUSION AND DISCUSSION 74
REFERENCES 79

APPENDICES 82
APPENDIX A: CODE FOR FASTENER MODELLING IN HYPERMESH .. 82
APPENDIX B: MODAL ANALYSIS RESULT BEFORE-AFTER OPTIMIZATION 87
CURRICULUM VITAE 91

NOMENCLATURE

Roman Letter Symbols

C_{D_0}	Zero lift drag coefficient
C_D	Drag coefficient
C_L	Lift coefficient
C_m	Pitching moment coefficient
N_{ult}	Ultimate load factor
V_{max}	Aircraft maximum speed, m/s
W_{dg}	Take-off gross weight of the aircraft.
W_{fw}	Weight of fuel in wing, kg
c	Chord length, m
P	Engine power, kW
A	Aspect ratio of the wing
D	Drag force, N
E	Young's modulus, N/m^2
L	Lifting force, N
M	Moment, N/mm
S	Wing area, m^2
V	Aircraft speed, m/s
b	Wing spanwise, m
d	Fastener diameter, mm
e	Oswald efficiency factor
p	Penalty factor
q	Dynamic pressure, N
t	Thickness, m
t/c	Thickness to chord ratio
u	Airspeed, m/s

Greek Letter Symbols

η_i	Pseudo-densities
Γ	Circulation, N/m
Λ	Wing sweep angle at 25% MAC
λ	Taper ratio

ρ	Air density, kg/m^3

Acronyms

BESO	Bi-directional Evolutionary Structural optimization
ESO	Evolutionary Structural optimization
MAC	Mean Aerodynamic Chord
MMPDS	Metallic Materials Properties Development and Standardization
SIMP	Solid Isotropic Material Penalization

LIST OF TABLES

Table 2.1 Input Data of Cessna 172 17
Table 2.2 Initial Weight Estimation Constant and Aircraft Class 19
Table 2.3 Weight Comparison with Real Cessna 172 Data 19
Table 2.4 Weight Comparison Raymer and Roskam Method 20
Table 2.5 Cessna 172R Airspeed Limitation 21
Table 2.6 Cessna 172R Load Factor Limitation 21
Table 2.7 Load Factor vs Lift Force 23
Table 2.8 Lifting Force on Wing Spanwise Stations 24
Table 2.9 Maximum Aerodynamic Force on Wing Structure 30
Table 3.1 Aerodynamic Forces Values on Chordwise 38
Table 3.2 Model Input Data for Analytical Calculations 45
Table 3.3 Finite Element Model and Analytical Results 45
Table 3.4 Model Force Moment Equilibrium 46
Table 3.5 Epsilon Value Check at Static Check Model 47
Table 3.6 Free to Free Modal Analysis Frequency Modes Results 48
Table 3.7 Wing Model Maximum Stress Results and Minimum Reserve Factors 54
Table 3.8 Wing Model First 10 Buckling Modes Reserve Factor 55
Table 3.9 Fastener Ultimate Shear and Tensile Allowable 56
Table 3.10 Fastener Shear and Tensile Reserve Factor for Wing Structures 59
Table 3.11 Wing Component Structural Weight and Real Data Comparison 59
Table 4.1 Topology Optimization Constraint and Boundary Conditions 63
Table 4.2 Spar Design Space Region Constraints and Boundary Condition 65
Table 4.3 Wing Model Maximum Stress Results and Minimum Reserve Factors 71
Table 4.4 Before and After Topology Optimization Frequency Comparison 72
Table 4.5 Wing Model First 10 Buckling Modes Reserve Factor 73
Table 4.6 First and After Optimization Weight of the Wing Structures 73
Table 5.1 Real and FEM Wing Weight Comparison 75
Table 5.2 Weight Comparison of Wing Structures Before and After Topology Optimization 77
Table Appendices B.1 Wing Model before Optimization First 15 Buckling Modes Reserve Factor 88
Table Appendices B.2 Wing Model After Optimization First 15 Buckling Modes Reserve Factor 90

LIST OF FIGURES

Figure 1.1 Cessna 172 Wingbox Topology Optimization Stages 2
Figure 1.2 Cessna 172R Wing Type and Strut Connection 3
Figure 1.3 Typical Wing Components 3
Figure 1.4 Cessna 172 Wing Internal Structure Layout 5
Figure 1.5 Spanwise Lift Distribution 7
Figure 1.6 The Force on Pressure Center 8
Figure 1.7 Pressure Center Positions by Angle of Attack 9
Figure 1.8 The Aerodynamic Forces on Aerodynamic Center 9
Figure 1.9 Typical V-g Diagram 11
Figure 1.10 Typical Topology Optimization 14
Figure 1.11 Homogenization Method Topology Optimization 15
Figure 2.1 Cessna 172R V-g Diagram 22
Figure 2.2 Typical Lift Distribution 24
Figure 2.3 Cessna 172R Wing Lift Distribution and Stations 25
Figure 2.4 Angle of Attack on Airfoil Profile 26
Figure 2.5 Cl v Angle of Attack 26
Figure 2.6 Cd v Angle of Attack 27
Figure 2.7 Cm v Angle of Attack 27
Figure 2.8 Drag Force versus Angle of Attack at 3.8 Load Factor 28
Figure 2.9 Velocity versus Angle of Attack at 3.8 Load Factor 29
Figure 2.10 Pitching Moment versus Angle of Attack at 3.8 Load Factor 29
Figure 3.1 Cessna 172R Wing Dimensions 31
Figure 3.2 Main and Secondary Spar View 32
Figure 3.3 Main and Secondary Spar Chordwise Location 32
Figure 3.4 Ribs Wing Spanwise Distribution 33
Figure 3.5 Ribs Spanwise Location 33
Figure 3.6 Stinger Chordwise Location 34
Figure 3.7 Stringers Chordwise Location 34
Figure 3.8 Stiffened Skin Panel Top View 35
Figure 3.9 Fastener Modelling Example from Skin and Spar Connection 36
Figure 3.10 Fastener to Fastener Distance Example from Main Spar 37
Figure 3.11 Cessna 172 Wing Model Boundary Condition 37

Figure 3.12 Wing Model Aerodynamic Forces Distribution Location 38
Figure 3.13 Wing Model Fuel Tank Location 39
Figure 3.14 Main Spar Thickness Map 39
Figure 3.15 Main Spar Width and Height Measurements 40
Figure 3.16 Secondary Spar Thickness Map 40
Figure 3.17 Secondary Spar Width and Height Measurements 41
Figure 3.18 Wing Model Ribs Thicknesses 41
Figure 3.19 Wing Model Skin Panel Thickness 42
Figure 3.20 Wing Model Strut Dimensions 42
Figure 3.21 Wing Model Stringers Width and Heights 43
Figure 3.22 Finite Element Model General View 44
Figure 3.23 Finite Element Model Applied Load Location 44
Figure 3.24 Wing Static Check Model 46
Figure 3.25 Wing Free to Free Modal Analysis Check Model 48
Figure 3.26 Wing Model Displacement Results 49
Figure 3.27 Upper Skin Stress Results 50
Figure 3.28 Lower Skin Stress Results 51
Figure 3.29 Main Spar Stress Results 51
Figure 3.30 Secondary Spar Stress Results 52
Figure 3.31 Ribs Stress Results 52
Figure 3.32 Stringers Stress Results 53
Figure 3.33 Strut Stress Results 53
Figure 3.34 First Buckling Mode of Wing Structure 55
Figure 3.35 Most Critical Fastener Shear Force Location on Main Spar 56
Figure 3.36 Most Critical Tensile Force Location on Main Spar 57
Figure 3.37 Most Critical Fastener Shear Force Location on Secondary Spar 57
Figure 3.38 Most Critical Tensile Force Location on Secondary Spar 57
Figure 3.39 Most Critical Shear Force Location on Ribs 58
Figure 3.40 Most Critical Tensile Force Location on Ribs 58
Figure 4.1 Rib Web Topology Optimization Design Spaces 60
Figure 4.2 Main Spar Topology Optimization Design Space 61
Figure 4.3 Main Rib for Topology Optimization Pattern 62
Figure 4.4 Solid Rib Optimization Design Space 62
Figure 4.5 Solid Rib Manufacturing Cutting Direction 63

Figure 4.6 Rib Topology Optimization Pattern..... 63
Figure 4.7 Rib Topology Result Applied 2D Main Model 64
Figure 4.8 Spar Topology Optimization Location 65
Figure 4.9 Spar Topology Optimization Location 65
Figure 4.10 Spar Topology Optimization Applied Model 66
Figure 4.11 Topology Optimization Result Model 67
Figure 4.12 Topology Optimization Model Displacement Results..... 67
Figure 4.13 Topology Optimization Model Upper Skin Stress Results..... 68
Figure 4.14 Topology Optimization Model Lower Skin Stress Results 68
Figure 4.15 Topology Optimization Model Spars Stress Results 69
Figure 4.16 Topology Optimization Model Ribs Stress Results..... 69
Figure 4.17 Topology Optimization Model Stringers Stress Results..... 70
Figure 4.18 Topology Optimization Model Strut Stress Results 70
Figure 4.19 Topology Optimization Model Main Spar Buckling Region 71
Figure 4.20 Topology Optimization Model Main Ribs Buckling Region 72
Figure Appendices B.1 First Bending Mode..... 87
Figure Appendices B.2 First Torsion Mode..... 87
Figure Appendices B.3 Second Bending Mode 88
Figure Appendices B.4 First Bending Mode..... 89
Figure Appendices B.5 First Torsion Mode..... 89
Figure Appendices B.6 Second Bending Mode 89

CHAPTER 1

INTRODUCTION

1.1 Aim and Stages of the Study

In aviation, the weight parameter is considered one of the most important characteristics of the aircraft. Weight directly affects many parameters such as the type of engine of the aircraft, the size and type of wings, fuel consumption and range of the aircraft. The fact that the gains obtained with the weight reduction were so high led the engineers to make lighter designs. For this reason, it was requested that the designs become lighter with different optimization methods and better designs were made with these optimization methods. Since weight plays such an important role in aircraft, different weight optimization methods have been developed. One of these methods is topology optimization, which has recently been preferred in jet aircraft [1] and general aviation aircraft [2].

The main purpose of this study is to apply topology optimization, which is one of the optimization methods commonly used in the aviation industry, on a sample aircraft component. Cessna 172 Skyhawk also known as 172R which is the best-selling training aircraft in the world [3], was chosen as the sample aircraft. During the study, analysis and analytical calculations were carried out on the wing component of Cessna 172. The main motivation of the study is to make the structure lighter with topology optimization, but there are other parameters that should be known about the wing component until the optimization stage of the study. In Figure 1.1, the stages to be followed until the topology optimization stage are shown. To evaluate the output of weight optimization of a structure, the initial weight of that structure must be obtained. In the study, it was aimed to show that the initial design weight of the wing component can be found approximately by analytical methods in terms of its originality and understanding of the engineering behind the data obtained. The results obtained with this analytical method will be compared with real-life data. After the initial weight is determined, the structure should be evaluated in terms of structural analysis while it

has this weight. In other words, before optimizing the Cessna 172 wing structure, it should be confirmed that it is in the safe zone with a similar structural arrangement. For this, structural analysis should be done by considering the material distribution in the internal structure of the wing structure and the most critical loading situation. At the end of these two phases, the structure will prove to be similar in weight and structurally durable to the currently produced Cessna 172 wing component. The weight optimization phase started after this point, weight reduction was made by using topology optimization in certain design areas of the structure and the initial and final weights of the wing component were compared. While determining the design areas for optimization, places such as the fuel tank wing root, which are the critical parts of the structure, are excluded from the optimization area.

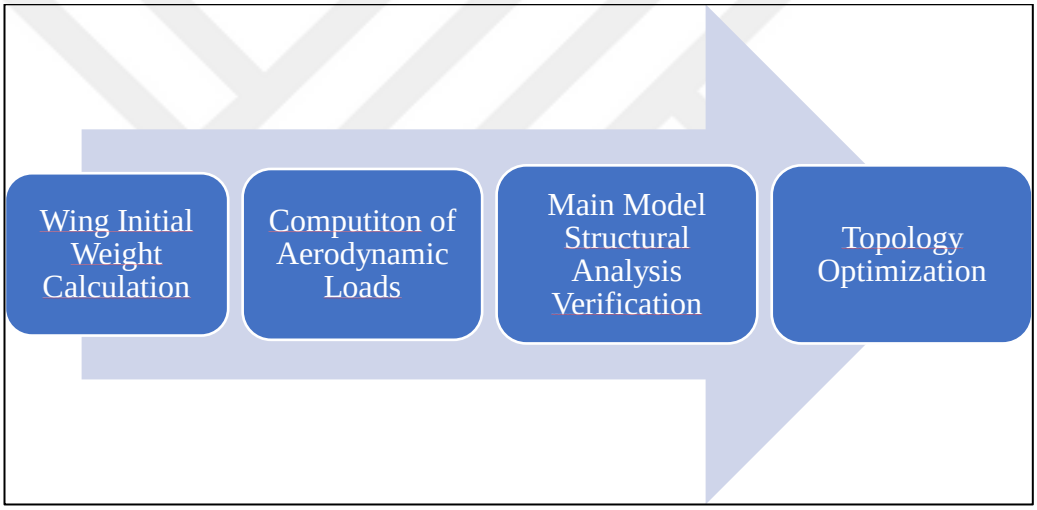

Figure 1.1 Cessna 172 Wingbox Topology Optimization Stages

1.2 Cessna 172 Wing Components

The force required for an aircraft to fly is called lift. The wing is the lift-generating component of the aircraft. The wing structure has many different shapes by connection type of the fuselage. Cessna 172 is a high wing aircraft. Cessna 172 model uses struts that are attached to the aircraft from the fuselage upwards. The main aim of these structures is to support the bending moment created at the root by the lift force acting on the wing of the aircraft. The wing type and strut connection of the aircraft model are shown in Figure 1.2 [4].



Figure 1.2 Cessna 172R Wing Type and Strut Connection [4]

In general, the wing structures are similar to each other and there are longitudinal and transverse elements in it. Considering the internal structure of a wing, longitudinal components are spar and stringers, while ribs are positioned perpendicular to these structures. These internal structures are enclosed by a surrounding skin panel. In addition to the structures inside the wing box, there are two structures known as the control surfaces of the wing. These are flap and aileron. While ailerons help the aircraft roll, flaps are needed to increase lift on take-off and landing [5]. In Figure 1.3 [5], the control surfaces and structural parts of an example wing component are seen.

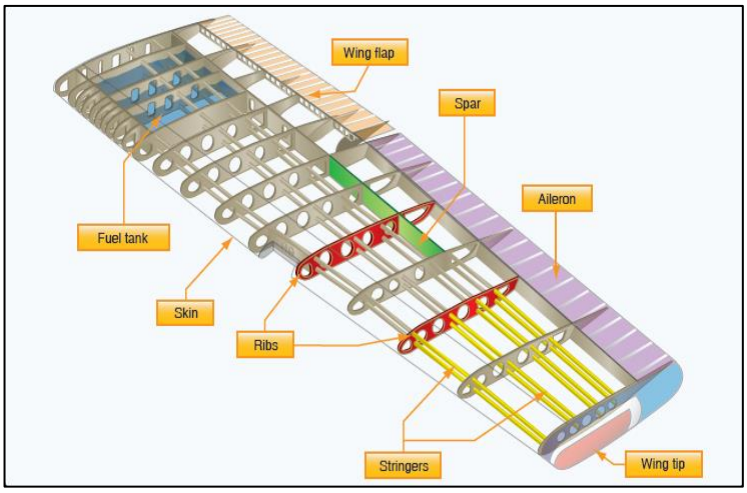

Figure 1.3 Typical Wing Components [5]

The spars, ribs and stringers, which are the main carrier elements in the wing structure, have separate tasks. In fixed-wing aircraft, the spars are the main carrier elements of the wing. Spars resist the bending moment due to the lift load on the wing. There are 2 spars in the Cessna 172 model. One of them is called front and the other is called rear spar. Front spar, also known as main spar, is the main carrier element. It is responsible for carrying most of the lifting force. The rear spar is the auxiliary beam to which the control surfaces are attached and is called the secondary spar. The ribs are positioned parallel to the aerodynamic airflow. They are the structures located between the two spars and are responsible for maintaining the stability of the skin panel. The function of stringers is similar to that of ribs, but they are used directly to support the skin panel. Stringer structures are not used in every aircraft, but they are used to prevent instability situations such as buckling that may occur on the skin panel. Stringers support the skin panel and create resistance against instability caused by the compression load on the skin panel. In addition to these main carrier structures, the fuel tank is usually placed inside the wing in airplanes. There are two supporting reasons for this. First, keeping all the fuel in fuselage in airplanes causes the thickness of the structure to increase and the aircraft to become heavier. Instead, placing the fuel tank inside the wing structure creates a weight force in the opposite direction of the lift force, helping both to lighten the structure and to carry extra fuel.

While the internal structure of the wing is being distributed, the locations of the spar and ribs are related to how the forces affect the structure. Cessna type aircraft are subsonic aircraft. This means that the speed of the aircraft is between 0 and 0.8 mach. In such aircraft, the aerodynamic center chord is approximately 25% of the leading edge [6]. The most dominant force in the wing structure is the lift force, and while most of it is produced in the root part of the airfoil, it decreases towards the tip. For this reason, the main spar, is usually positioned close to the aerodynamic center of the chord. The location of the secondary spar is usually determined by the size of the control surfaces. The distribution of the wing interior structure of Cessna 172 is shown in Figure 1.4 [7]. Cessna 172 has a main spar located approximately 20-25% of the chord, while a secondary spar is located 65-75% away to connect control surfaces. The location of the spars in the structure is almost similar in most wing structures. Considering the number of ribs, it consists of 11 ribs in total. Here, unlike other

aircraft, ribs are not concentrated only at the root of the wing and also are distributed at average equal distances along the wing. The main reason for this is that the load of the lift is carried with the help of the strut with the spars. With the reduction of loads in the root area, the ribs are positioned to prevent buckling in the skin panel.

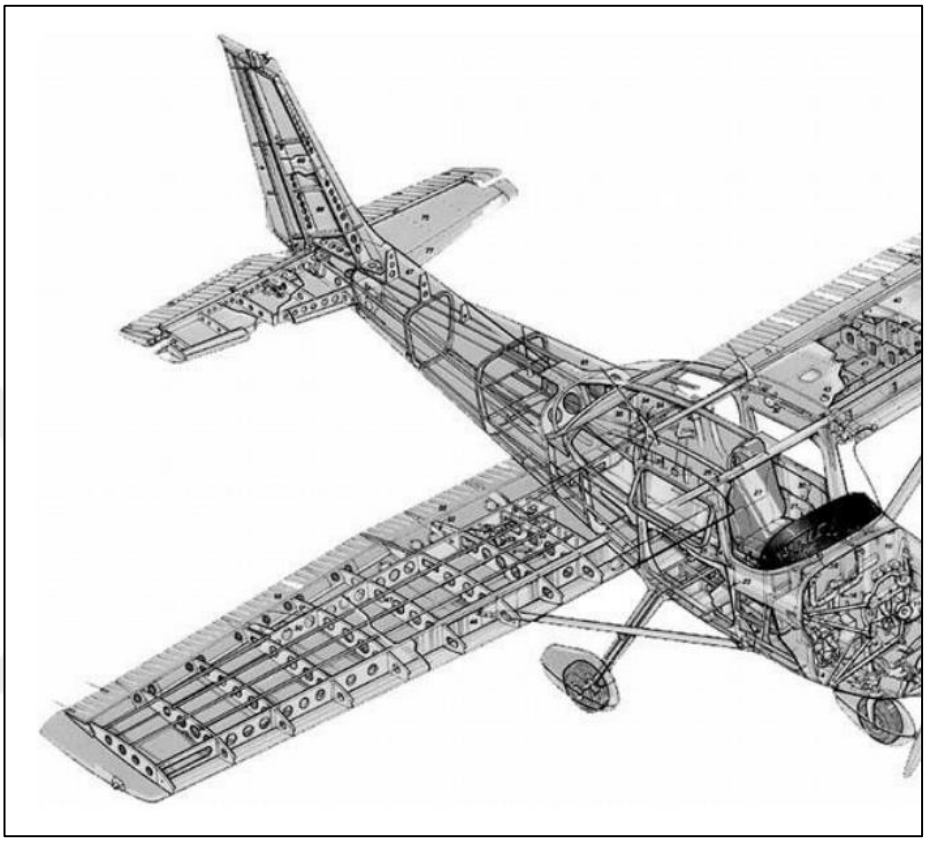

Figure 1.4 Cessna 172 Wing Internal Structure Layout [7]

1.3 Acting Forces on Wing Component and Initial Weight Calculation

The thickness dimensioning of the structural elements of an aircraft and their position in the interior structure are determined by the loads on the component. While performing the structural analysis of the aircraft, the most critical loading condition is determined. Dimensioning of the structure is performed according to this load case. Considering the loading condition of the wing component, the most effective force on the structure is the lift force. For this reason, when trying to calculate the structural strength of a wing structure, the maximum lift force on the structure should be

calculated. The reason for this is that, if the wing structure is resistant to the most critical situation, it will also become safe against other loads. It is possible to make a simple approximation when calculating the lift force on the wing. If the entire lift force of the aircraft is resisted by the wings and the gravitational acceleration to which the aircraft will be exposed is applied directly to the wings as a pressure load, results that are not far from reality can be obtained. However, lift is quite high this load situation and causes the thickness of the structure and the component weight to increase. The lift distribution on a wing is not uniform, and it is generally elliptic in subsonic aircraft as in Figure 1.5 [6]. There is a decreasing load distribution from the root to the tip of the wing. Although the magnitude of the lift force acting in total is same, the bending moment that will occur at the root of the wing in case of uniform loading is quite high compared to the elliptic loading. This causes an increase in the thickness of the structure and the component weight in the case of loading. The following Equation (1.1) can be used to calculate the lift force on the wing [8]. Thanks to the equation, the lift force acting on the wing structure is found. There are many unknowns in this equation. The speed of the airplane, the wetted area of the wing, and the lift coefficient can be computed with analytical methods [6]. However, on aircraft already flying, this can be found easily into the unknown. In this way, the most critical lift condition on the wing structure can be calculated.

$$L = \frac{1}{2}\rho V^2 S C_L \tag{1.1}$$

where L is the lift force, ρ is the air density, V is the aircraft speed, S is the wing area, C_L is the lift coefficient.

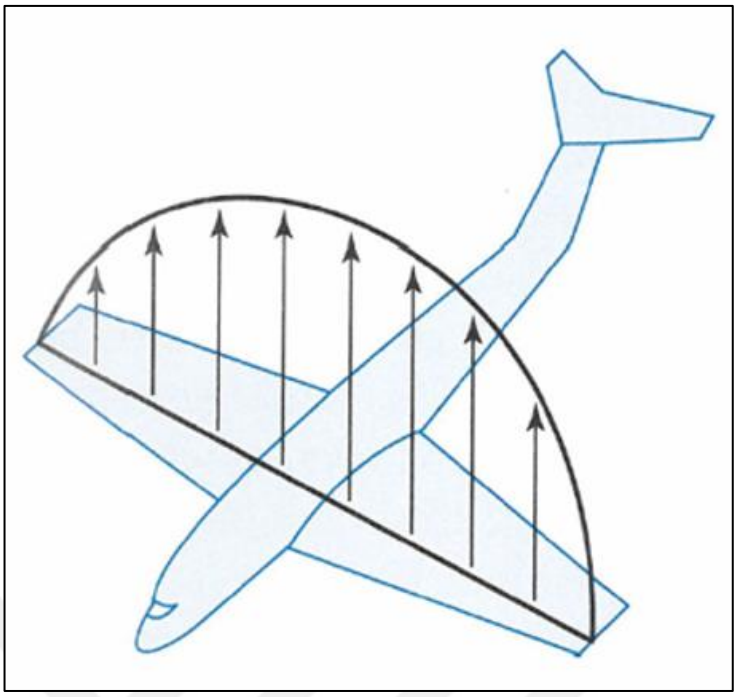

Figure 1.5 Spanwise Lift Distribution [6]

As the angle of attack of the aircraft increases, the lift force on it also increases. However, it also increases the drag force, which has a negative effect of increasing the lift force. This is because the surface of the airfoil in contact with the air increases. Therefore, a drag force is created on the aircraft in addition to the lift force. Equation (1.2) [9] can be used to calculate drag force. To find the load at which drag force is maximum, it is necessary to know the stall speed of the aircraft, the wing wetted area and the maximum drag coefficient. Since unknown data other than drag coefficient are found when calculating the lift force, it should be focused on calculating the maximum drag coefficient. There are two ways to calculate this coefficient. First, it can be found from the drag coefficient versus lift coefficient graph of the wing profile. Another method is to find it analytically from Equation (1.3) [6]. The efficiency factor, or Oswald efficiency factor (e), is considered 1.0 for aircraft with elliptical lift distribution. However, for aircraft with general aviation status, this value is in the range of 0.8-0.9 [6]. The aspect ratio of the aircraft can be accessed from the aircraft's own data. Zero lift drag coefficient of the aircraft generally estimated as 0.02 for general aviation type aircraft. However, this coefficient can be found from the airfoil graphs [10].

$$D = \frac{1}{2}\rho V^2 S C_D \tag{1.2}$$

where D is the drag force, ρ is the air density, V is the aircraft speed, S is the wing area, C_D is the drag coefficient.

$$C_D = C_{D_0} + \frac{{C_L}^2}{\pi A e} \tag{1.3}$$

where C_{D_0} is the zero lift drag coefficient, A is the aspect ratio of the wing, e is the Oswald efficiency factor, S is the wing area, C_L is the lift coefficient.

After calculating the magnitudes of the lift and drag force, it is necessary to know from which point these forces act on the structure. The center of pressure is an important concept when designing an aircraft. An unsymmetrical air profile not only provides lift, but also generates a moment. An airplane's center of pressure is the point at which all aerodynamic loads can be represented by a single force vector without moment [11]. However, this point changes with the angle of attack of the aircraft. The aerodynamic center is the point where the pitching moment produced by the aerodynamic forces is constant with the angle of attack. In Figure 1.6 [6], forces acting on center of pressure and change of the location of pressure center relatively angle of attack in Figure 1.7 [6] can be seen. Therefore, force computation on aerodynamic center is more suitable compared to pressure center.

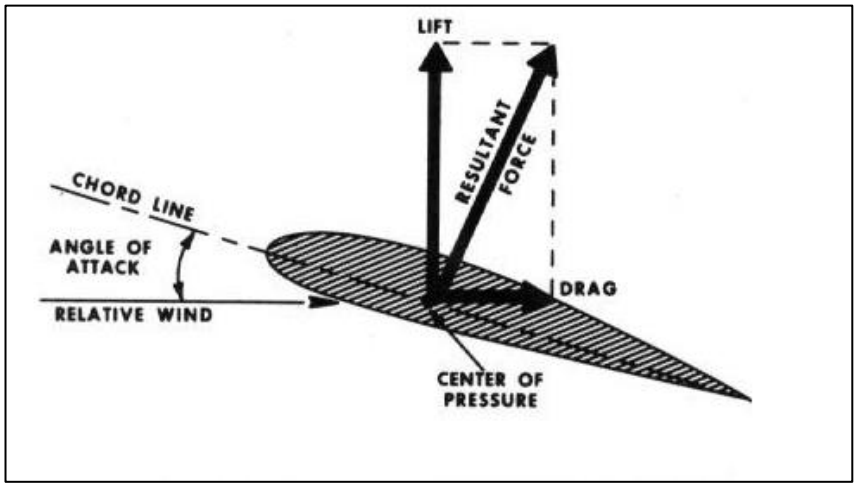

Figure 1.6 The Force on Pressure Center [6]

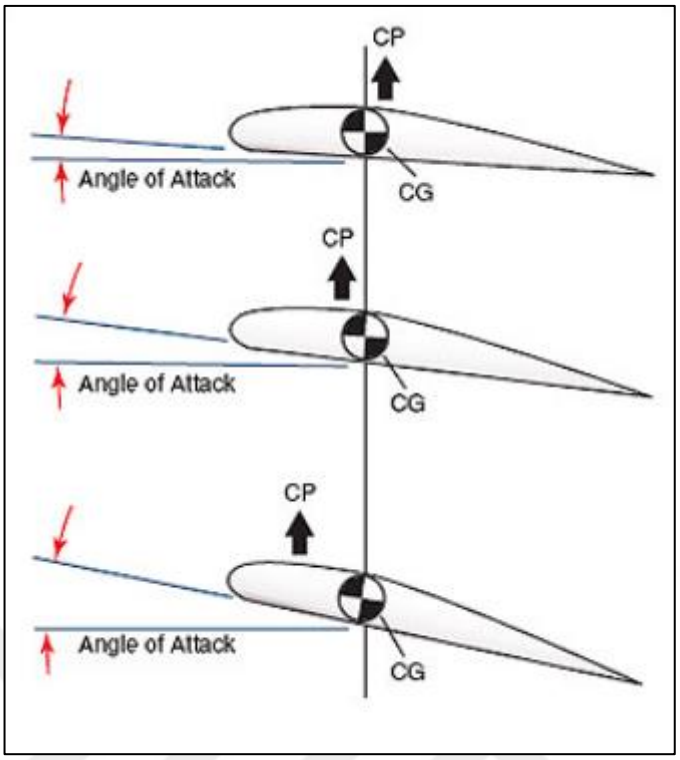

Figure 1.7 Pressure Center Positions by Angle of Attack [6]

In other words, the place where the aerodynamic moment remains constant is called the aerodynamic center of the airfoil. In subsonic aircraft, the wing theory shows that the lift force due to the angle of attack acts on the airfoil at a point about 25% from the leading edge. In wind tunnel tests, the aerodynamic center deviates 1% or 2% from this quarter point [9]. In Figure 1.8 [9], lift, drag and pitching moment forces on the aerodynamic center can be seen.

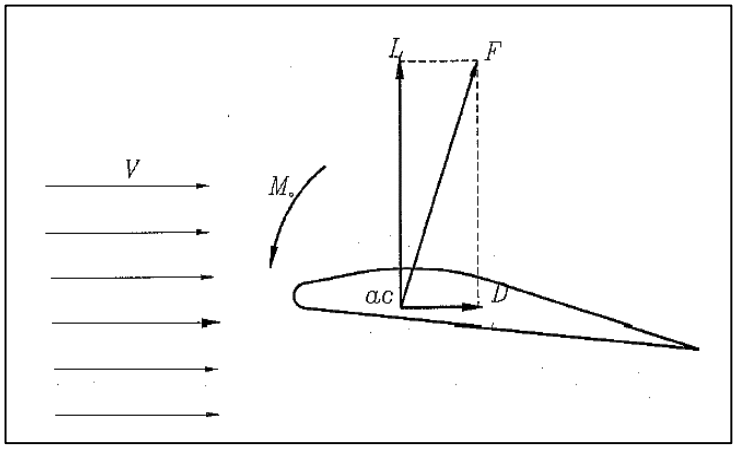

Figure 1.8 The Aerodynamic Forces on Aerodynamic Center

The lift and drag forces acting on the aerodynamic center are described in the topics in this section. Equation (1.4) can be used to find the pitching moment acting on the aerodynamic center [12]. All equation unknown data can be accessed from the aircraft's own data [13]. The pitching moment coefficient can be calculated from the pitching moment versus angle of attack graphs of the airfoil used in the airfoil [10]. Thus, the necessary forces for the static analysis of the wing structure and the location where the forces acted were found.

$$C_m \frac{M}{qSc} \tag{1.4}$$

where C_m is the pitching moment coefficient, M is the moment, q is the dynamic pressure, S is the wing area, c is the chord length of the wing.

Even if the calculation formulations of the loads are known, it is important to predict in which case they will occur. At this point, comments can be made about the loading situations that an aircraft may encounter along the flight envelope. The V-g graph, which is a graph showing the structural strength of an example aircraft according to certain speeds and load factors, is shown in Figure 1.9 [5]. Loading situations that an aircraft may encounter along the flight envelope are shown. While creating this flight envelope, data such as stall, manoeuvre, maximum cruise and never speed of the aircraft should be known. Thanks to this graph, when performing the structural analysis of an aircraft, the loading conditions are calculated and information about the forces acting on the structure is obtained. The load factor of the aircraft, on the other hand, shows the limit required to prevent the structure from being statically damaged. The load factor is determined by the structural analysis engineer and the manoeuvres and speeds of the aircraft are determined according to this load factor value. Therefore, this diagram plays an important role in determining the loading conditions of an aircraft. With these input values, the structural strength of the components is checked.

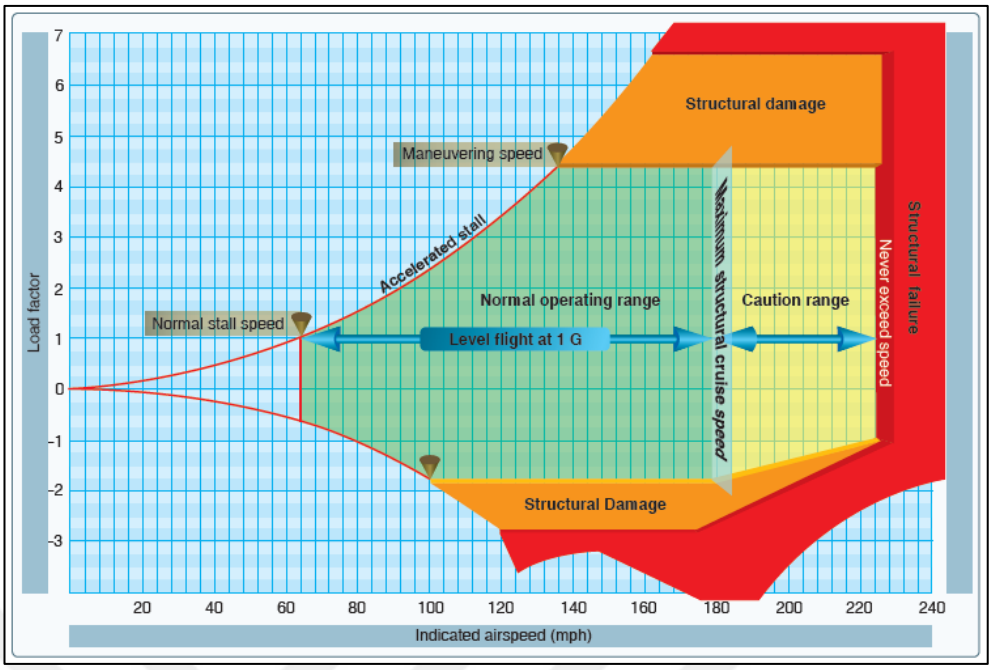

Figure 1.9 Typical V-g Diagram [5]

After understanding the loads acting on the wing component and where they affect it, the initial weight of the structure should be known to compare the component weights before and after optimization. If the aircraft has been built before, this data can be accessed from the aircraft's required document. But there are also some analytical ways of determining the initial weight. While designing aircraft, different stages are passed through. The first of these is conceptual design. At this stage, the approximate weight of each component of the aircraft is calculated and the total take-off weight of the aircraft is determined as an estimation. In this way, an idea about the center of gravity, stability and performance of the aircraft can be obtained before the aircraft takes off. Different methods have been put forward when weight estimation of components in an aircraft. The first of these is FLOPS (Flight Optimization System), a program recently used by NASA. The FLOPS method emerged by NASA in the 1980s and its development continued until 2011. The math and algorithm in this method are complicated [14]. This method was created to evaluate the component weights and technological systems of the aircraft during the conceptual design phase of the aircraft. However, other methods used since long times in the literature that can be used analytically are the methods of Roskam and Raymer. The Roskam method, on the other hand, allows the designer to make a weight estimation like Raymer's method

during the conceptual design phase. One of Roskam's approximate weight finding methodologies is directly on Cessna group planes. In Equation (1.5) [15], the weight approach formulation of the wing structure can be seen belonging to the Cessna group and connected to the strut and fuselage. The fixed values in this formulation of Roskam were created by statistical evaluation of the data of the pre-produced aircraft. Raymer, on the other hand, offered a method for calculating aircraft belonging to the general aviation category, not directly related to a single aircraft. In Equation (1.6) [6] there is a formula for calculating the weight of a general aviation class aircraft using the Raymer method. The weight of an aircraft's wing component can be estimated using this method from Raymer. When these 3 weight estimation methods are compared and the purpose of the study is considered, Roskam and Raymer's methods are seen as the most effective and efficient ways. The reasons for choosing these methodologies are that the history of the aircraft is very old, it has an easy aircraft geometry, and the methods have been applied before.

$$W_{wing} = 0.002933 S^{1.018} A^{2.473} {N_{ult}}^{0.611} \tag{1.5}$$

where S is the wing area, A is aspect ratio of the wing, N_{ult} is the ultimate load factor.

$$W_{wing} = 0.036 S^{0.758} W_{fw}^{0.0035} \left(\frac{A}{cos^2 \Lambda}\right)^{0.6} q^{0.006} \lambda^{0.04} x \left(\frac{100\ t/c}{cos\Lambda}\right)^{-0.3} (N_{ult} W_{dg})^{0.49} \tag{1.6}$$

where S is the wing area, A is aspect ratio of the wing, N_{ult} is the ultimate load factor, q is the dynamic pressure, t/c is the thickness to chord ratio, Λ is the wing sweep at 25% mean aerodynamic chord, λ is the taper ratio, W_{fw} is the weight of fuel in wing, W_{dg} is the take-off gross weight of the aircraft..

While calculating the weight of the wing component, there are steps in calculating the unknown values in the relevant formulations. First, it is necessary to know the take-off weight of the aircraft and the ultimate load factor according to the manoeuvres of the aircraft. As the weight of the aircraft and the maximum gravitational force it can withstand increase, the weight of the wing increases in direct proportion. After this stage, information about the wing geometry should be obtained. The wetted area of the

wing, the dynamic pressure it is exposed to during the cruise, the thickness chord ratio of the used airfoil and the taper angle should be known by the designer. If these unknowns are for a previously manufactured and tested aircraft, the information is already available in the handbooks of the aircraft [16]. The initial weight of the wing component can be calculated using Roskam's and Raymer's weight estimation methods and compared with the actual weight of the aircraft. In this way, the margin of error between analytical calculation and real data can be determined.

1.4 Topology Optimization Methods

Size and shape optimization, which are two samples of optimizations, was widely used to increase the performance of aircraft by reducing the weight of it [17]. The topology optimization method was revealed by the research carried out by Bendsøe and Kikuchi in recent years [18]. This method, along with the other two methods, started to attract attention by well-established companies in the aviation industry such as Lockheed Martin [19] and Airbus [20]. Thanks to this method, the material is distributed in a way that determines the load paths according to the loading conditions and boundary conditions of the aircraft. For this reason, it has played a major role in making it a preferred optimization method in aircraft structures in the aviation industry. Simply defined, topology optimization aims to find the optimum structural distribution under user given objectives, constraints, loads, and boundary conditions. The main principle of size optimization is to optimize the physical dimensions of the structure. In shape optimization, the boundary surfaces of the geometries can be defined as parameters so that the outer boundaries of the structure geometry can reach the optimum. Although size and shape optimization provide lightness in the structure, the result of the optimization results in a result depending on the initial state of the design. The advantage of topology optimization over size and shape optimization is that it optimizes the structure regardless of the initial boundaries of the geometry. Figure 1.10 shows how an optimized structure is output from a structure in general topology optimization [21].

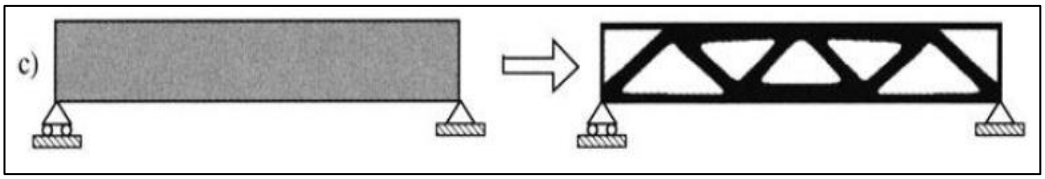

Figure 1.10 Typical Topology Optimization [21]

When Topology optimization first came out, the main problem was large scale integer problems, so it was creating a lot of time and expense. Thereupon, the homogenization method was introduced by Bendsøe and Kikuchi to reach the result more quickly. The structure resulting from the classical topology optimization is as in Figure 1.10. But the difference that separates the homogenization method from traditional topology optimization is the complex mathematics behind it. The structure has been created many microstructures. Each microstructure is evaluated through homogenization according to some properties such as stiffness. The homogenization method performs the optimization process by iteratively changing the size of each cell. It has been observed that while getting the output results of this complex mathematics, it is still not at the desired place in terms of time. The structure resulting from the homogenization method is as in Figure 1.11 [22]. As can be seen in Figure 1.11, a macro structure consists of many microstructures and the densities of these microstructures were determined according to some criteria. As a result of these conditions, the microstructures had different densities and combined to form a new macrostructure.

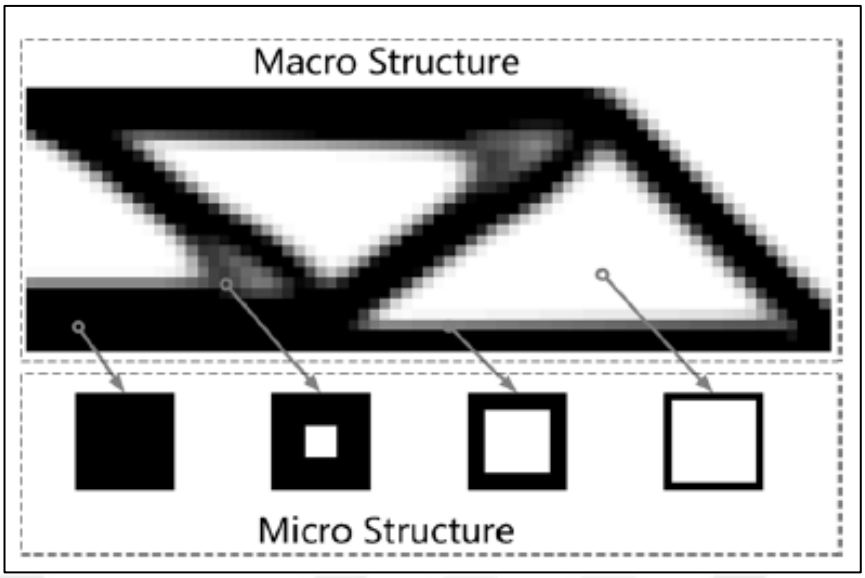

Figure 1.11 Homogenization Method Topology Optimization [22]

Right after the homogenization method, Bendsøe and Kikuchi [23] developed density-based approach, which is a simplified methodology compared to the mathematical background homogenization method. When an intermediate density value ranging from 0 to 1 is assigned with the formulation in Equation 1.7 instead of the method of homogenizing the microstructure in the structure, the stiffness of the element is penalized to a small value. In this way, it ensures that the pseudo-density variable η_i changes between 0 and 1 during optimization. This method is also known as SIMP (Solid Isotropic Material Penalization) [24]. To better interpret the data given from this topology optimization, Bendsøe [25] showed that there is a connection between the rigidity of the structure and the amount of material at this density. At the same time, considering the ease of application, the SIMP method has become the most preferred among topology optimization methods [21].

$$P(\eta_i) = \eta_i^p \tag{1.7}$$

where η_i is the pseudo-densities, p is the penalty factor.

ESO (Evolutionary structural optimization) is another popular topology optimization approach. This method was improved by Xie and Steven [26]. The main purpose here is to define the volume restriction determined by the user as a goal, and until this

restriction is reached, the non-essential materials in the structure are gradually removed in accordance with the defined criteria. The advantage of the ESO method is that it is conceptually simple. For this reason, it has been used in solving various design problems [27]. Although popular, this topology optimization approach has not been preferred. The reason for this is that it is not possible to add the removed material back. During the optimization, it leads to unexpected failures in the structure since the material only progresses during the iterations. To overcome this, Bi-directional ESO (BESO) version has been enhanced [28]. With this method, the negative aspects of ESO were avoided and a robust and efficient result was achieved in microstructural designs according to the SIMP method. Apart from the density-dependent methods, there are boundary variation methods. Level set method is one of the most researched among these methods [29]. The reason for this is its advantage in complex geometries. However, more research needs to be done before it can be used in industrial products [30]. Within the scope of the study, it is the SIMP methodology, which has an ancient history and has an advantage in time and mathematics. One of the most important features of this methodology is that it has been previously studied in the aviation industry.

CHAPTER 2

FINITE ELEMENT MODEL INPUT

2.1 Aircraft Wing Component Weight Computation

The initial weight of the Cessna 172 should be known before weight reduction can be made with topology optimization of the wing structure. To estimate the weight of an aircraft, the aircraft data produced in the past are evaluated statistically. Putting this process into equations with physics-based models means a great deal of time and effort. However, many companies are still developing their own equations to better converge to the initial weight of the components. There is no exact way to calculate the initial weight of an aircraft that has not flown before. Therefore, in this study, the equation used by Raymer for general aviation aircraft [6] and the Cessna method in Roskam's book [15] were used to calculate the approximate weight of the wing. Then, these data were compared with the actual values of the Cessna 172 itself. First, aircraft geometric data can be accessed from documents. These data are given in Table 2.1 [16] below.

Table 2.1 Input Data of Cessna 172 [16]

Data	Value	Unit
Wing Referenced Area	16.16	m^2
Wing Fuel Tank Weight	53	kg
Aspect Ratio	7.5	-
Thickness Chord Ratio	0.12	-
Taper Ratio	0.7	-
Chord Length	1.74	m
Sweep Angle	0	$degree$
Maximum Speed	83.85	m/s
Cruise Speed	62.76	m/s
Ultimate Load Factor	5.7	-
Engine	134	kW

As the first method, equation (1.6) given below is used for the component weight method of Raymer's general aviation aircraft. The weight obtained from this equation

includes the weight of the flaps and ailerons, but the weight of the mechanisms is not included in these structures. In addition, this equation was written in accordance with the British system, but the data obtained were translated according to the SI unit. At this point, the referenced area of the wing, the taper ratio of the wing and the wing profile information are given in Table 2.1. In addition, fuel tanks are added to the wings to carry more fuel on most aircraft. Fuel tanks also help the structure from a structural point of view, as they are in the opposite direction to the lift force coming to the wing. Each wing of the Cessna 172 has a fuel carrying capacity of 53 kg (14 gallons). There are data that cannot be obtained in the equation. First, calculating the gross weight of an aircraft is one of the first steps in the conceptual design phase. It is sufficient to know the engine power to calculate an estimated first take-off weight of an airplane. Equation (2.1), which can be used when calculating the initial take-off weight, is given below. The constant values here have been made into an equation with reference to the old planes. In Table 2.2 below, some coefficients are calculated according to the category types of the aircraft. It should be noted that the constants in the equations in this table; it was obtained according to knots of airspeed and horsepower units of engine power. The maximum speed and engine power information of Cessna 172 can be reached from Table 2.1. At this point, it is important to choose the Cessna 172's aviation name type correctly [41]. Cessna 172 is in the category known as general aviation. From here, there are only two options that can be selected from the table. In the 172 model, a single motor was used as the thrust source. Therefore, the values to be used in the equation are included in the general aviation-single engine section of Table 2.2 [6].

$$W_{dg} = P.a.{V_{max}}^{C} \tag{2.1}$$

where V_{max} is the aircraft maximum speed, P is the engine power.

Table 2.2 Initial Weight Estimation Constant and Aircraft Class

Aircraft Class	a	C
Sailplane-powered	0.043	0
Homebuilt metal/wood	0.005	0.57
Homebuilt composite	0.004	0.57
General aviation-single engine	**0.025**	**0.22**
General aviation-twin engine	0.036	0.32
Agricultural aircraft	0.009	0.5
Twin turboprop	0.013	0.5
Flying boat	0.03	0.23

With the replacement of these values in equation 2.1, the approximate take-off weight of the Cessna 172 could be calculated. When the data of the aircraft is examined, the maximum take-off weight is known as 1111 kg (2450 lb) in normal category type aircraft [16]. In Table 2.3 below, the inputs and weight output of this equation are shown. When the actual weight data is compared with the theoretical data obtained from the equation, there is an error margin of 4.14%.

Table 2.3 Weight Comparison with Real Cessna 172 Data

Data	Value	Unit (SI)
a	0.025	-
C	0.22	-
V_{max}	83.85	m/s
$Engine\ hp$	134	kW
$W_0\ (Theoritical)$	1065	kg
$W_0\ (Real\ Data)$	1111	kg
$\boldsymbol{Error\ Rate}$	**4.14**	%

The only unknown in Equation 2.2 is the dynamic pressure parameter represented by q. Dynamic pressure, on the other hand, can be obtained by the equation in equation (2.2) [12]. The type of fluid in the equation is air, and its specific mass is 0.97 kg/m^3 (0.00189 slug/ft^3) at 7500 ft, at the altitude at which the plane cruises. The cruise speed of Cessna 172 is 62.7 m/s (122 knots). With the help of the related equations, the approximate weight of the wing component of the aircraft can be calculated according to the Raymer method.

$$q = \frac{1}{2}\ \rho u^2 \tag{2.2}$$

where u is the air speed, ρ is the air density.

Another method to be used in this study to calculate the initial weight of the wing component is Roskam's Cessna method. Roskam has created a special equation for Cessna type training aircraft. In these equations, there are physical approximations for two types of wing structures produced as strut and cantilever. Due to the Cessna 172 structure, the wing structure is connected to the fuselage with the help of strut. This columnar structure helps the structure while carrying the lift force from the wing, but it disrupts the air flow in terms of aerodynamics. Roskam's component weight calculation for strut braced Cessna wings is shown in Equation (1.5). This equation has been obtained according to the British system, so the obtained data will be converted to SI unit after the equation. All the unknowns required at this point are among the Cessna 172 data given in Table 2.1.

The results of the first weight calculation methods used to verify the structural strength of the Cessna 172 wing component at its own weight are given in Table 2.4. The actual weight of the Cessna 172 for a single wing is 53.62 kg (118 lb.). As can be seen in Table 2.4, the deviation margin of the 2 methods according to the obtained values is shown.

Table 2.4 Weight Comparison Raymer and Roskam Method

Method	Wing Weight (kg)	Wing Weight (lb)	Error Rate (%)
Raymer Method	45.21	99.59	15.6
Roskam Method	53.71	118.31	**0.26**

The equation created by Raymer for general aviation predicts a structure that is approximately 15.6 percent lighter. It's not a good enough approximation, even if it's not too far from reality. On the other hand, the method specially developed by Roskam for Cessna group aircraft is very close to the real value and the deviation margin is 0.26 percent. Therefore, Roskam's methodology was chosen for the weight of the wing component. In the main motivation of this study, real life data is not intended to be used directly to find the initial weight of an aircraft wing component.

2.2 Computing Aerodynamic Force on Wing

To analyse the structural strength of the Cessna 172's wing component, it is necessary to know the loading situation. The forces acting on the wing structure are lift, drag and pitching moment. At this point, it is the loading conditions are important for the structural analysis. In other words, what is one of the most critical loading conditions for the wing and at what location it occurs. To learn this, the Cessna 172's V-g diagram must be known. While creating this diagram, values such as maximum load factor, maximum cruise, never exceed and manoeuvre speed should be known. Since Cessna 172 is an aircraft that has been flown many times before, speed and load factor restrictions can be easily reached, and V-g diagram can be created. While the speed values of Cessna 172 are seen in Table 2.5 and Table 2.6 [31] shows the maximum positive and negative load factor values that the aircraft can encounter. The load factor value is the gravitational force that the earth creates on the mass. This value varies according to the manoeuvring movements of the aircraft and each aircraft has different limitations of this value.

Table 2.5 Cessna 172R Airspeed Limitation

Speed Type	Speed	Unit
Stall Speed	24.18	m/s
Manoeuvre Limit	49.9	m/s
Maximum Cruise	62.76	m/s
Never Exceed Speed	83.85	m/s

Table 2.6 Cessna 172R Load Factor Limitation

Limit Type	Load Factor (g)
Positive Limit	3.8
Negative Limit	1.52

With the values obtained, the V-g diagram for the normal category of the C172R Skyhawk aircraft was created. The speed-load factor diagram of the Cessna 172R model is shown in Figure 2.1 According to this diagram, an approximation can be made for the forces acting on the wing. At this point, the limits to be considered are 3.8 g positive and 1.52 g negative limitations. These values give information about how much the load will be on the structure. In aircraft, when considering the structural

strength, it is desired to provide strength up to 1.5 times the loads applied at the limit load factor level. The region shown as structural damage shows the part up to 1.5 times this limit with the limit load factor. For example, in the Cessna 172R, this value is between 3.8-5.7 g in the positive range. In this region, the structure may be damaged, but the structure cannot fail. In the region between (+3.8) – (-1.52) load factor values, no structural damage should occur. The caution range region is the region between the aircraft's maximum cruise, never exceed speeds and limit g forces. In this area, attention should be paid to manoeuvres.

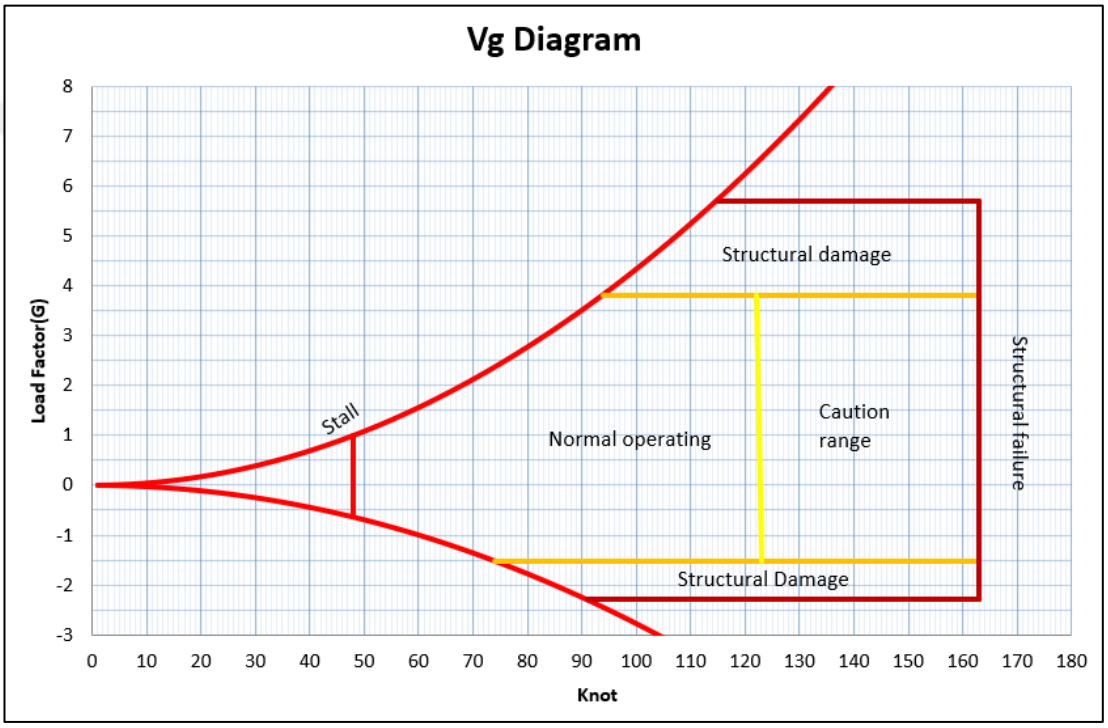

Figure 2.1 Cessna 172R V-g Diagram

2.2.1 Spanwise Lifting Force Distribution

The largest load on the wing component is the lift force [6]. The amount of this force is important for the distribution of the internal structure of the wing and the thickness of these structures. Lift formulation, Equation (1.1) is mentioned in the first chapter. The speed vs load factor diagram of Cessna 172 is shown in Figure 2.1. The highest limit factor in this diagram is 3.8 g. This means that the lift force impact on the wings

of the aircraft is 3.8 times its weight. The ratio of the lift load to the weight of the aircraft is the formulation of Equation (2.3).

$$\frac{L}{W_{dg}} = Load\ Factor = \frac{1}{2W_{dg}}\rho V^2 S C_L \tag{2.3}$$

It is known from the Cessna 172R document that the aircraft is 1111 kg. This means that the lift force on the wing component is 3.8 times its weight. The point to be considered here is the case in which the wing is exposed to this load. Table 2.7 shows the size of the installations that the wing is exposed to in 1, 2 and 3.8 g.

Table 2.7 Load Factor vs Lift Force

Load Factor(g)	**Lift Force(N)**
1	10911.66
2	21823.33
3.8	41464.32

The total lift load on the wing was calculated as 41464.3 N. The lift load on a single wing is half of it, that is 20732 N. In this study, it was assumed that this load is distributed as elliptic on the wing. Cessna 172R's total wingspan length is 11 meters, but the length of each wing component is 4.9 meters, as a 1.2 -meter part is included in the body. In equation 2.4 [8], the circulation (Γ) value must be known to find the lift distribution along Spanwise. After this value is found, a lift distribution similar to Figure 2.2 [8] is seen. The area under the curve represents the lift load and can be found from the point where spanwise comes.

$$\Gamma(y) = \Gamma_0\sqrt{1 - (\frac{2y}{b})^2} \tag{2.4}$$

where Γ is the circulation, b is the wing spanwise, y is the spanwise location.

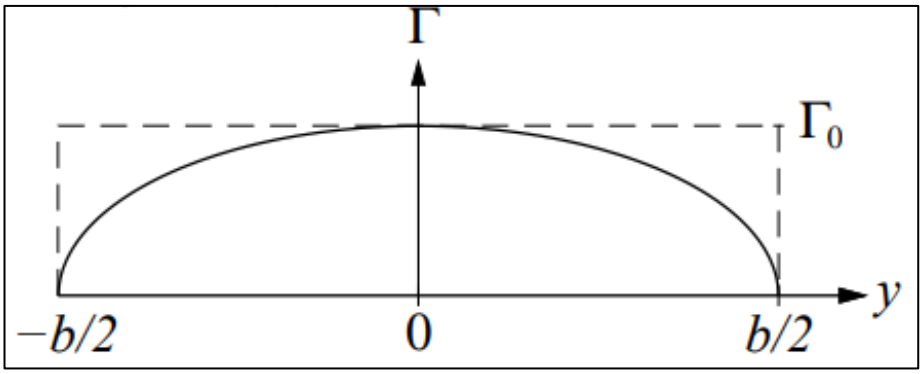

Figure 2.2 Typical Lift Distribution

With the help of Equation 2.6, the lift loading status may be found on a wing opening of 4.9 m. In Figure 2.3, the lift distribution of 172R is shown as an example, and for the application of the load to the finite element model, spanwise is divided into 7 regions and the area under the curve is calculated for each region. For these 7 regions, lift was calculated separately. At this point, the amount of load for each load station obtained from diagram and the location on the spanwise is shown in Table 2.8. These load points will be integrated into the finite element model in later chapters.

Table 2.8 Lifting Force on Wing Spanwise Stations

Station	Lifting Force (N)	Spanwise Location (mm)
1	3943.78	367.5
2	3853.08	1225
3	3664.86	1960
4	3362.56	2695
5	2909.98	3430
6	2211.32	4165
7	786.78	4777.5

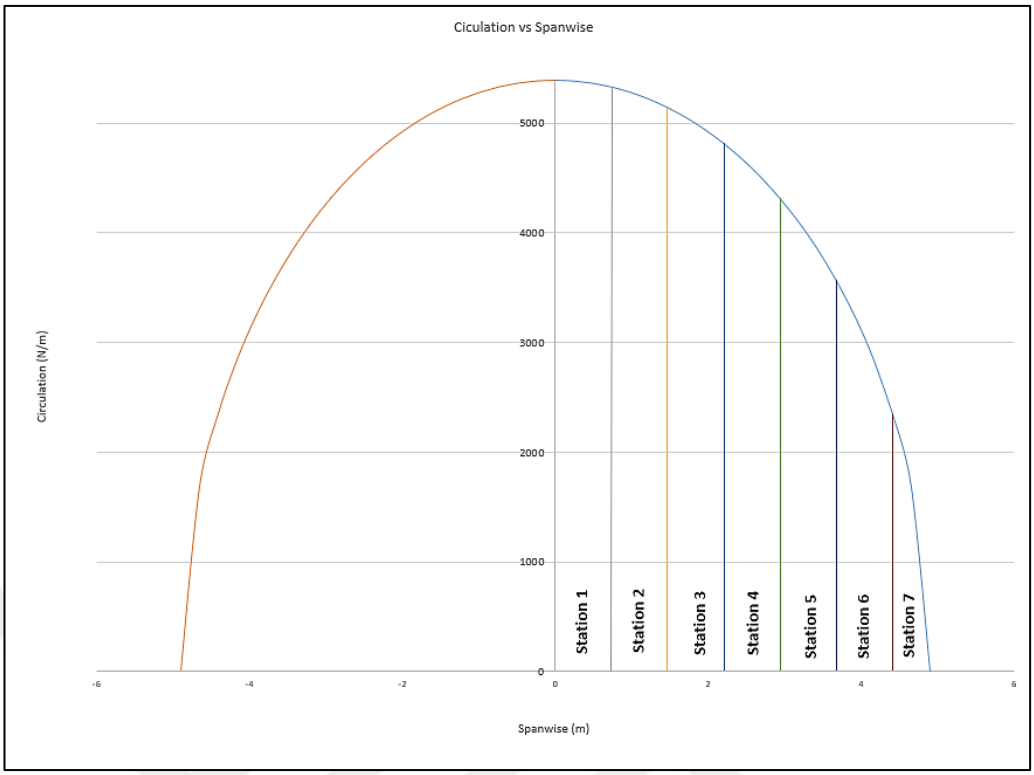

Figure 2.3 Cessna 172R Wing Lift Distribution and Stations

2.2.2 Drag Force and Pitching Moment

Depending on the limit factor value, the angle of attack value was not taken into consideration when calculating the maximum lift load on the aircraft. This was because the variability of the lift coefficient, air speed, or the specific weight of the fluid can be changed but the maximum lift load stayed the same. In this chapter, the drag force and pitching moment on the aircraft will be found. Some iterations need to be made because the most critical case is chosen for the wing of the aircraft. In these iterations, while the lift load is maximum, it was noted that the wing and the pitching moment are the highest values that the wing may face. Angle of attack is one of the most important variables that may affect the drag force and pitching moment that may occur on the wing. Like Figure 2.4 [8], the angle of the angle of attack wing profile between the chord line and the fluid is the direction of the fluid. As angle of attack increases, it also increases with the increase in the lift coefficient on the wing [8]. Therefore, these angles are limited to 15-20 values for wing profiles. The wing profile used on the

Cessna 172R plane is NACA2412 [16]. This wing profile of the maximum angle of attack is 15-16.

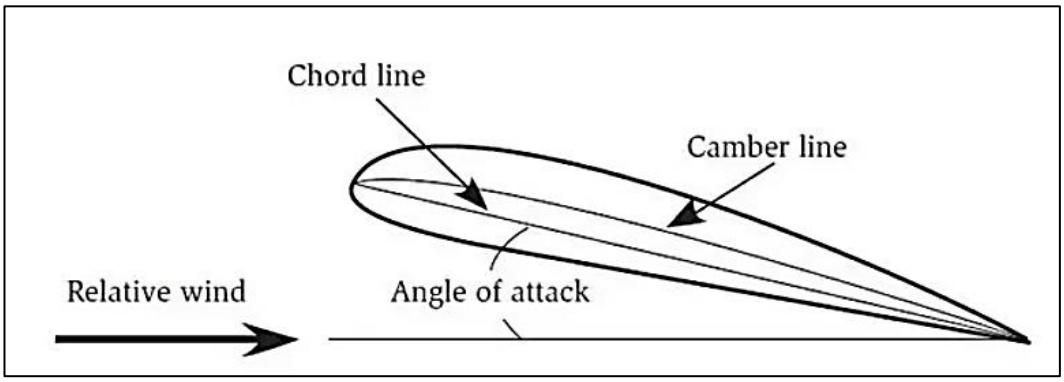

Figure 2.4 Angle of Attack on Airfoil Profile

For the presence of the most critical drag and pitching moment loads, the NACA2412 profile at 1000000 Reynold number of lift, drag and pitching moment coefficient and angle of attack associated graphics are shown in Figure 2.5, 2.6 and 2.7 respectively [10]. The most critical angle of attack will be identified and drag and pitching moment will be calculated.

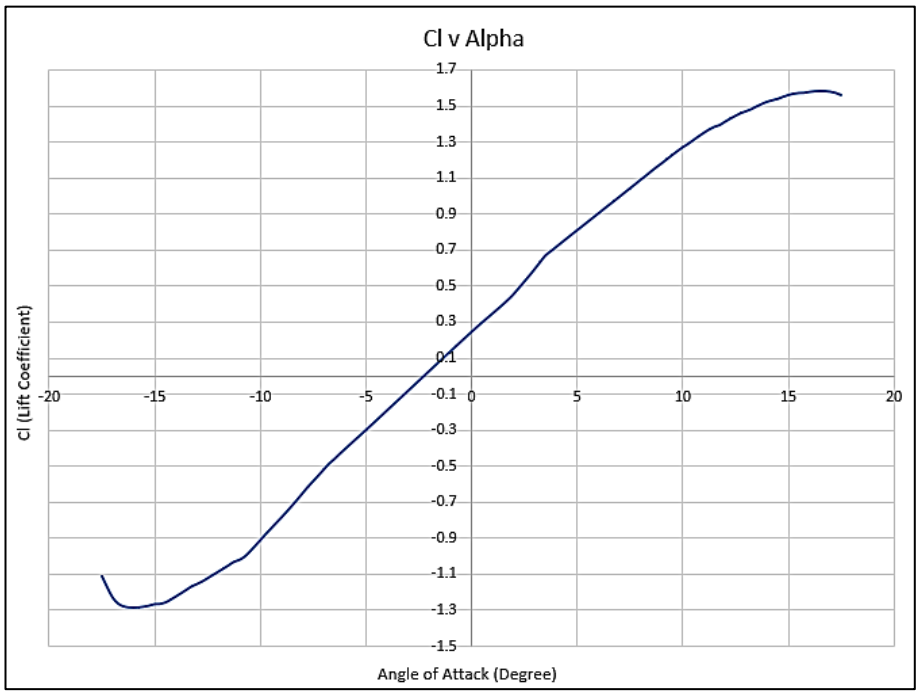

Figure 2.5 Cl v Angle of Attack

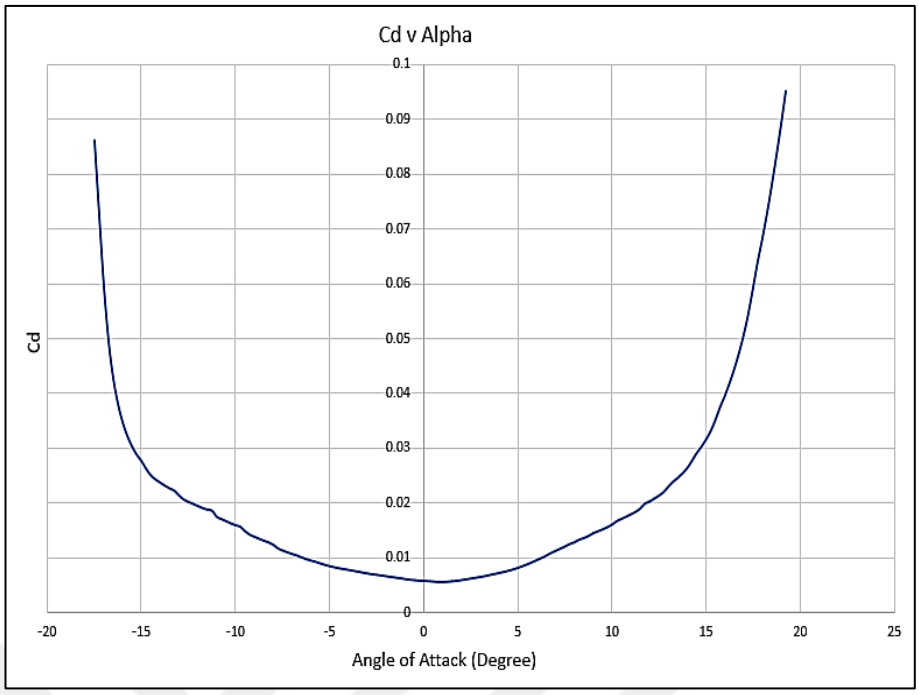

Figure 2.6 Cd v Angle of Attack

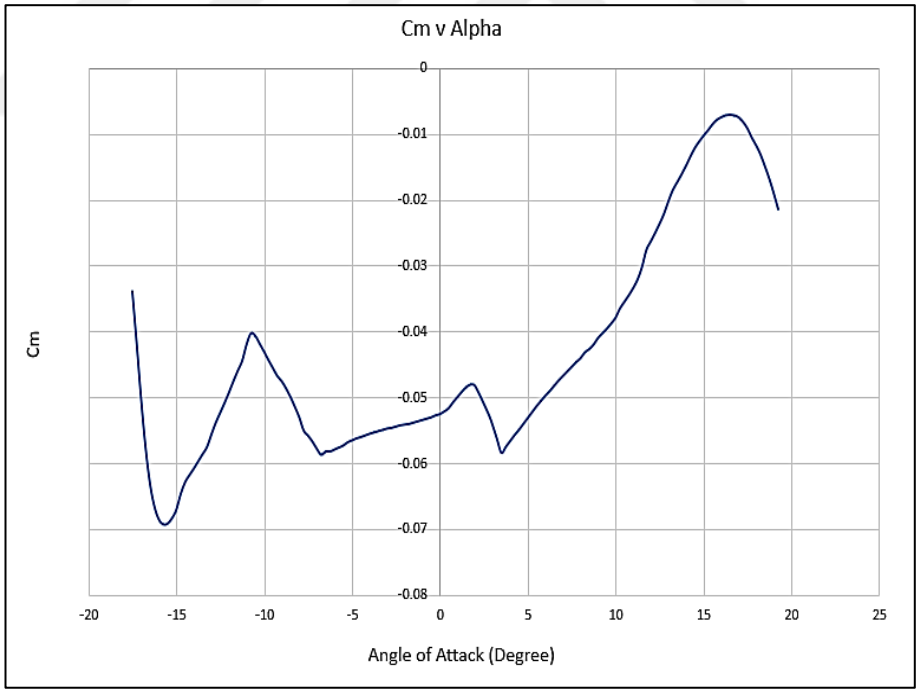

Figure 2.7 Cm v Angle of Attack

While the total lift load was 41464 N, the speed of the airfoil lift coefficients versus angle of attack graph was found for each angle. Here, the aircraft operation ceiling of

the aircraft was taken as 2286 m (7500 ft) to be fixed specific weight of the air. The speed graph has been shown for the Cessna 172R aircraft to resist the load of 3.8 g of force according to any angle of attack value. Drag force and pitching moment graphics have been created according to these speed and angle of attack values. Related data can be seen in Figure 2.8, 2.9 and 2.10. Equation 1.2 [9] for drag force and Equation 1.4 [12] for pitching moment were used to calculate these values. Cessna 172R's never exceed speed is 83.85 m/s. For this, the above graphs are suitable for calculations between 4.25-15 Degree. Other speed values cannot be met by the engine of the aircraft.

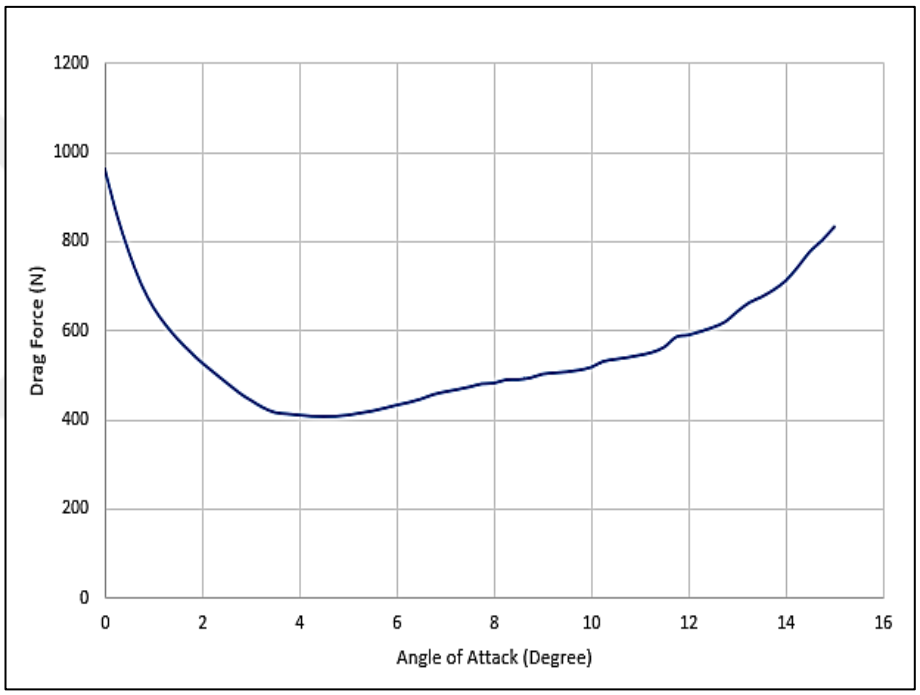

Figure 2.8 Drag Force versus Angle of Attack at 3.8 Load Factor

Considering the drag load and pitching moment values, the maximum value between the angle of attacks of pitching moment and drag force. Maximum values created for the finite element model to be applied to the model are as in Table 2.9.

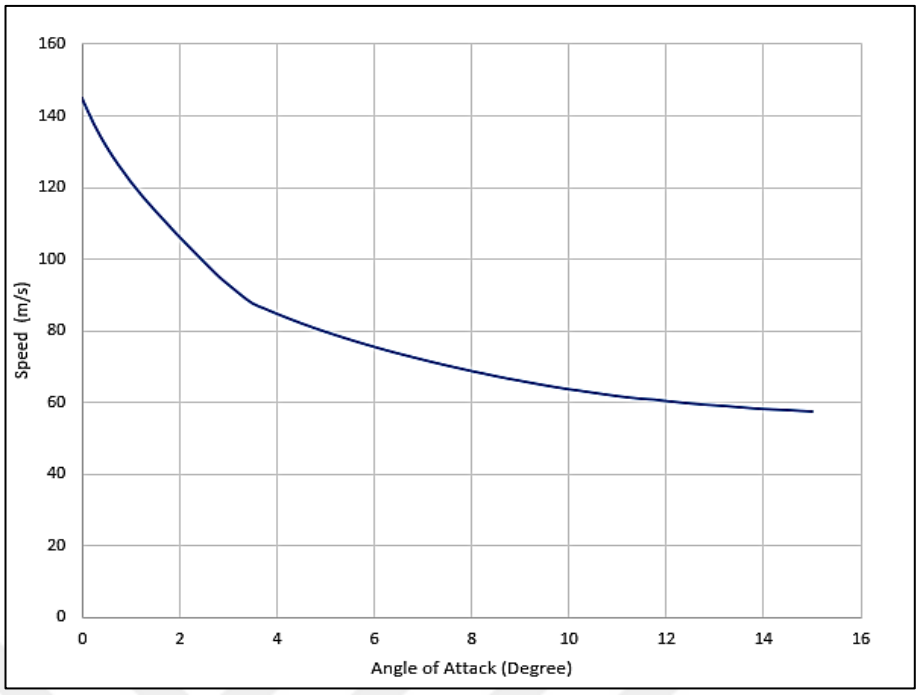

Figure 2.9 Velocity versus Angle of Attack at 3.8 Load Factor

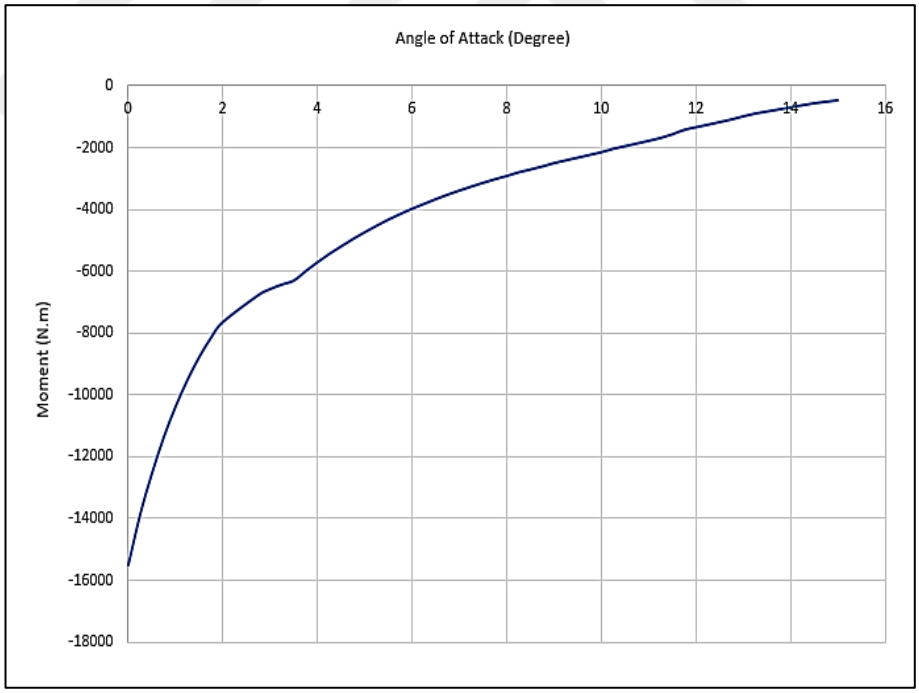

Figure 2.10 Pitching Moment versus Angle of Attack at 3.8 Load Factor

Table 2.9 Maximum Aerodynamic Force on Wing Structure

Aerodynamic Forces	Value	Unit
Lift	41464	N
Drag	835	N
Pitching Moment	-5432	Nm

In the Chapter 2, the force, which is effective above the wing structure, and initial weight estimation were made to compare its weight. In the next chapter, the finite element model of Cessna 172 will establish, and the data obtained in this section will be integrated into the model and the results will be examined.

CHAPTER 3

FINITE ELEMENT MODELING

3.1 Determination of Internal Structures Location

While creating the finite element model, Altair Hypermesh was used for modeling and Optistruct was used for the solver. When establishing the finite element model of Cessna 172, it is necessary to know the spanwise length, chord length and the location of the structures in the inner structure of the skin. Figure 3.1 shows NACA2412, which is the wing profile used for Cessna 172R, and the dimensions of the component. The wingspan is 4900 mm for a single wing, while the chord length is 1738 mm [41]. The taper ratio of the wing is 0.7, and the chord width narrows towards the tip. The global x-coordinate is from the leading to trailing edge of the wing in the positive direction.

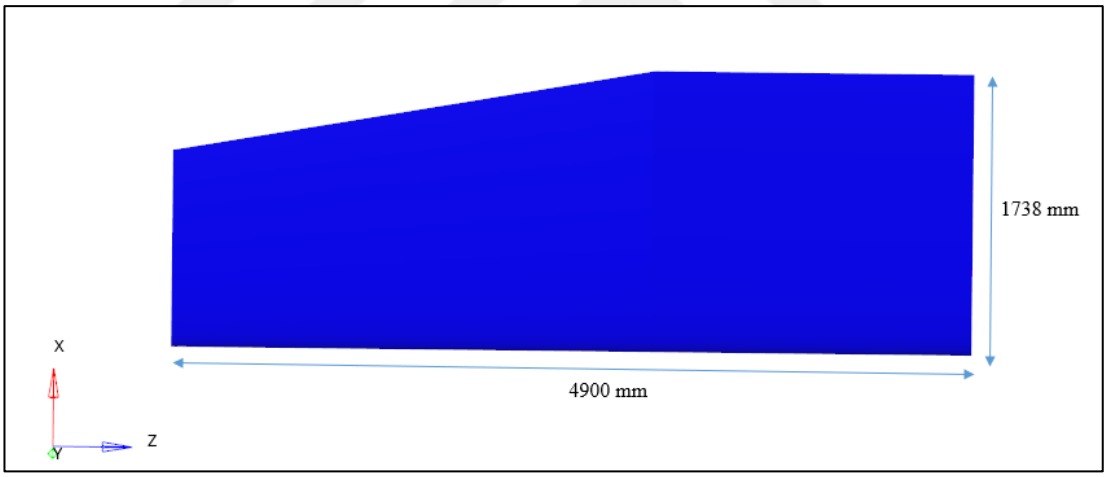

Figure 3.1 Cessna 172R Wing Dimensions

When looking at the internal structure, the force that has been calculated in chapter 2 and that affects the structure the most is the lift force. The main carrier structures of the incoming lift load of the wing structure are the spars. Cessna 172 has 2 C type spars. The first one is the main carrier spar and the other is the secondary spar. The location of these spars in general is not clear, but generally, the first spar corresponds to 18-25 percent of the chord and the other 55-70 percent of the chord [35]. The main

reason for this is that the aerodynamic center usually corresponds to 25% of the chord in airplanes [9]. For this reason, it is desirable to position the main carrier spar close to the aerodynamic center, where the load is concentrated. However, the location of the auxiliary spar is determined by the control surfaces. Figure 3.2 shows the spars, and Figure 3.3 shows the positions of these spars on the chord.

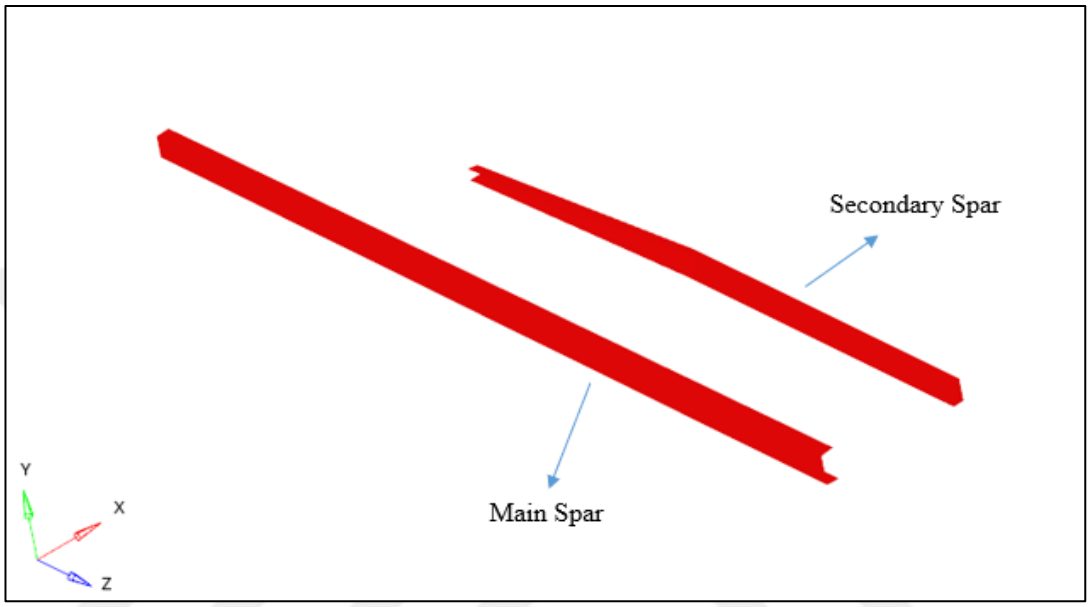

Figure 3.2 Main and Secondary Spar View

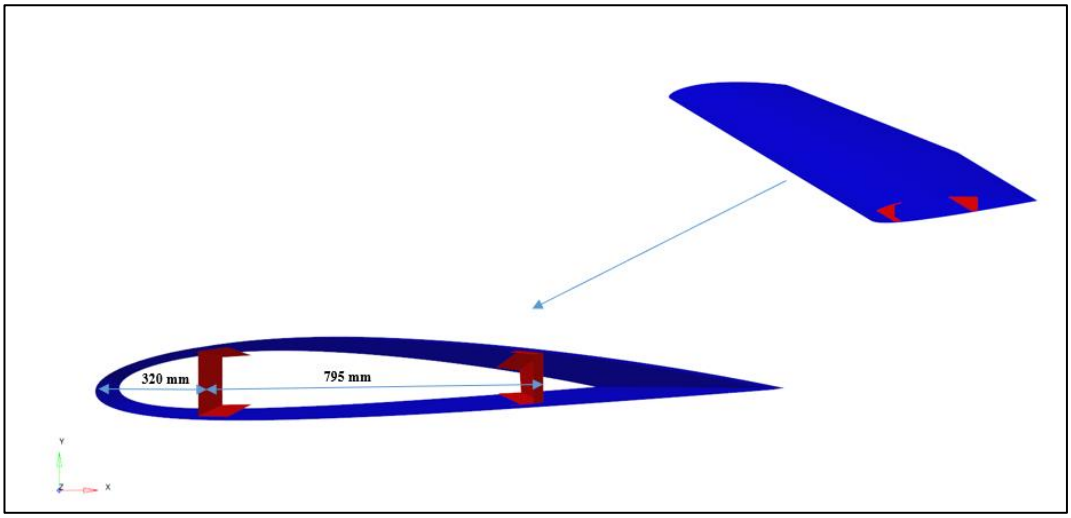

Figure 3.3 Main and Secondary Spar Chordwise Location

The main spar, which is 320 mm from the leading edge, corresponds to approximately 18% of the chord, and the secondary spar, which is 1115 mm away, corresponds to 64%. The positions of the ribs in the spanwise after the spars are shown in Figure 3.4. However, the locations of the first and last rib are marked. Accordingly, the locations of the ribs spanwise in the global z direction are shown in Figure 3.5.

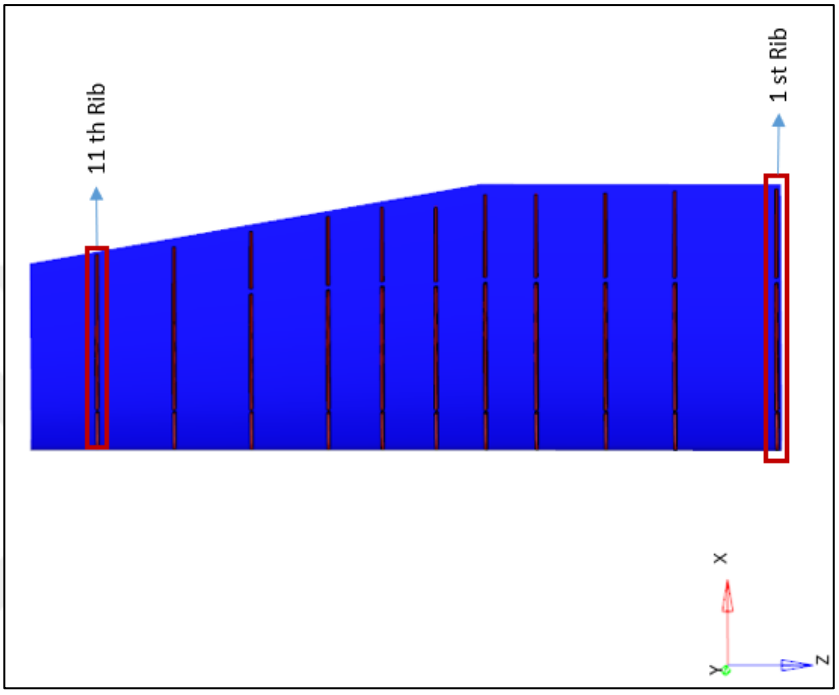

Figure 3.4 Ribs Wing Spanwise Distribution

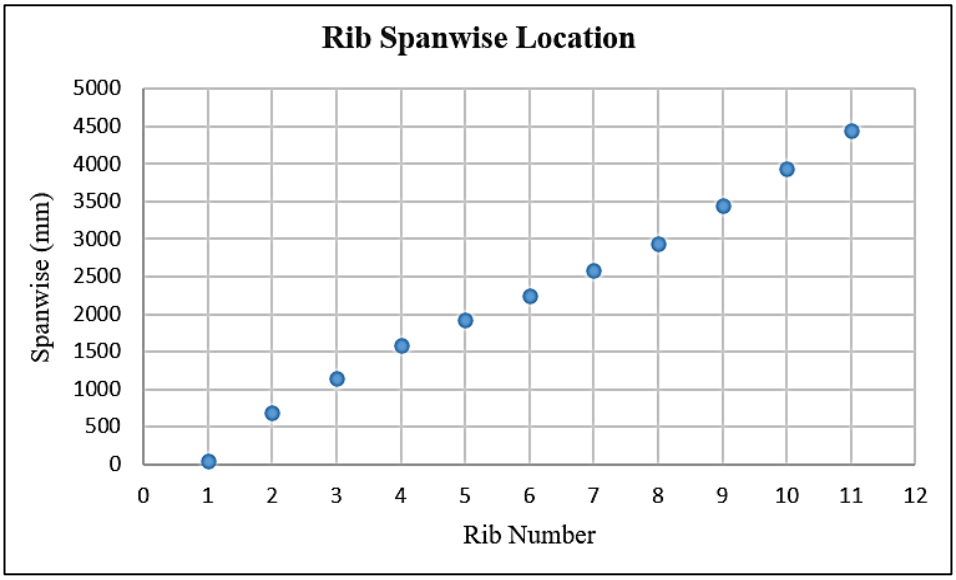

Figure 3.5 Ribs Spanwise Location

After the main structures forming the wing structure were completed, some auxiliary structures were added to prevent the skin panel from buckling failure. The first of these is stringers. Stringers are longitudinal members like spars and are used to support the wing structure. Another point is that the skin panels are created stiffened due to the low thickness of the skin panel and the large gaps between ribs and spars. The locations of the stringers on the chordwise are shown in Figure 3.6. The points it located in the wing chordwise are shown in Figure 3.7. The pattern created for the skin panel is shown in Figure 3.8. When creating the skin panel, the gap between the stiffeners varies between about 40 and 60 mm. Supporting the skin panel with stiffeners in this way prevents buckling failure [42].

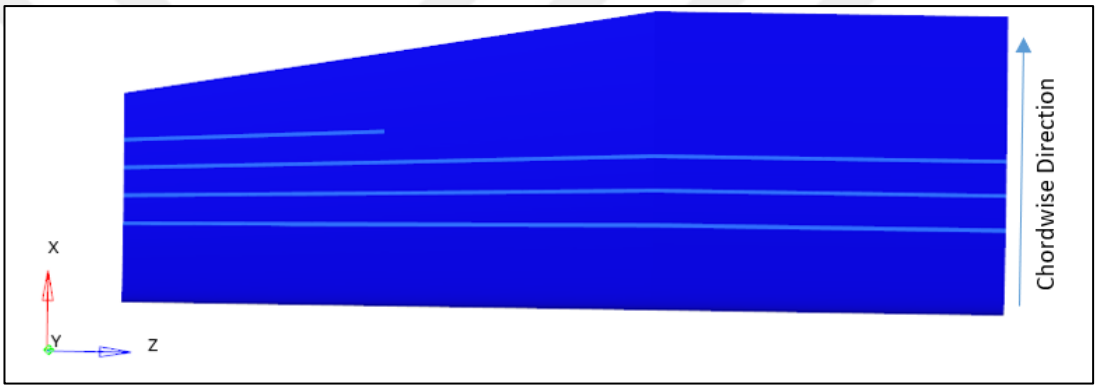

Figure 3.6 Stinger Chordwise Location

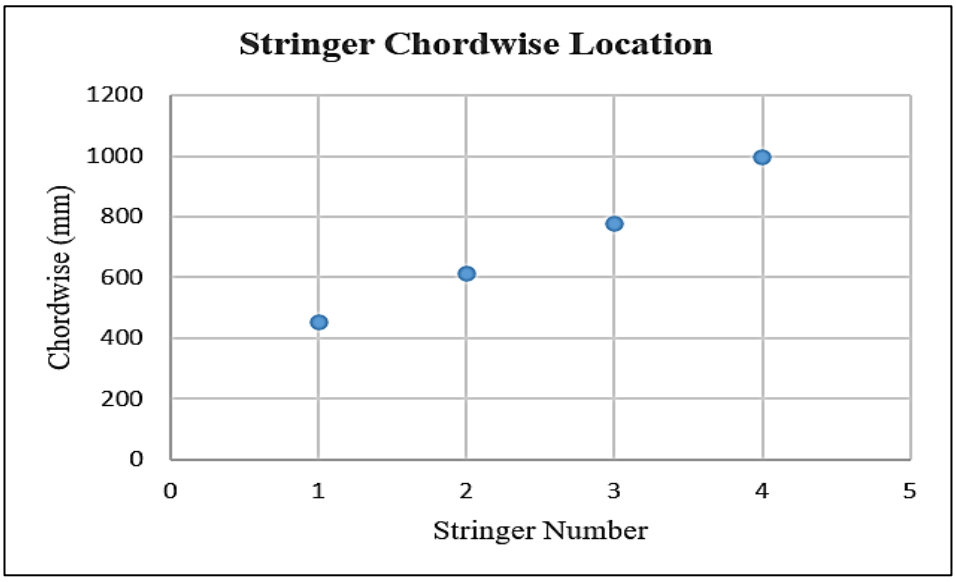

Figure 3.7 Stringers Chordwise Location

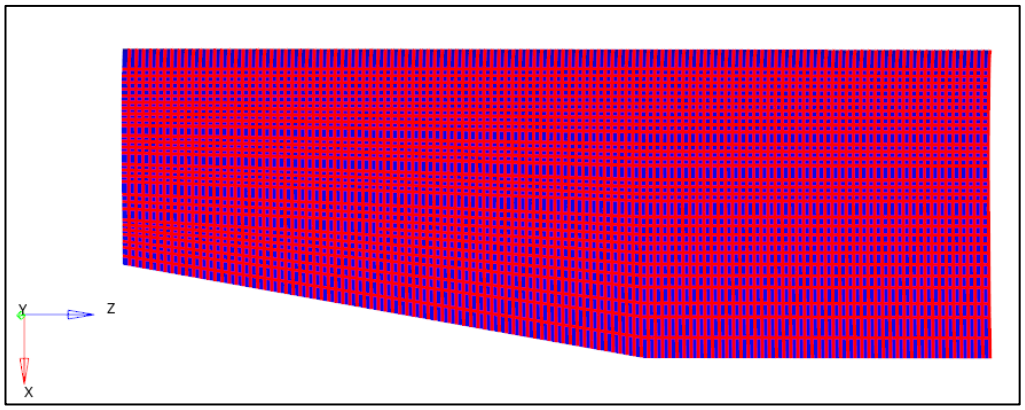

Figure 3.8 Stiffened Skin Panel Top View

3.2 Wing 2D Finite Element Modelling

While creating the finite element model, spar, rib, and skins were modelled in 2 dimensions (2D). Stringer, strut and skin panel stiffeners were modelled in 1 dimension (1D). While modelling, spars, ribs and skin panels are connected to each other with fasteners in order to reflect reality. However, the wings and control surfaces of the fasteners are accepted as one piece. The reasons for 2D modelling are that it is much better than 3D in terms of time and cost, and besides, the 3D model takes so long that it is almost insoluble while getting the buckling results. In addition, 2D modelling facilitates iterative variation of the thickness of the structure since there is no definite structure in the study. Stringer, strut, and skin panel stiffeners are 1D modelled. Cbar element was used during modelling. The main reason for this is that these elements do not actually carry the bending load but only the axial load. The reason for using cbeam element instead of cbar is that bar element only carries axial load [36].

When it comes to fastener modelling, rbe3-bush-rbe3 modelling was done. While the load on the structure is transferred to each other with the help of the rbe3 element, the stiffness of the bush element in the modelling is like that of the fastener in real life. With the stiffness values of the bush in the axial and shear directions of the element, it shows a behaviour like the fastener. An example of fastener modelling is shown in Figure 3.9.

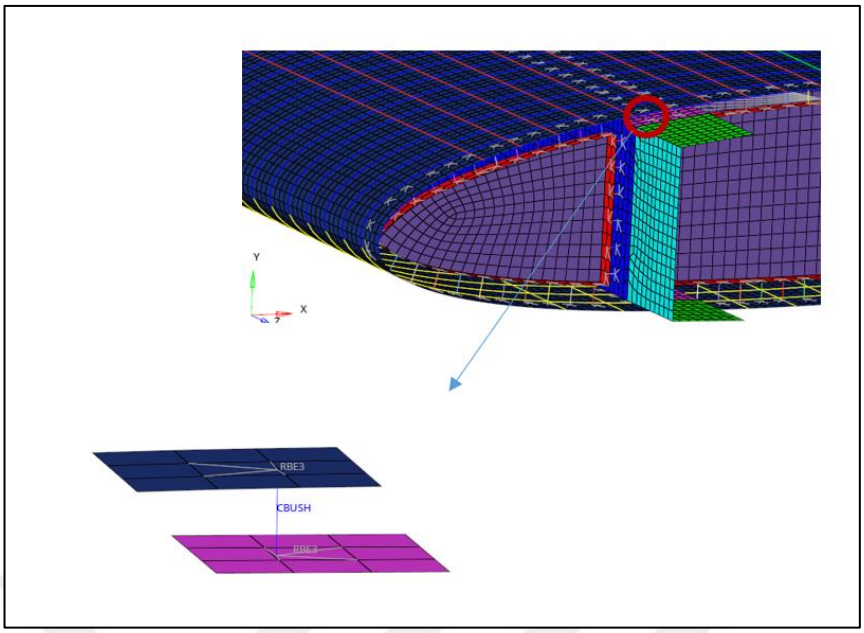

Figure 3.9 Fastener Modelling Example from Skin and Spar Connection

Huth formulation was used to calculate stiffeners of fasteners. With this formulation, a model close to reality is created. Between the 2D fastener modelling and the model tested in real life, there is a 5-10 percent deviation margin between the forces carried by the fasteners [38]. While calculating the stiffness of the fastener with the Huth formulation, the Equation 3.1 formulation is used.

$$C_i = \left(\frac{t_1+t_2}{2d}\right)^a . \frac{b}{n}\left(\frac{1}{t_1E_1} + \frac{1}{nt_2E_2} + \frac{1}{2t_1E_f} + \frac{1}{2nt_2E_f}\right) \tag{3.1}$$

where t plate thickness, E is the plate elastic modulus, d is the fastener diameter, n is the fastener row number, a is the constant for metal structures 0.667, E_f is the fastener elastic modulus.

To calculate the stiffness of the fastener, the thickness and material of the two plates to which the fastener is attached, the Young's modulus, the diameter and material of the fastener must be known. In addition, the stiffness that the fastener shows between different materials is also different. For this reason, there are many factors that affect the stiffness of the rivet. Another important issue is the distance between the fasteners. The distance between the fasteners is 4-5 times diameter of the fastener to prevent the fasteners from being affected by each other and to prevent the plate from buckling

failure due to the distance between them [39]. The distance between 2 fasteners on the spar is shown as an example in Figure 3.10. During the study, 4.8 mm rivets were used as fastener diameter and the distance between each other was taken as 4.5 D.

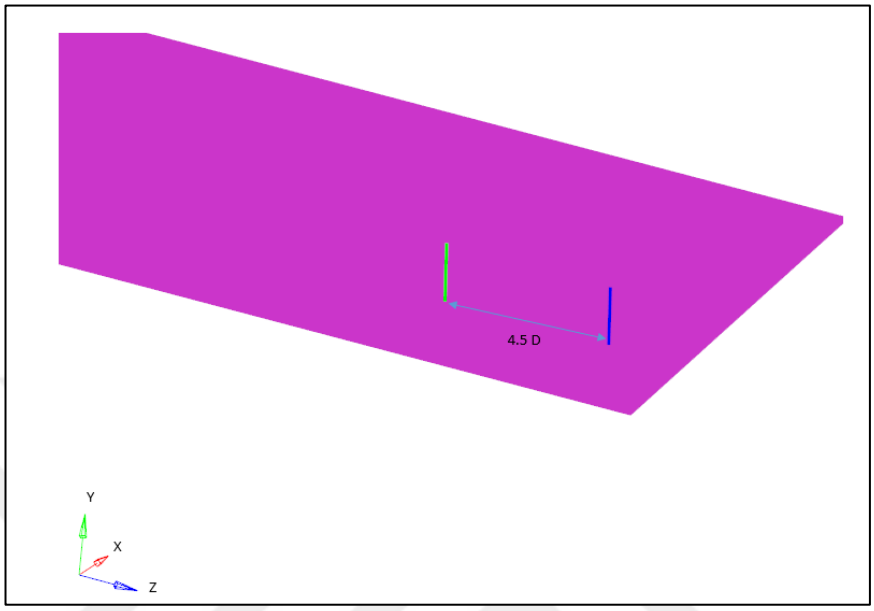

Figure 3.10 Fastener to Fastener Distance Example from Main Spar

After the modelling of the structures has been determined, there are two points required to run the model. The first of these is the boundary conditions of the structure. While determining the boundary conditions of the wing structure, its connections with the body were closed in translation. The tip of the strut and the junction of the spars with the body were determined as boundary condition points. The boundary conditions of the model are shown in Figure 3.11.

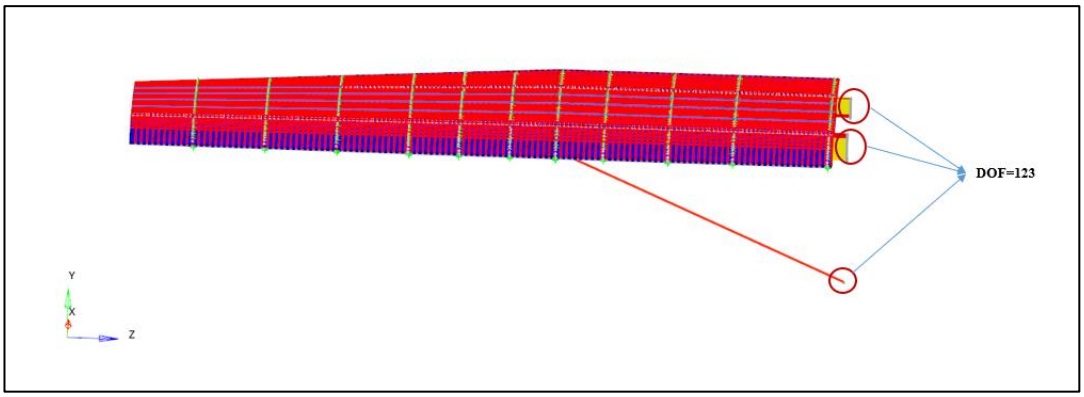

Figure 3.11 Cessna 172 Wing Model Boundary Condition

The second important point is the size of the loads and the location they are applied. While applying the loads, rbe3 elements were used, and the aerodynamic load was applied to 7 different stations. The point of application of stations is 25% from the leading edge on the chord. Along the chordwise, the application points and the magnitude of the loads are shown in Figure 3.12 and their values are given in Table 3.1. In Figure 3.13, the load elements used to model the fuel tank in the wing structure are shown. Cessna 172 carries approximately 45.5 kg of fuel on each wing [16].

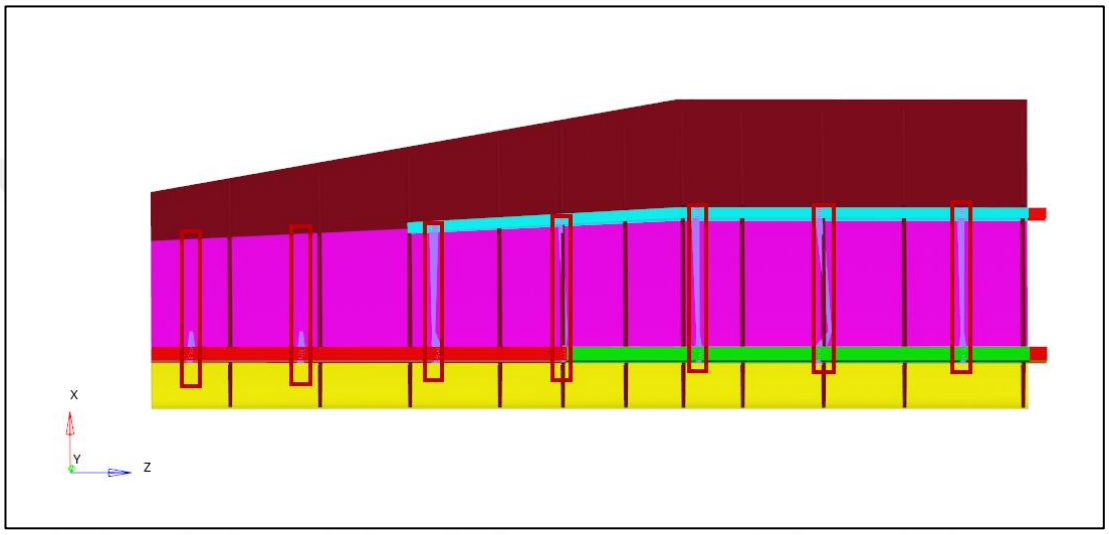

Figure 3.12 Wing Model Aerodynamic Forces Distribution Location

Table 3.1 Aerodynamic Forces Values on Chordwise

Station	Lifting Force (N)	Drag Force (N)	Pitching Moment (N.mm)	Spanwise Location (mm)
1	3943.78	59.64	-388000	367.5
2	3853.08	59.64	-388000	1225
3	3664.86	59.64	-388000	1960
4	3362.56	59.64	-388000	2695
5	2909.98	59.64	-388000	3430
6	2211.32	59.64	-388000	4165
7	786.78	59.64	-388000	4777.5

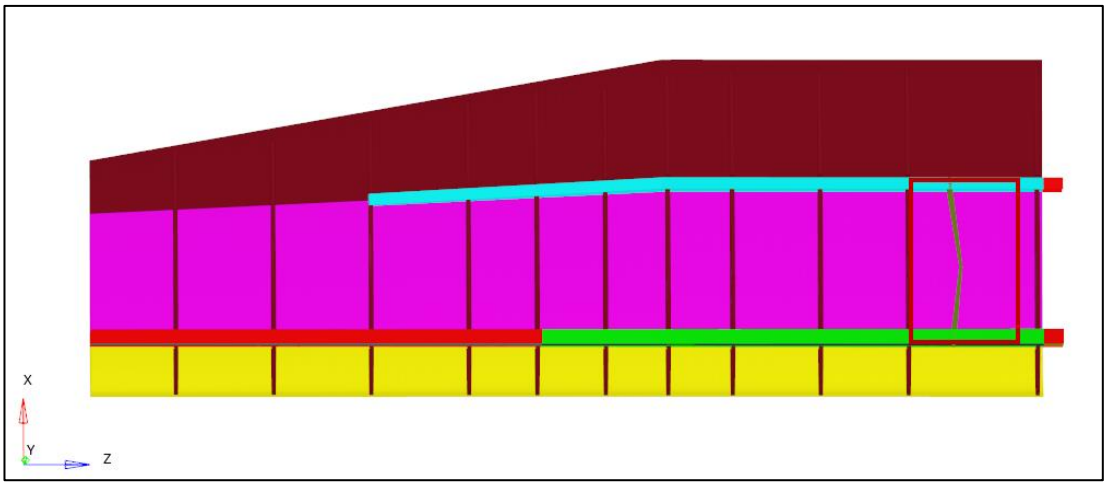

Figure 3.13 Wing Model Fuel Tank Location

The locations and magnitudes of the forces applied on the model are shown. In the model, thickness, one of the most important parameters affecting the load paths and the stiffness of the structure, are shown for each structure. The thickness distribution of the main spar and the dimensions of the structure are in Figures 3.14 and 3.15, respectively.

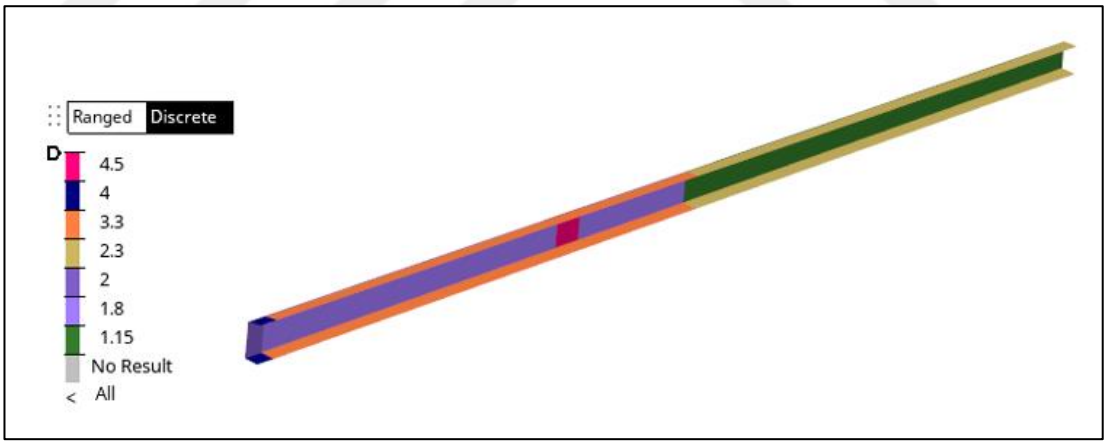

Figure 3.14 Main Spar Thickness Map

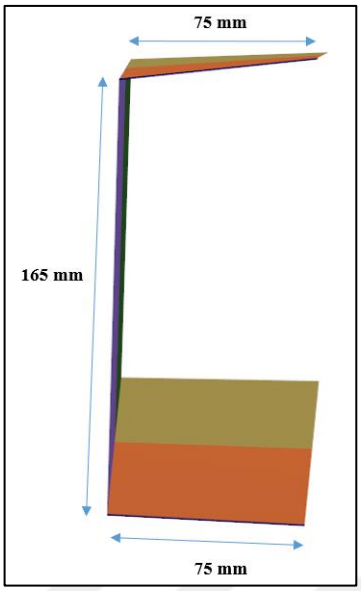

Figure 3.15 Main Spar Width and Height Measurements

The thickness distribution and dimensions of the secondary spar are shown in Figures 3.16 and 3.17. There is a thickness thinning from the root of the wing to the tip in both spars. This is because the moment at the root gradually decreases towards the tip of the wing.

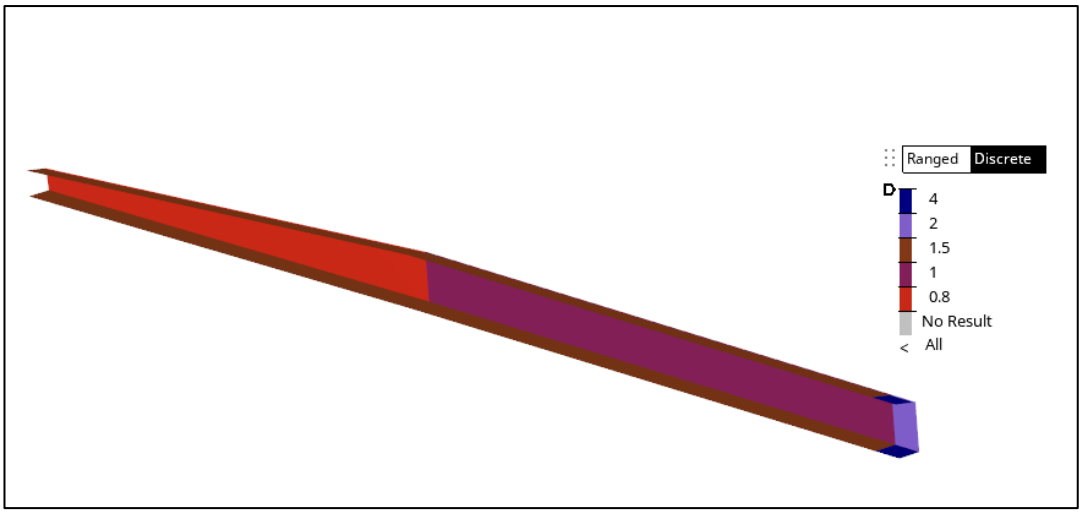

Figure 3.16 Secondary Spar Thickness Map

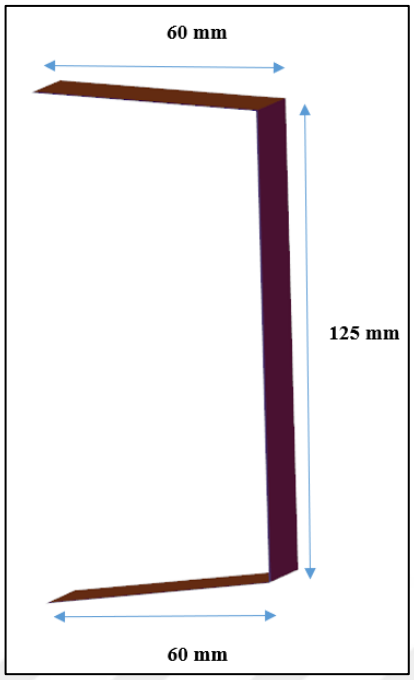

Figure 3.17 Secondary Spar Width and Height Measurements

The cap and web thickness of the ribs are the same everywhere and are shown in Figure 3.18 The dimensions of the ribs vary along the chordwise as they depend on the shape of the skin. For this reason, only the thickness map is given. The skin thickness is the same in all locations and is 0.508 mm. The thickness distribution of the skin panels can be found in Figure 3.19.

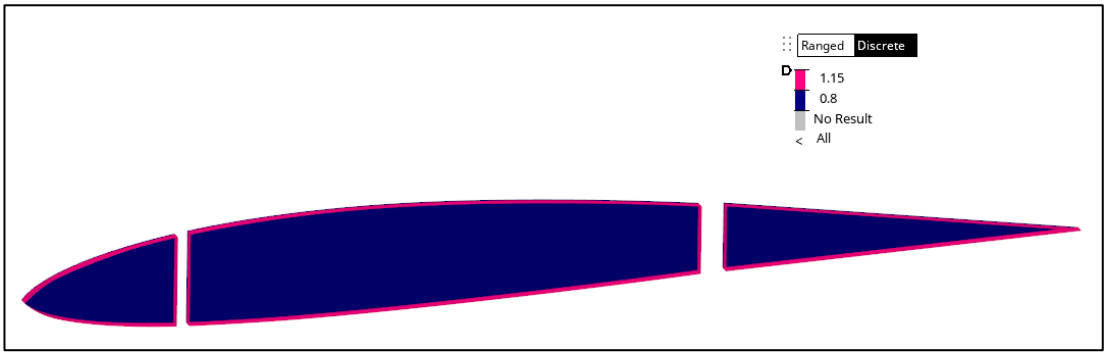

Figure 3.18 Wing Model Ribs Thicknesses

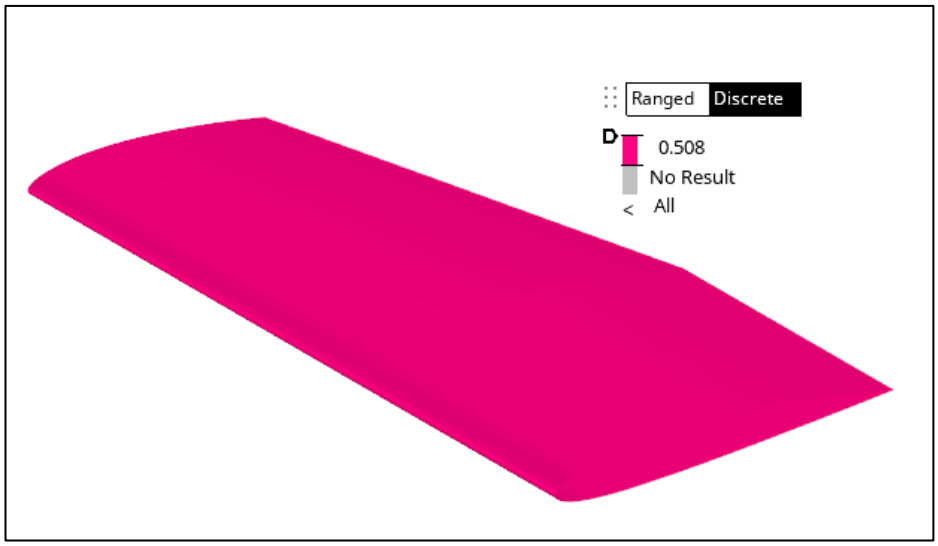

Figure 3.19 Wing Model Skin Panel Thickness

The strut structure that allows the wing to receive support from the fuselage and the stringers used to support the skin panel are modelled as 1 dimension. The 3-dimension view of the strut and stringers is given in Figures 3.20 and 3.21. The length of the strut is 2170 mm. Stringers are placed at different points along the chordwise. Stringer structures with different lengths are equal in thickness and width.

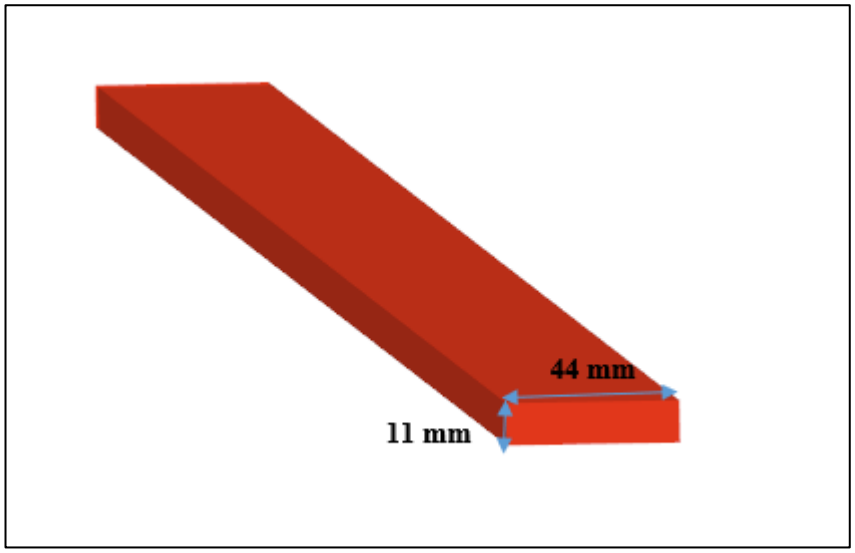

Figure 3.20 Wing Model Strut Dimensions

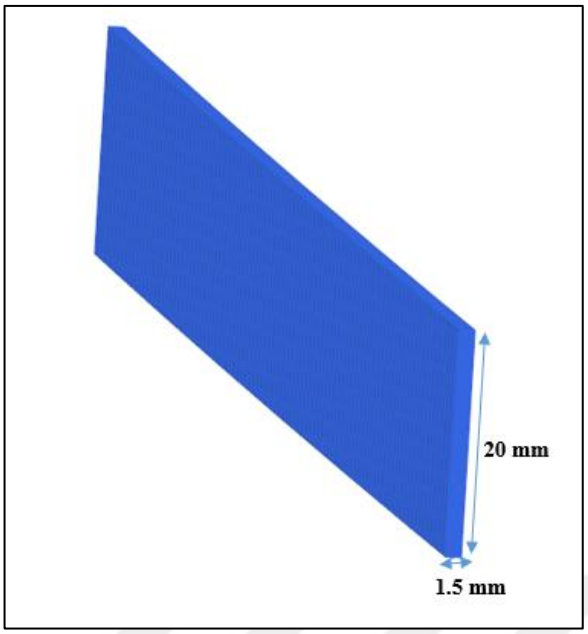

Figure 3.21 Wing Model Stringers Width and Heights

After giving information about the dimensions of all the structures used in the model and how they are modelled, it is necessary to make sure that the model is correct. The created model was tried to be modelled very similar to the wing interior structure of Cessna172R, and a safe structure was tried to be obtained before the optimization stage by creating a mass close to real-life value.

3.3 Finite Element Model Validation

There are some methods to verify the final element model created before the post-process stage. The most known of these methods are static and free to free modal check. The main purpose of these checks is to understand the accuracy of the load flow in the final element model and to determine whether there is an unstable element in the structure.

3.3.1 Analytical Calculation Check

To see that the model gives realistic results, some analytical verifications have been tried to be made through static and modal analysis. Firstly, displacement for static analysis and then first bending mode, which is the first mode for modal analysis, are examined. While performing the analyses, the strut structure was removed. Since the

strut will add an extra boundary condition, the calculation is made on the main structure. In this structure, there are spar, skin, rib and fasteners, which are the main structures. As the boundary condition, it is determined as the tip of the spars. The main model used in the two validations is shown in Figure 3.22.

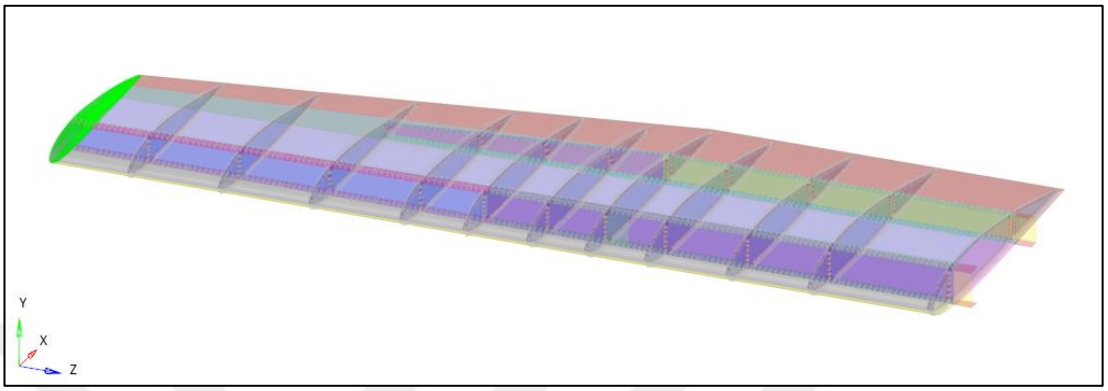

Figure 3.22 Finite Element Model General View

In the model used for static verification, a load of 1000 N is applied from the type of blade. Equation 3.2 was used to calculate the cantilever beam deflection analytically. The loaded version of the model is in Figure 3.23.

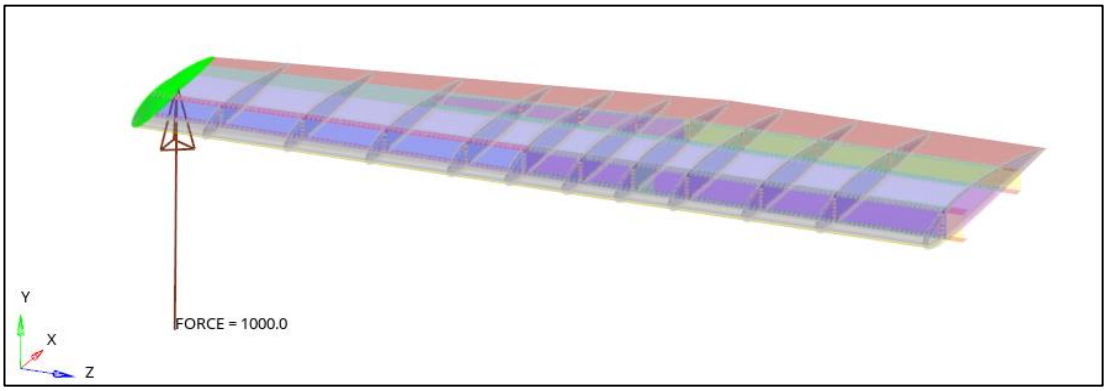

Figure 3.23 Finite Element Model Applied Load Location

$$\delta_{max} = \frac{PL^3}{3EI} \tag{3.2}$$

where δ_{max} is the maximum deflection tip of the beam, P is the load, L is the length of the beam, E is the Young's modulus, I is the area moment of inertia.

For the modal analysis, the structure was again accepted as a cantilever beam. The model is as in Figure 3.22. There is no applied load in the model. It is fixed only from the ends of the spars. To find the first natural frequency, the formulation is as in Equation 3.3.

$$f = \frac{K}{2L^2\pi}\sqrt{EI/m} \tag{3.3}$$

where f is the frequency of vibration, $K = 3.52$ for first bending mode, m is the mass/unit length.

The information required for modal and static calculations is given in Table 3.2.

Table 3.2 Model Input Data for Analytical Calculations

Data	Value	Unit
Beam Length	4900	mm
Second Moment of Inertia	9028727	mm^4
Young Modulus	73000	MPa
Structure Mass	39.5	kg

The displacement and natural frequency comparisons of the static and modal solutions of the model are given in Table 3.3.

Table 3.3 Finite Element Model and Analytical Results

Model	Data	FEM	Analytical	Unit	Error Rate (%)
Static	Displacement	55.48	59.51	mm	**7.24**
Modal	Frequency	7.62	6.67	Hz	**12.48**

The reason for the difference here is that the wing structure is structurally like the cantilever beam but does not have the same properties. The main purpose here is to show that the results obtained from the finite element are not far from analytical results.

3.3.2 Static Analysis Check

A static check was made before applying the structurally real loads of the wing model to the structure. During this control process, a gravitational force of 1 g was applied to the structure in X, Y and Z. There are 2 parameters to understand whether the structure is statically stable. The first of these is that the same amount of force must be read from the points determined as the boundary condition of a force applied to a structure in static equilibrium position. Figure 3.24 shows the model created for static analysis check. The values read from the constraint points of this structure are shown in Table 3.4. The boundary conditions in the structure are the same as in the main model.

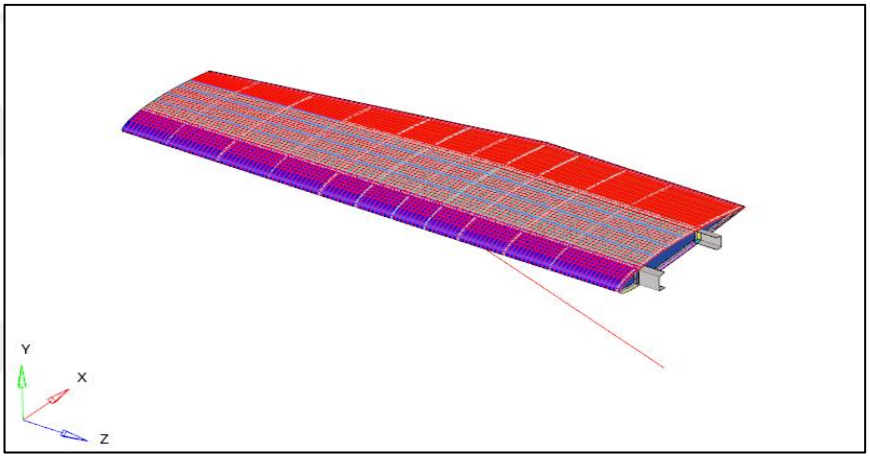

Figure 3.24 Wing Static Check Model

Table 3.4 Model Force Moment Equilibrium

Label	X-Force	Y-Force	Z-Force	X-Moment	Y-Moment	Z-Moment
Applied Load	0.0E+00	5.5E+02	0.0E+00	1.1E+06	0.0E+00	3.7E+05
Sum at Constraint	-2.8E-07	-5.5E+02	5.1E-07	-1.1E+06	2.7E-04	-3.7E+05

As can be seen in Table 3.4, all loads applied on the 6 degree of freedom have counterforces at the constraint points. Some of the dummy forces found at the constraint points are errors from mathematical calculations within the model. In addition, the second control is knowing the epsilon value. Epsilon value shows the margin of error within the model. As a result of the modelling, this value being between

$10e^{-6}$ and $10e^{-9}$ indicates that the model is statically balanced. Table 3.5 shows the epsilon value of the model.

Table 3.5 Epsilon Value Check at Static Check Model

Subcase	Epsilon at Model
Gravitational Forces	1.83E-09

3.3.3 Free to Free Modal Analysis Check

After it was understood that the loads were in balance in static check, free to free check was performed to control modelling errors and non-connected elements in the model. What is desired to be seen on the model with this check is that the first 6 natural frequency modes should be very close to 0. The mode after that must be greater than 0. Figure 3.25 shows the finite element model created for modal check. The element and property structure in the model are the same. There are two differences between static and free to free modal check. First, there is no boundary condition in the model because it is free to free. At the same time, there is no force applied on the model. As a result of this modelling, the first 6 natural frequency modes of the structure should come very close to 0 for modal analysis. Zero natural frequency means that the structure can have rigid movement without any excitation. This is expected as there is no boundary condition. The 8 natural frequency values obtained from the modal analysis are shown in Table 3.6.

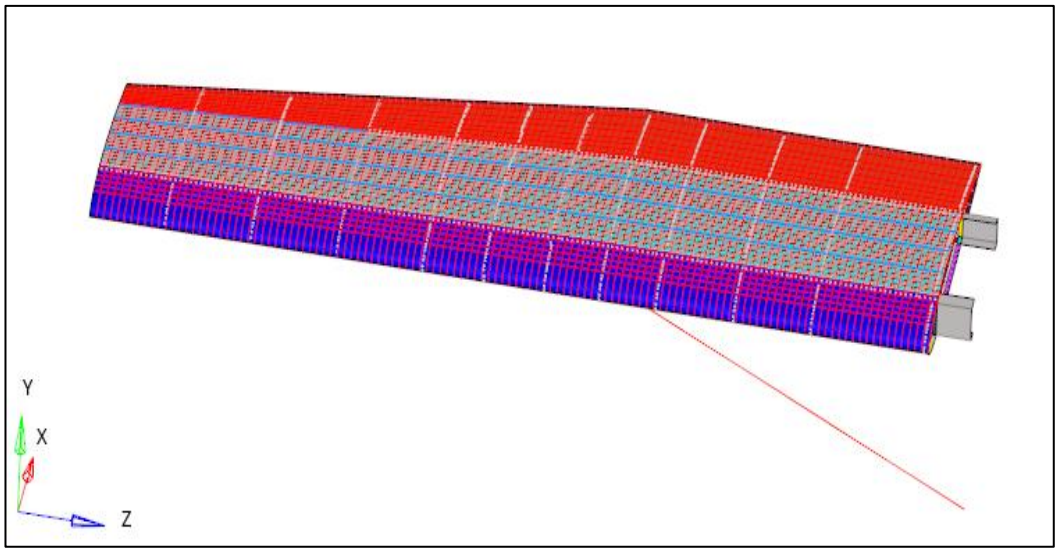

Figure 3.25 Wing Free to Free Modal Analysis Check Model

Table 3.6 Free to Free Modal Analysis Frequency Modes Results

Mode	Frequency
1	**8.82E-04**
2	**9.55E-04**
3	**1.05E-03**
4	**1.37E-03**
5	**1.50E-03**
6	**1.53E-03**
7	1.28E+00
8	4.31E+00

3.4 Finite Element Model Results

The wing model created was tried to be established very close to the real model of Cessna 172. For the critical loading situation, the highest drag force, lift force and pitching moment were taken and combined. The Aluminium 2024 series is used as the material for the entire structure. The values required for the analysis of the material were taken from the MMPDS published by the Federal Aviation Administration. After proving that the model works correctly in the previous stage, some data should be checked to show the static strength of the structure. Within the scope of this study, the most important points for the structural were tried to be checked. During these checks, the stress, displacement, and buckling results of the structure were checked. In

addition, the strength of the fasteners that provide load transfer in the structure were also checked.

3.4.1 Displacement Results

Although the displacement restriction for the wing is not known exactly, a displacement of 5 percent of half the wing length will be allowed at the wing tip point [43]. But since Cessna 172 has strut help, the length from strut to wing type is taken. The length from the attachment point of the strut to the wing type is approximately 3000 mm. In other words, the required maximum displacement value is around 150 mm for the wing component. The maximum displacement of the wing structure should not exceed this value. The displacement value for the loading condition of the wing structure is shown in Figure 3.26.

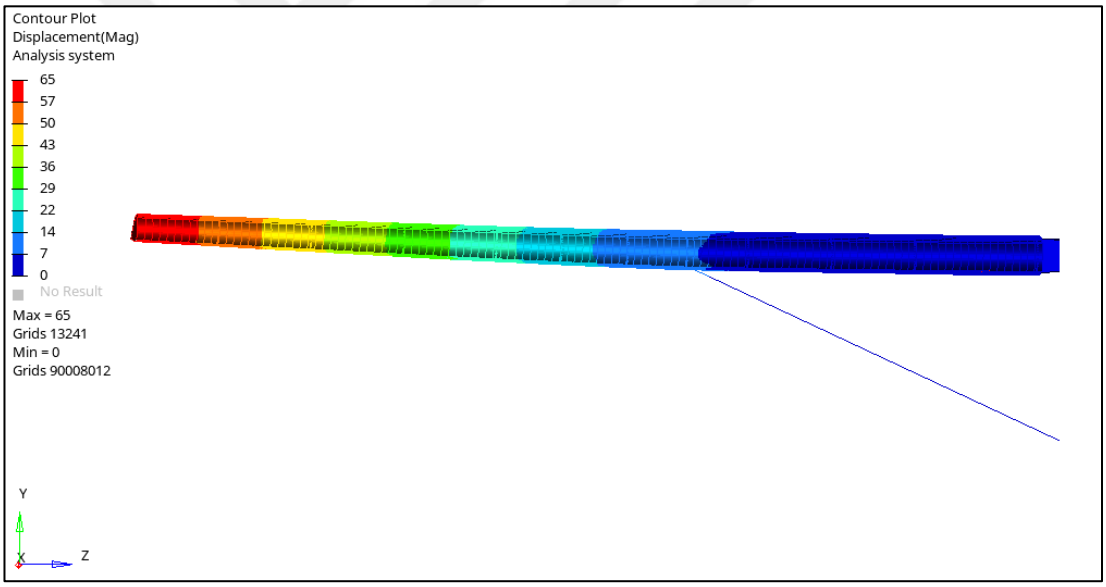

Figure 3.26 Wing Model Displacement Results

The maximum displacement of the wing model is well below the specified value. The building is in the safe zone in terms of displacement.

3.4.2 Stress Results

Another important constraint for the structure after the displacement evaluation is stress. The stress restriction varies according to the yield and ultimate strength of the

material. According to Code of Federal Regulations Part 23, the structure must not suffer any damage at the limit load. Ultimate loading is 1.5 times the limit loading. The structure may be damaged but must not fail. It is not necessary to evaluate within two criteria. The reason for this is that the ultimate value of the material of the Aluminum 2024 series is less than 1.5 times the limit value. When the calculation is made according to the ultimate value, the safety factor will be obtained above 1 for the limit value. Therefore, the stress value was considered as ultimate. The ultimate value of Aluminum 2024 is 428 MPa [40]. According to this material value, spars, ribs, skin, strut and stringers stress results are shown and safety factors are calculated. The Von-Mises stress distribution for each structural part is shown in the figures below. Values multiplied by 1.5 and are at ultimate loading.

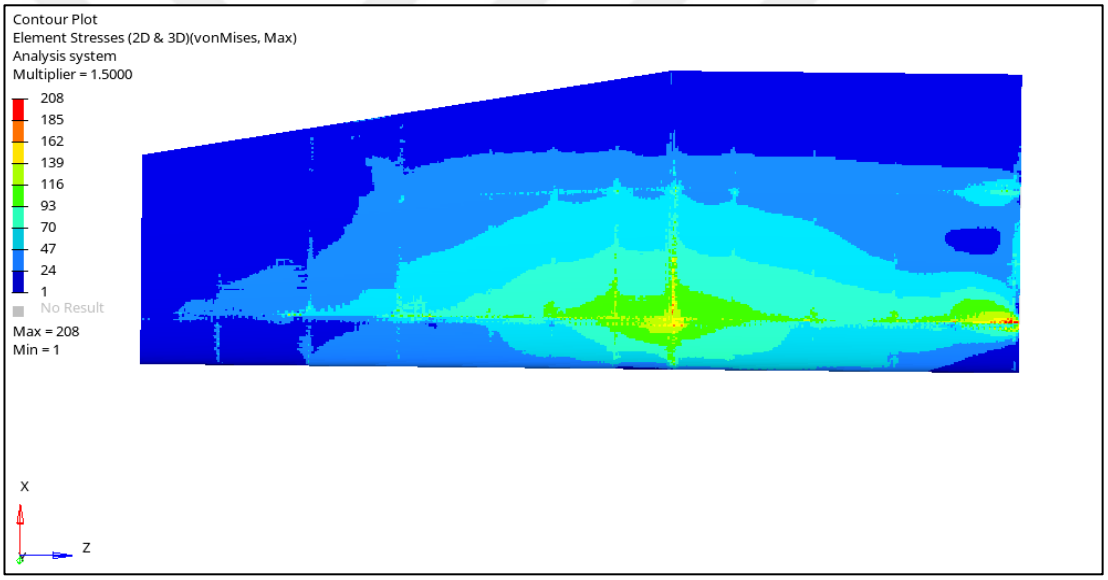

Figure 3.27 Upper Skin Stress Results

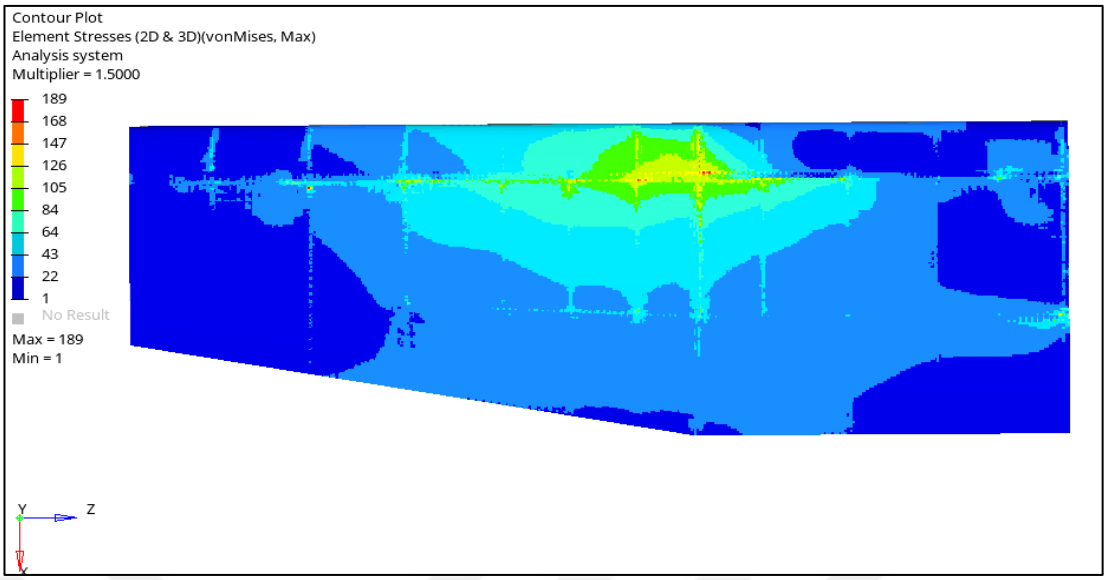

Figure 3.28 Lower Skin Stress Results

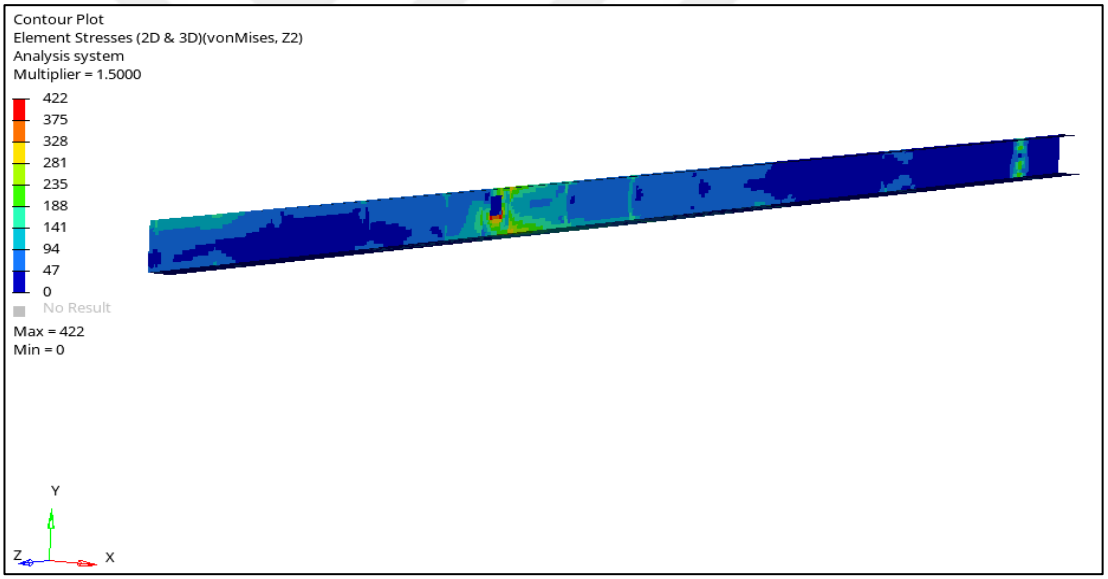

Figure 3.29 Main Spar Stress Results

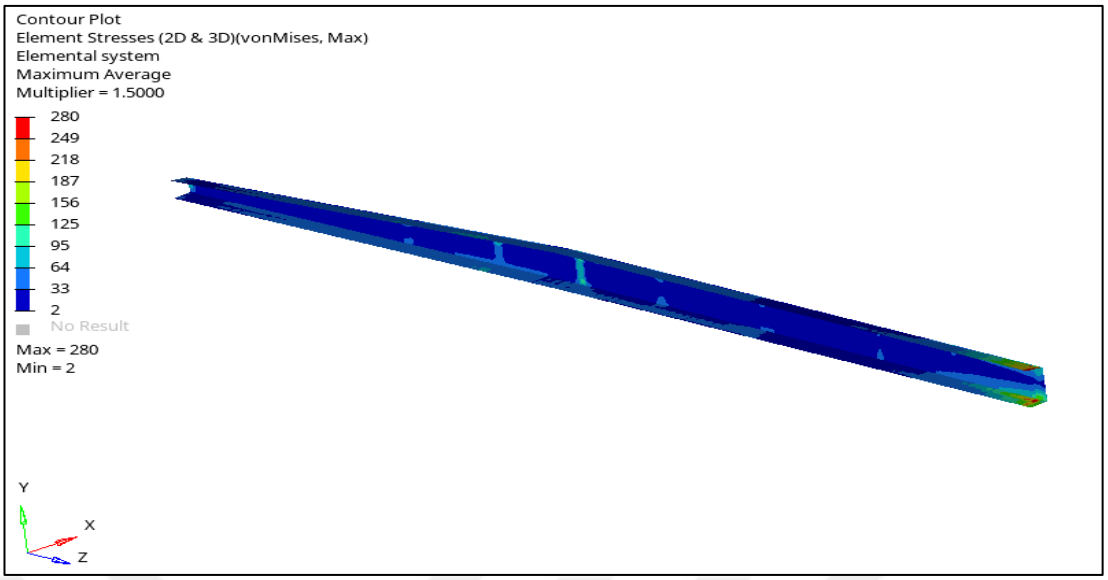

Figure 3.30 Secondary Spar Stress Results

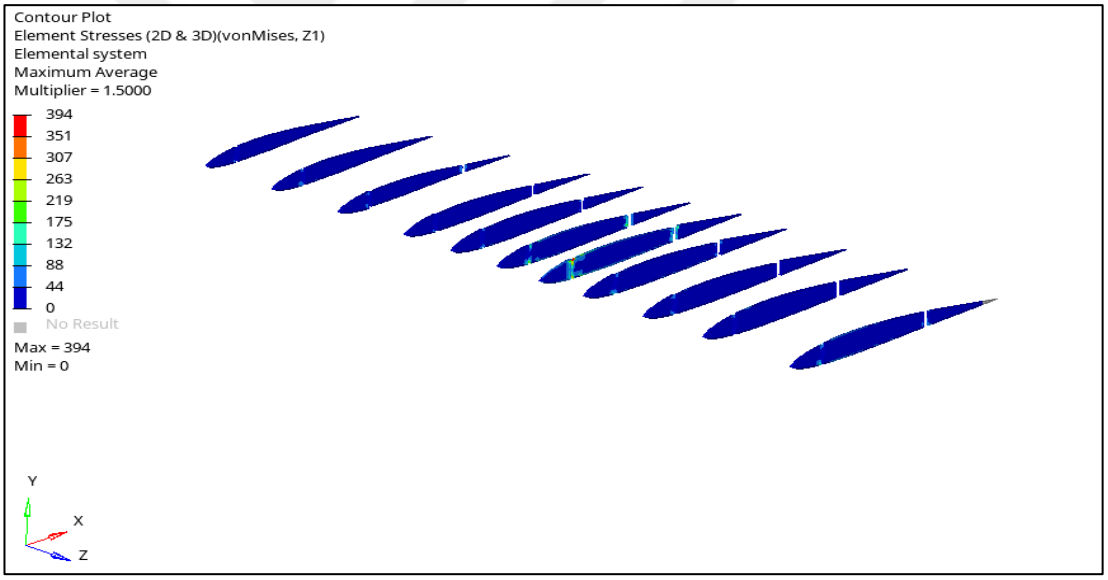

Figure 3.31 Ribs Stress Results

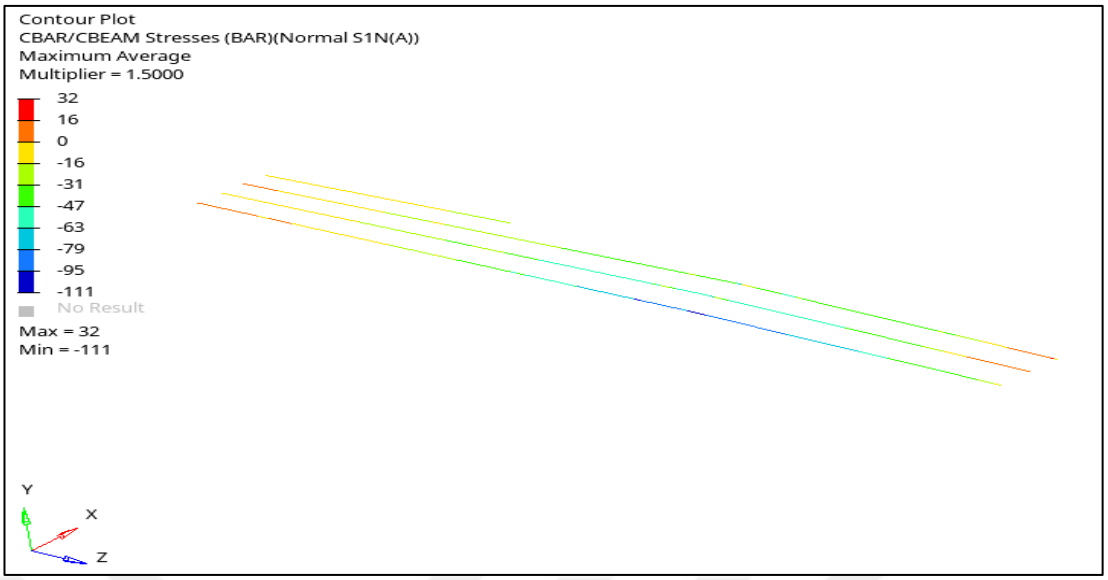

Figure 3.32 Stringers Stress Results

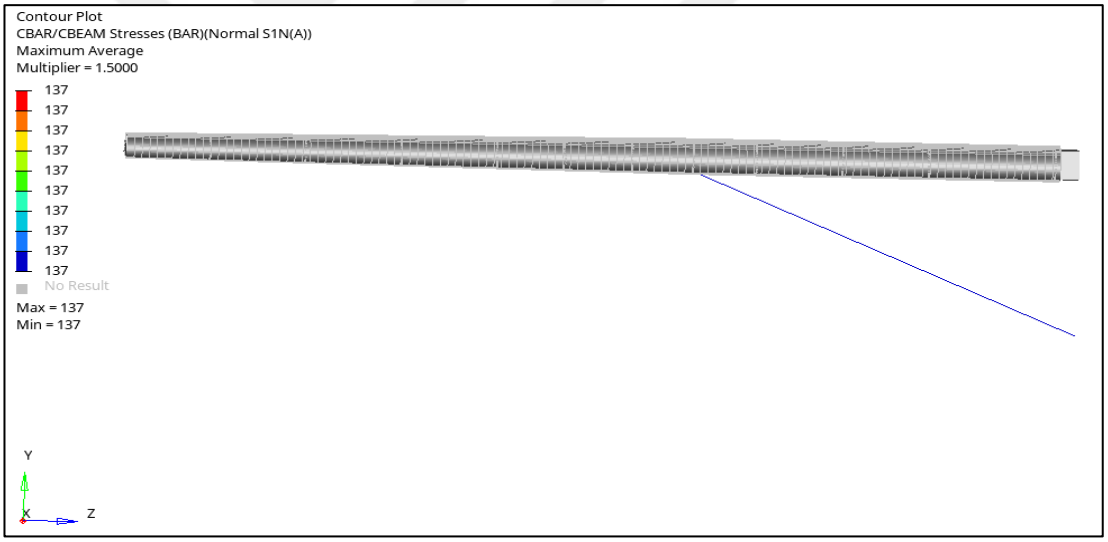

Figure 3.33 Strut Stress Results

After showing the stress data, reserve factor values are shown in Table 3.7 The reserve factor for stress of each structure is above 1 in the ultimate case.

Table 3.7 Wing Model Maximum Stress Results and Minimum Reserve Factors

Structure	Maximum Stress (MPa)	Min Reserve Factor
Upper Skin	208	2.06
Lower Skin	189	2.26
Main Spar	422	1.02
Secondary Spar	280	1.53
Ribs	394	1.09
Stringer	111	3.86
Strut	137	3.12

3.4.3 Buckling Results

There are two main causes of sudden damage to a mechanical structure: material damage and structural instability, commonly referred to as buckling. If the ratio of the cross-section to the length of a thin column, which is forced from its axis, is small, buckling may occur in this column [33,34]. The load at which buckling occurs depends on the stiffness of the structure, not its strength. This is a stability problem. The calculated stress in the part does not necessarily exceed or approach the stress limits for buckling to occur. For this reason, buckling may occur far below the safe strength values.

The buckling reserve factor values of the model must be greater than 1 under limit loading. A total of 10 buckling modes were requested during modelling. The most critical area in terms of buckling in the structure is the skin panels shown in Figure 3.34. This is because it has both a thin structure and large surface areas. The location is shown for the most critical buckling safety factor value, and the critical areas obtained in other modes are on the skin panel and close to each other. The reason for this is that a hard point has occurred in the structure because it is the region where the strut is attached. The values reached from the first 10 modes are shown in Table 3.8 and lowest safety factor value is 1.05.

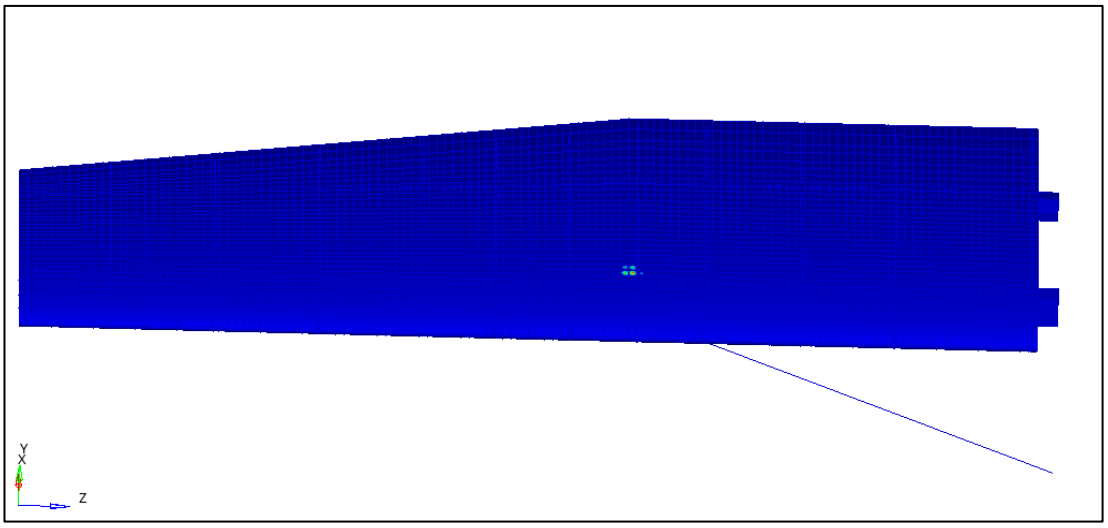

Figure 3.34 First Buckling Mode of Wing Structure

Table 3.8 Wing Model First 10 Buckling Modes Reserve Factor

Buckling Mode	Reserve Factor
1	**1.05**
2	1.08
3	1.09
4	1.11
5	1.12
6	1.14
7	1.18
8	1.21
9	1.21
10	1.21

With the data obtained from the buckling analysis, it has been shown that the strength of the structure in terms of buckling failure is in the safe zone. When considered as the main structural parts, the safety factor of the model is above 1 in stress and buckling. At this point, another point to be considered is the factor of safety of fasteners.

3.4.4 Fastener Force Results

The main components that provide load transfer in the structure are fasteners. Although it has little effect on the structure in terms of size and weight, it provides load transfer between structures. While showing the strength of the structure, it is

necessary to show that the fasteners in the structure are in the safe zone. The fasteners used in the wing model are in two different diameters. Since spars are the main load-carrying structures, 4.8 mm diameter rivets are used, while 3.2 mm diameter rivets are used for ribs. PER IFI-126 GRADE 26 was chosen as the fasteners sealed blind rivet [32]. While looking at the loads of fasteners, they were examined as main, secondary spar and ribs. At this point, it is sufficient to calculate the reserve factor of the fastener that draws the highest load for each structure. When looking at the strength of the fastener, it is necessary to look at both shear and tensile strength. The strength of the selected fastener is given in Table 3.9.

Table 3.9 Fastener Ultimate Shear and Tensile Allowable

Fastener Diameter (mm)	Ultimate Shear Allowable (N)	Ultimate Tensile Ultimate (N)
3.2	1070	1250
4.8	2220	3070

The main spar, secondary spar and rib regions were examined to look at the fastener strengths. For these locations, the fastener with the most critical shear load and tensile load was examined. In this way, minimum fastener safety factor has been obtained for these regions. The fastener with the highest shear load for the main spar is shown in Figure 3.35, and the location of the fastener with the highest tensile force is shown in Figure 3.36.

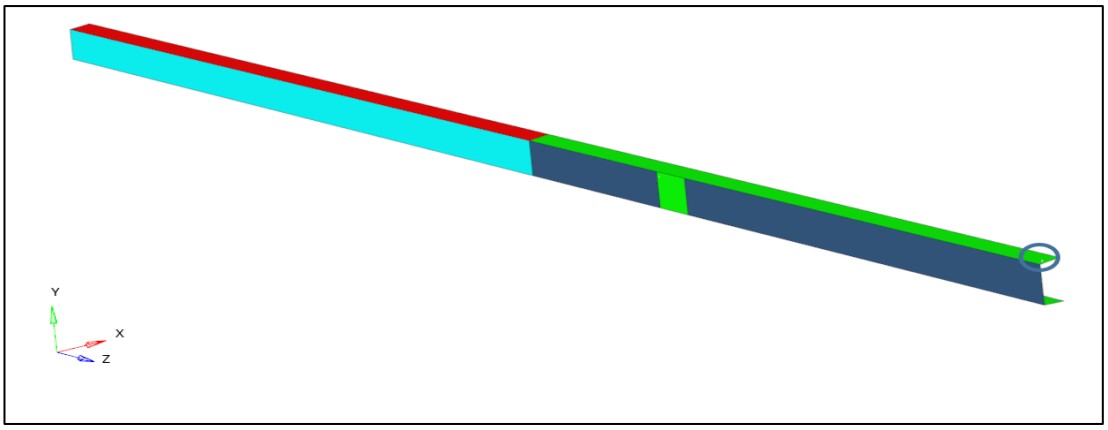

Figure 3.35 Most Critical Fastener Shear Force Location on Main Spar

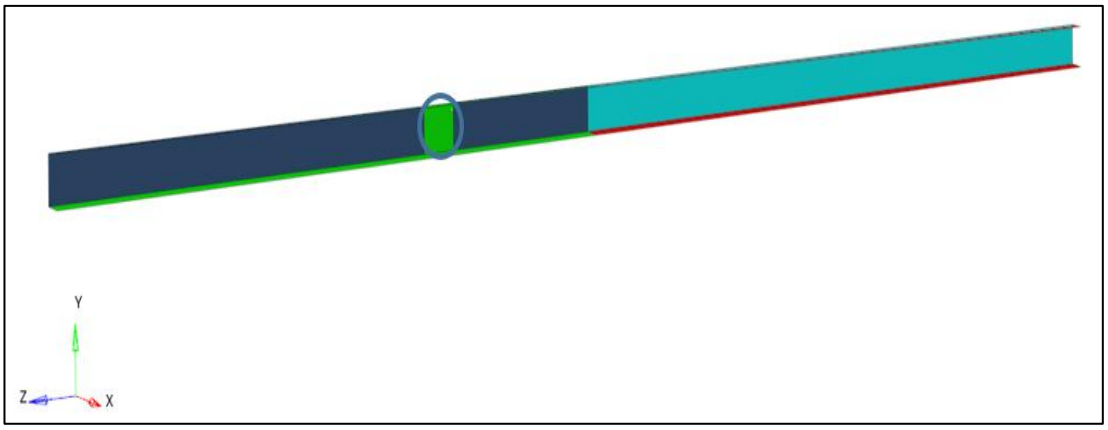

Figure 3.36 Most Critical Tensile Force Location on Main Spar

The fastener with the highest shear load for the secondary spar is shown in Figure 3.37, and the location of the fastener with the highest tensile force is shown in Figure 3.38.

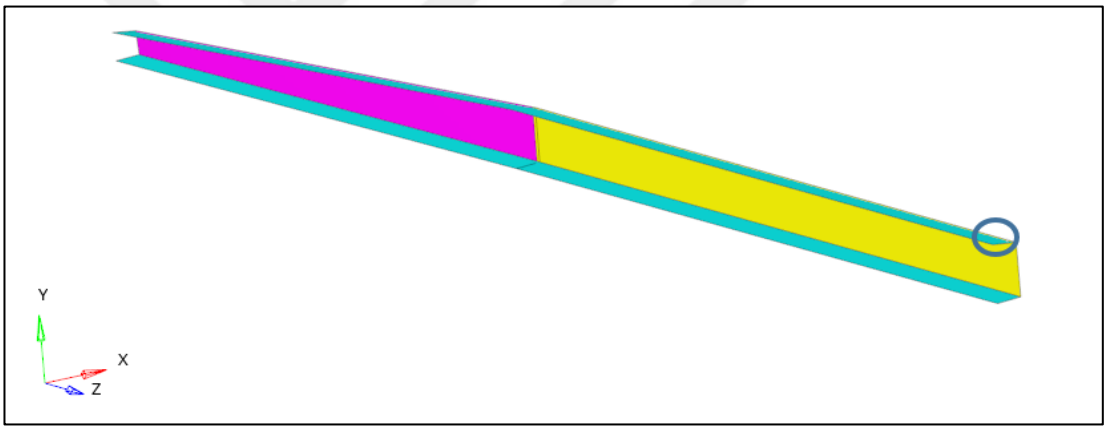

Figure 3.37 Most Critical Fastener Shear Force Location on Secondary Spar

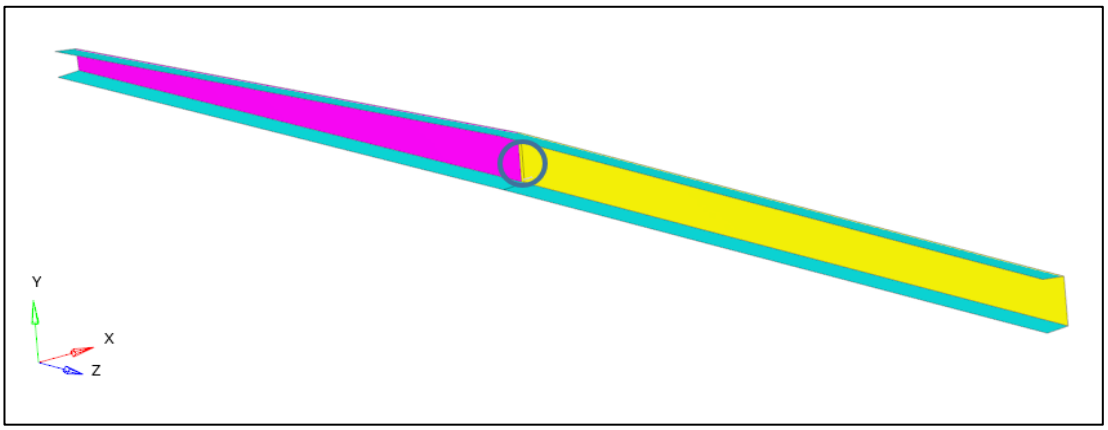

Figure 3.38 Most Critical Tensile Force Location on Secondary Spar

For spars, the highest shear force location is at the wing joint, while the highest tension comes from the fastener connection with the rib where the strut joint is. Ribs are shown in Figure 3.39 and 3.40 by selecting the rib with the most critical loads, which has not been examined individually. The fastener with the maximum shear and tensile load is on the same rib and is on the rib closest to the strut.

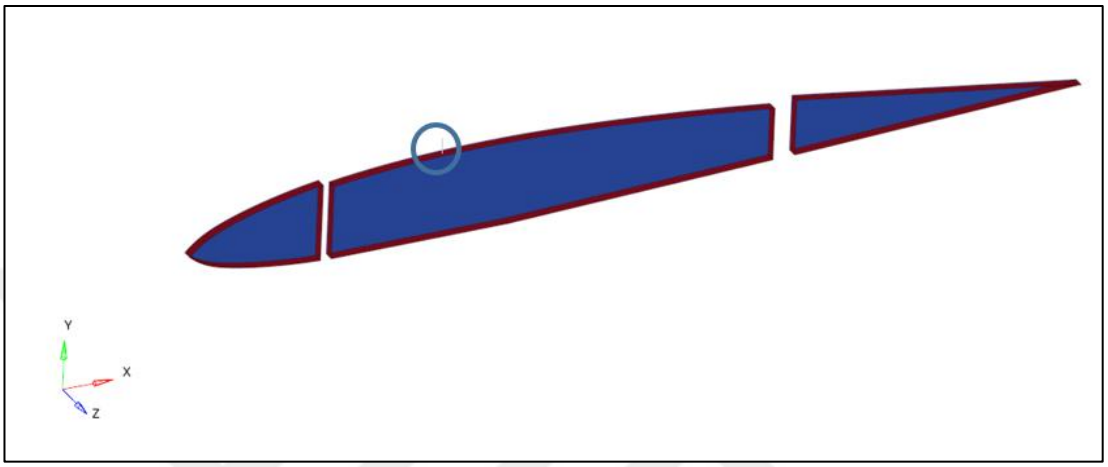

Figure 3.39 Most Critical Shear Force Location on Ribs

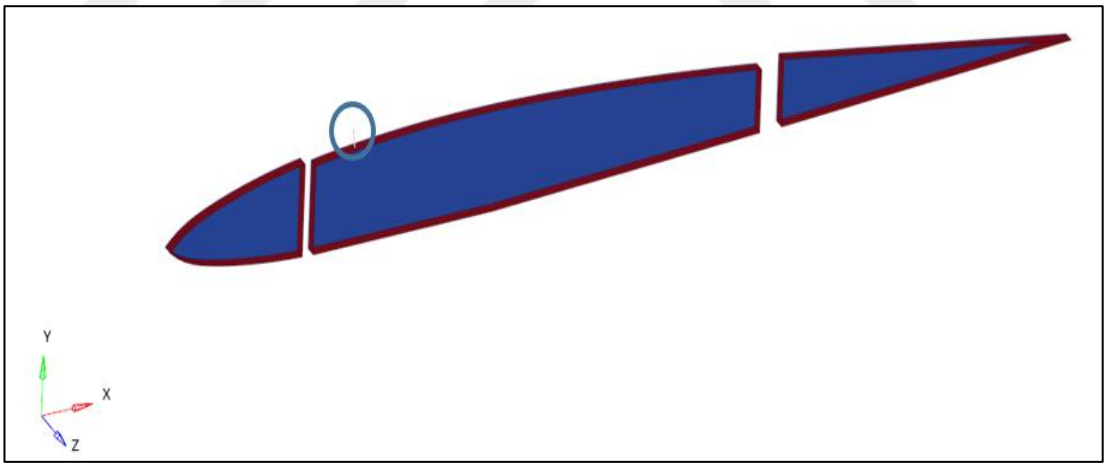

Figure 3.40 Most Critical Tensile Force Location on Ribs

After determining the critical locations of the fasteners, the minimum reserve factor values of the fasteners in these locations are shown in Table 3.10.

Table 3.10 Fastener Shear and Tensile Reserve Factor for Wing Structures

Location	Maximum Shear Force (N)	Maximum Tensile Force (N)	Minimum Shear RF	Minimum Tensile RF
Main Spar	1881.98	1078.34	1.18	2.85
Secondary Spar	1105.51	242.54	2.01	12.66
Ribs	246.65	459.32	4.34	2.72

3.4.5 Weight of Wing Structures

After the first verification of the model prepared for Cessna 172, its structural strength was checked, and it was proven to be in the safe zone. The necessary and important evaluation within the scope of this study for the finite element model prepared for Cessna 172 is the weight comparison. Actual weight data was calculated as 53.71 kg in chapter 2. The value obtained with the finite element model is 53.87 kg. The weight of the fasteners is also included in the model. Data is given in Table 3.11.

Table 3.11 Wing Component Structural Weight and Real Data Comparison

Structures	Weight (kg)	Error Rate (%)
Skins	30.60	
Spars	11.72	
Ribs	5.86	
Strut	2.91	
Stringers	1.3	
Fastener	1.48	
Wing FEM Total Weight	**53.87**	
Cessna 172 Real Wing Weight	**53.71**	**0.29**

When the weight data obtained were compared, a value very close to the real one was obtained. With this weight value, the structural safety of the building has also been calculated and shown. After this stage, topology optimization was used to make the structure lighter.

CHAPTER 4

TOPOLOGY OPTIMIZATION RESULTS

After the Cessna wing model has been verified very close to its actual weight, the internal structure will be lightened by topology optimization. At this stage, while reducing the weight, the design space areas should be determined first. Topology optimization is not possible in structures such as skin panels and stringers. In addition, since optimization cannot be made in fastener locations, ie flanges of ribs and spars, web locations in the internal structure remain. For this reason, there are 2 main groups as design space regions. First, the web regions of ribs are shown in Figure 4.1 below. The other is the part of the main spar web after the strut connection. The reason why the optimization cannot be applied to all web regions of the spars is that the structure is desired to be continuous in the fuel zone and the secondary spar is connected to the control surfaces. For this reason, the only region where topology optimization will be applied on spar is shown in Figure 4.2.

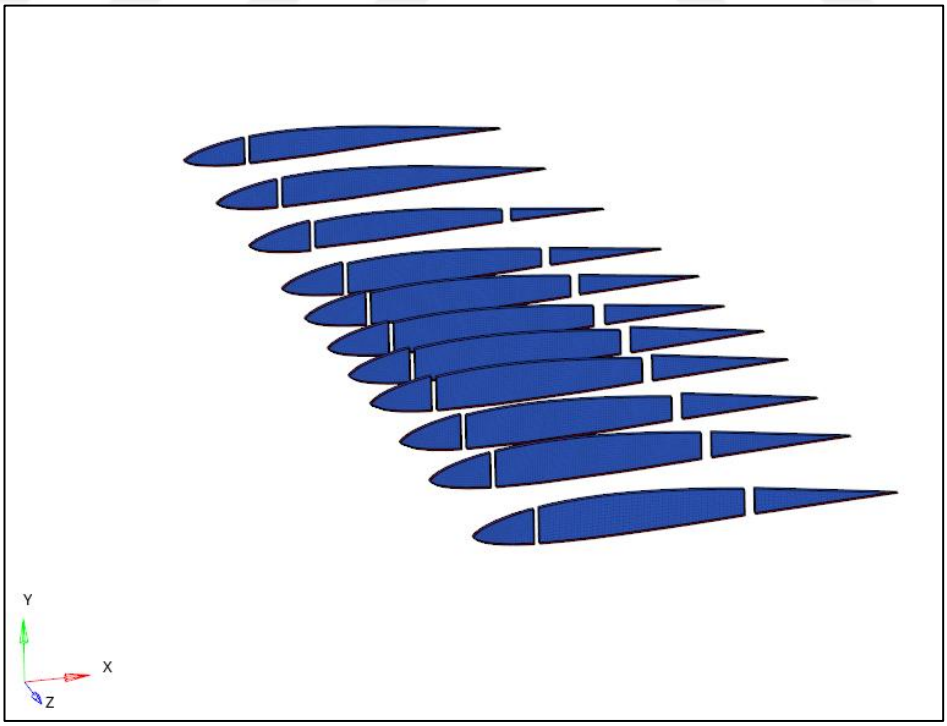

Figure 4.1 Rib Web Topology Optimization Design Spaces

In this topology optimization, which consists of two stages, topology optimization was applied in 2 different ways. While a 3-dimension structure was used for ribs, 2-dimension topology optimization was made for spar.

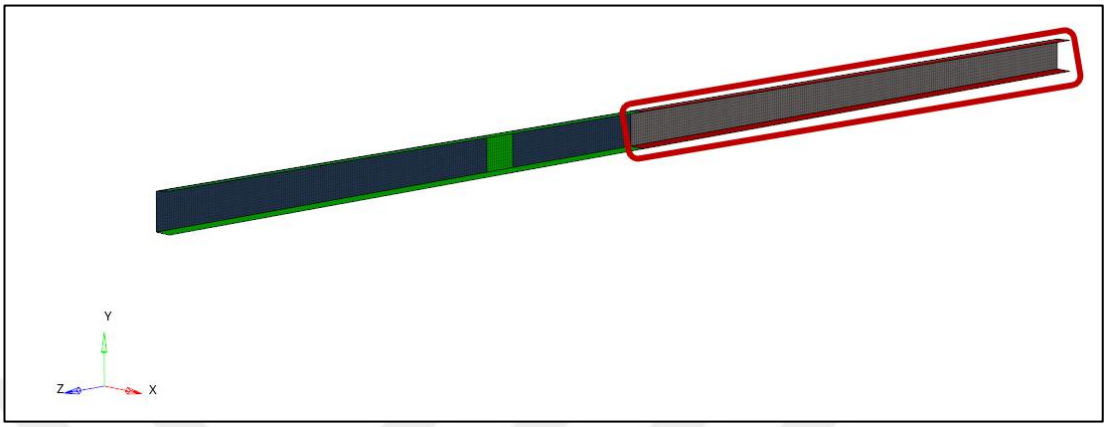

Figure 4.2 Main Spar Topology Optimization Design Space

4.1 Rib Topology Optimization

The design area determined for the topology optimization of the ribs is shown in Figure 4.1. Thereupon, topology optimization for ribs started. At this stage, topology optimization only gives an idea in terms of design. The main point here is the ease of production. For production, a single pattern has been tried to be obtained on the ribs and this pattern will be applied to the web region of all other ribs. To find a sample topology optimization pattern for the ribs, the rib with the most critical stress and fastener force in the main model was selected. This rib is the rib closest to the strut connection seen in Figure 4.3. To apply topology optimization to the 3D part, the rib selected as an example was removed from the model, and the model was created by connecting it with the help of a 3D modelled rib. The reason why a certain amount is kept away from the caps while optimizing the rib topology is because the cut-outs must be at a minimum h/6 distance from the caps [34].

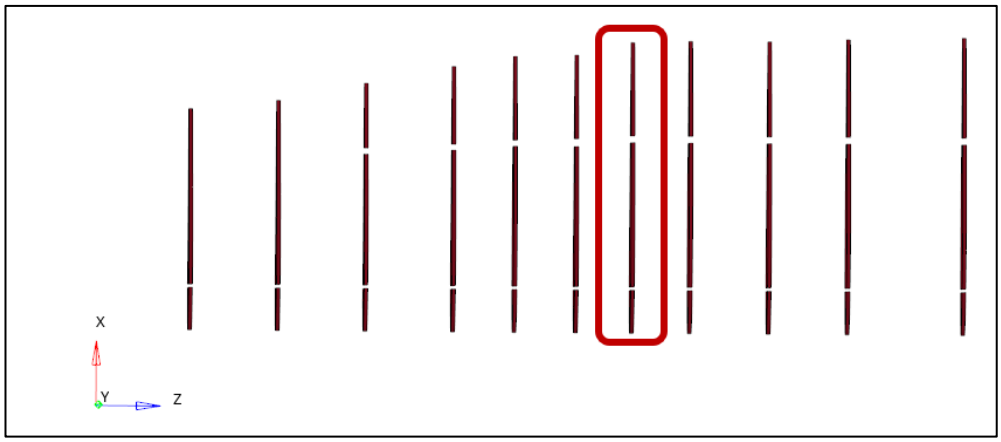

Figure 4.3 Main Rib for Topology Optimization Pattern

The green area of the designing space of the model is shown in Figure 4.4. Rib consists of 3 parts. No cut out is made on the part at the trailing edge. This is because the control surfaces are attached to these ribs. Since the area is small on the leading edge, a classic lighting hole is opened by applying a single pattern.

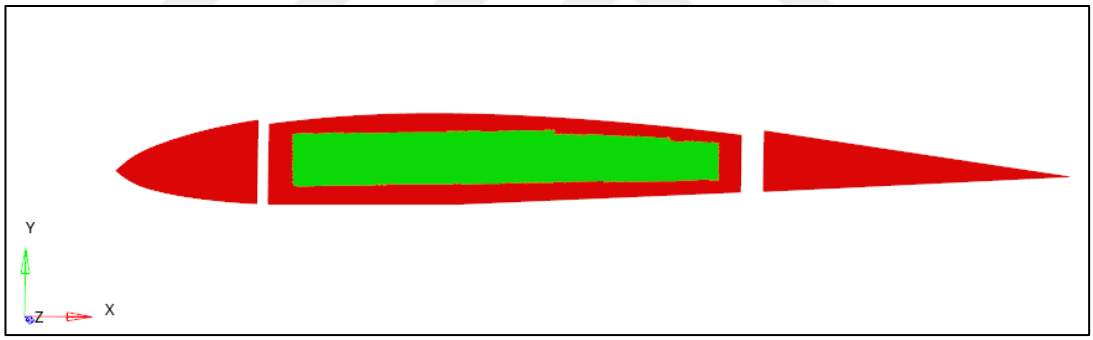

Figure 4.4 Solid Rib Optimization Design Space

The reason for 3D modelling is that the cutting direction can be determined for manufacturing during 3D topology optimization. The rib cutting method, which is essential for the pattern, is shown in Figure 4.5.

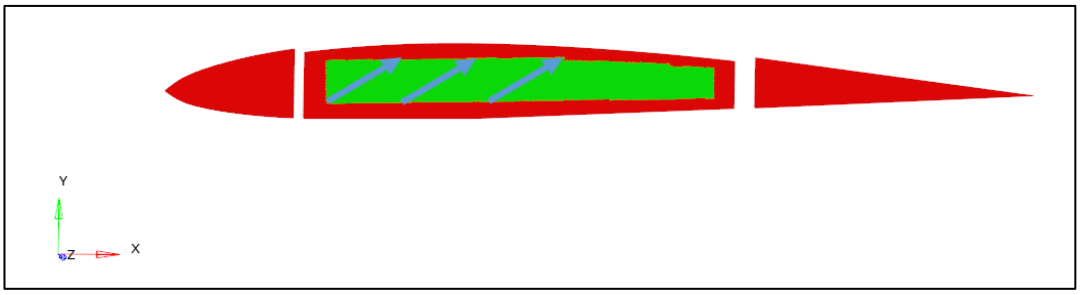

Figure 4.5 Solid Rib Manufacturing Cutting Direction

Some constraints need to be determined for the results of the model. Stress constraint has been applied to prevent the structure from failing in terms of static analysis. It has been determined as volume fraction constraint to set how much material will be removed from the design region. Objectively, it was desired that the structure should reach minimum compliance, that is, have maximum stiffness. The information of constraints is given in Table 4.1.

Table 4.1 Topology Optimization Constraint and Boundary Conditions

Constraint	Lower Bound	Upper Bound
Von-Misses Stress	150 MPa	200 MPa
Volume Fraction	0.1	0.5

The rib pattern reached by the structure after 35 iterations is shown in Figure 4.6. The structure here must be applied to the ribs in the 2D structure. The reason for applying this structure to a 2D structure is that it enables buckling and other analyses of the structure to be done faster and in a reasonable time [37].



Figure 4.6 Rib Topology Optimization Pattern

The application of the rib pattern obtained because of the topology optimization to all ribs is shown in Figure 4.7. The same or very similar pattern is used for all ribs. The cut out on the leading edge was applied in the same way for the whole structure with a 30 mm diameter.

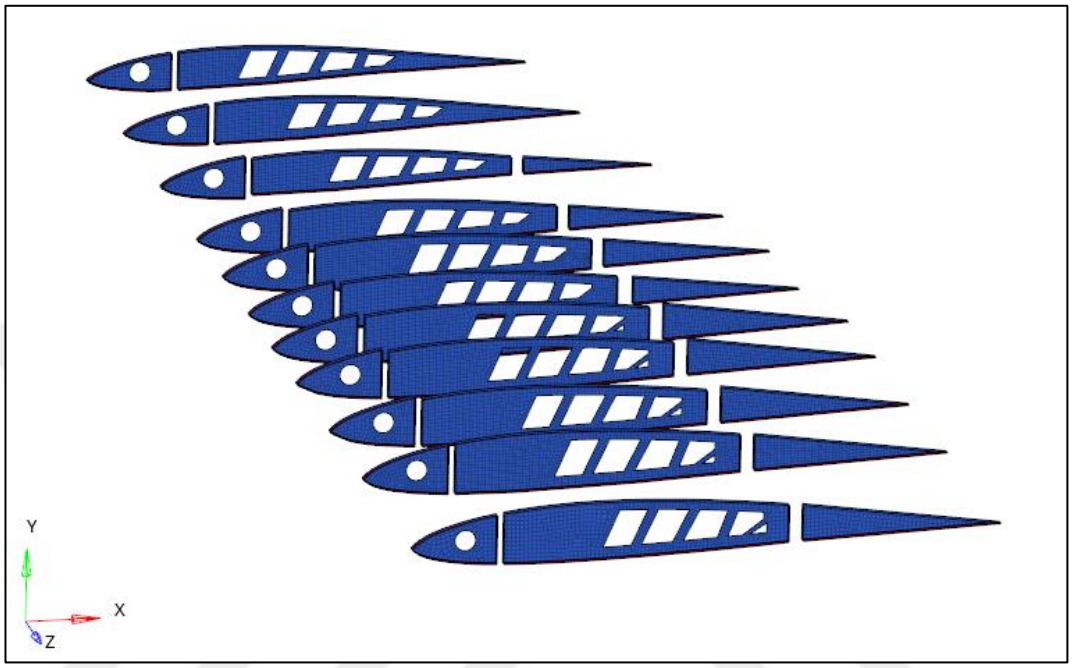

Figure 4.7 Rib Topology Result Applied 2D Main Model

After the topology optimization result of the ribs was applied to the 2D main model, the optimization result was started for the determined design space of the main spar.

4.2 Spar Topology Optimization

Since only one will be produced while applying the spar topology optimization with the design space determined, it was decided to drill holes in the form of a classic lightening hole in order not to use a different manufacturing pattern. The web of the spar is divided into 7 different zones to determine the parts to be drilled while cutting out the web region of the spar. The topology optimization of the ribs has been studied on the integrated model. 7 regions determined as design space on spar are shown in Figure 4.8.

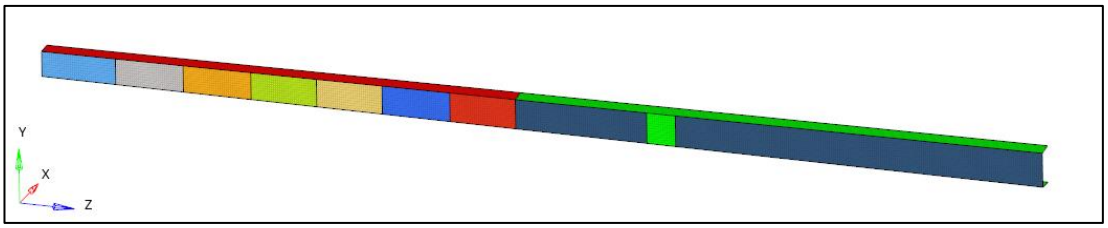

Figure 4.8 Spar Topology Optimization Location

It is seen that the spar web is divided into 7 same amount different regions after strut connection. In this part of the study, 2D topology optimization will be applied to the structure. While applying 2D topology optimization to these regions, some constraints and objectives were determined. Objectively, it was desired to keep the displacement of the spar to a minimum. There is the same constraint for each region. As applied to ribs, there are fraction and stress restrictions on volume. The boundary conditions of the constraints are shown in Table 4.2.

Table 4.2 Spar Design Space Region Constraints and Boundary Condition

Constraint	Lower Bound	Upper Bound
Von-Misses Stress	150 MPa	200 MPa
Volume Fraction	0.2	0.4

A topology optimization pattern is obtained from the determined constraints, objective, and design space. The pattern is shown in Figure 4.9. The blue areas seen in this figure are the locations that can be cut out. The red areas are the parts where the stress can be high, which is inconvenient to remove the material.

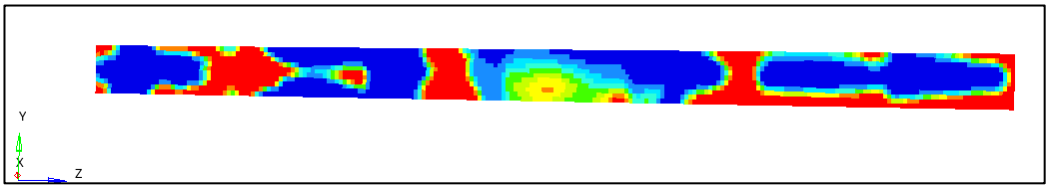

Figure 4.9 Spar Topology Optimization Location

Cut outs were made in areas where stress is low, and material can be extracted. The optimized state of the spar structure by opening cut outs in these regions is in Figure 4.10.

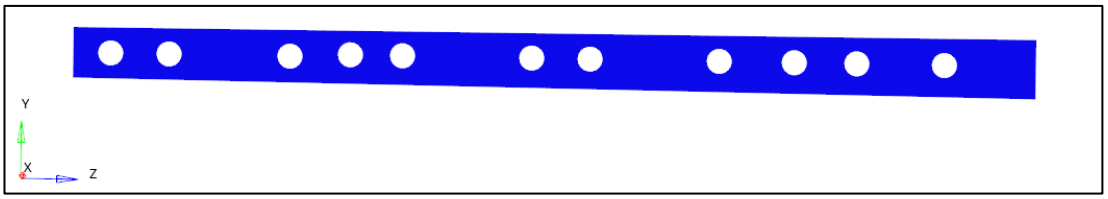

Figure 4.10 Spar Topology Optimization Applied Model

The model was created by drilling 11 lightening holes in total. The diameter of these cut outs is determined as 60 mm and is the same everywhere on the spar. When topology optimization is applied in spar, the topology optimization part of the model is over. After this point, the structural strength of the model should be checked, as was done in chapter 3.

4.3 Topology Optimization Model Results

In chapter 3, the structurally critical values for the first model are checked. However, after the topology optimization was made, weakening occurred in some parts of the structure. For this reason, the model obtained from optimization should be examined again. The results will be examined in terms of displacement, stress, buckling and weight on the model. Fasteners do not need to be re-examined, because cut outs in the model will affect the structure the most in terms of stress and buckling. Since the location of the fasteners was not changed, no significant change was observed in the load passing over it. The optimized spar and ribs of the model are shown in Figure 4.11 together.

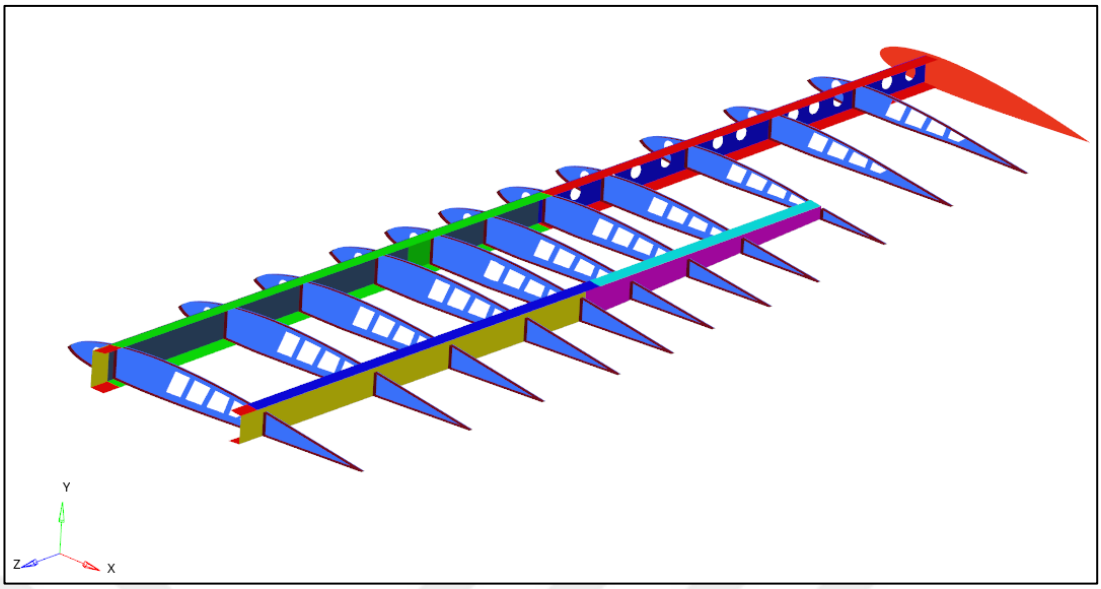

Figure 4.11 Topology Optimization Result Model

Since the changes in the displacement of the model are very small, it is in the safe zone with the optimization applied. Displacement result and deformation zones can be seen in Figure 4.12.

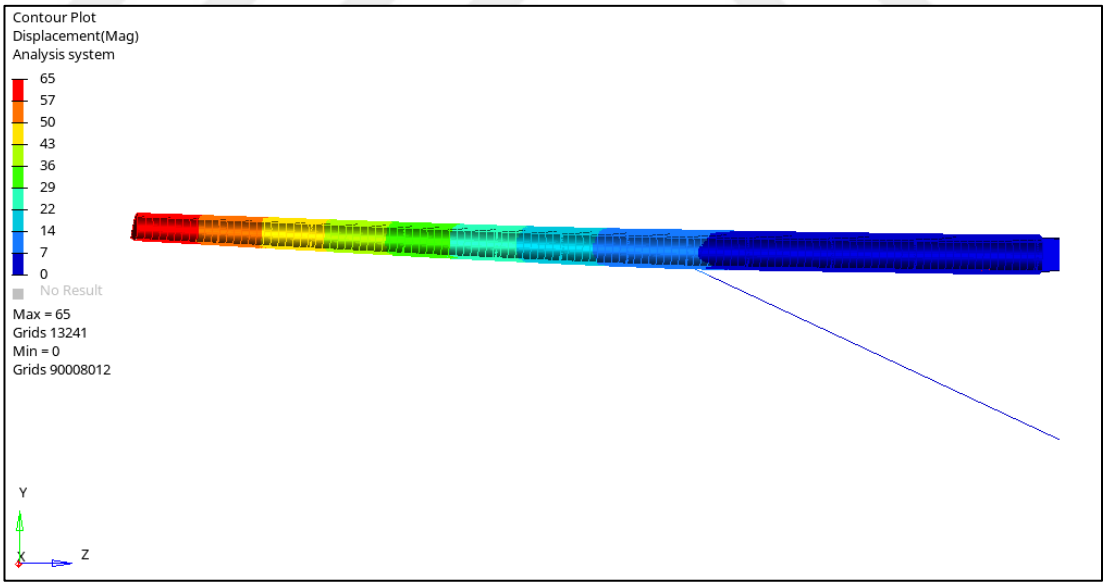

Figure 4.12 Topology Optimization Model Displacement Results

Stress data was determined as constraint as 428 MPa in ultimate. Within the framework of this restriction, stress information of the structures in the model is given in the figures below.

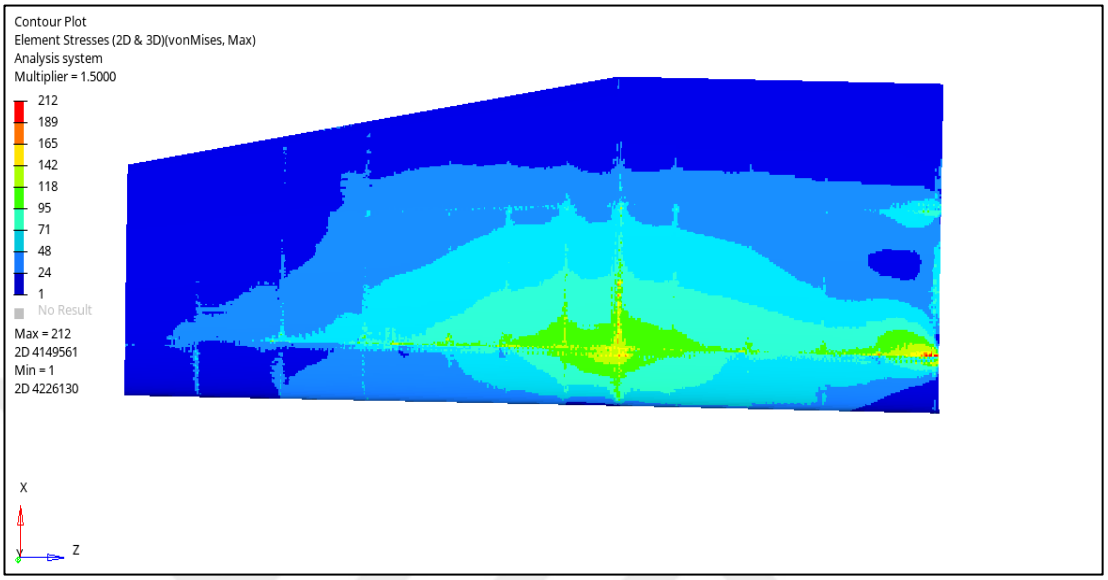

Figure 4.13 Topology Optimization Model Upper Skin Stress Results

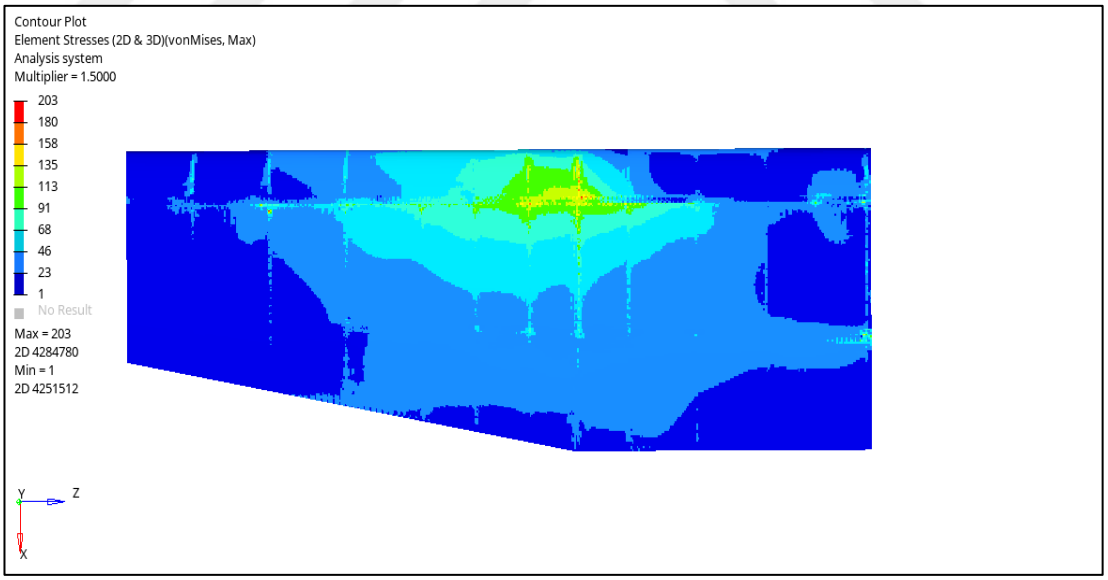

Figure 4.14 Topology Optimization Model Lower Skin Stress Results

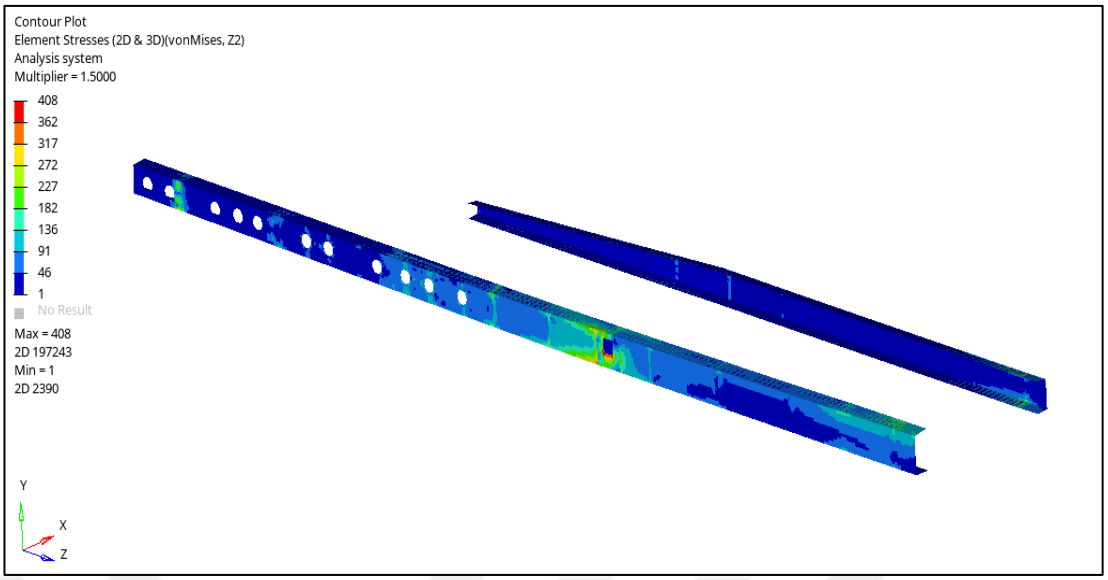

Figure 4.15 Topology Optimization Model Spars Stress Results

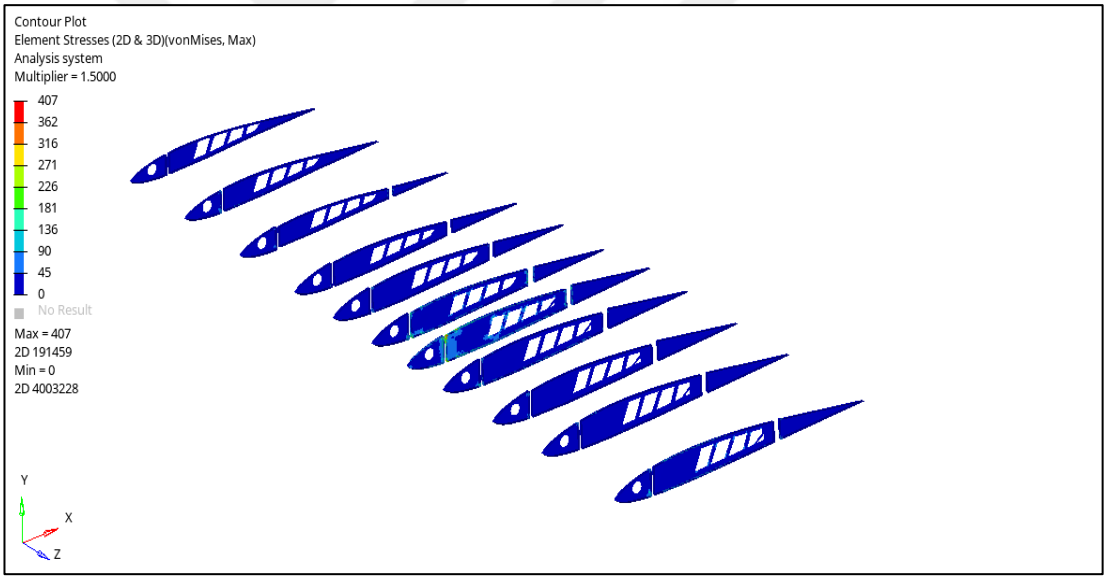

Figure 4.16 Topology Optimization Model Ribs Stress Results

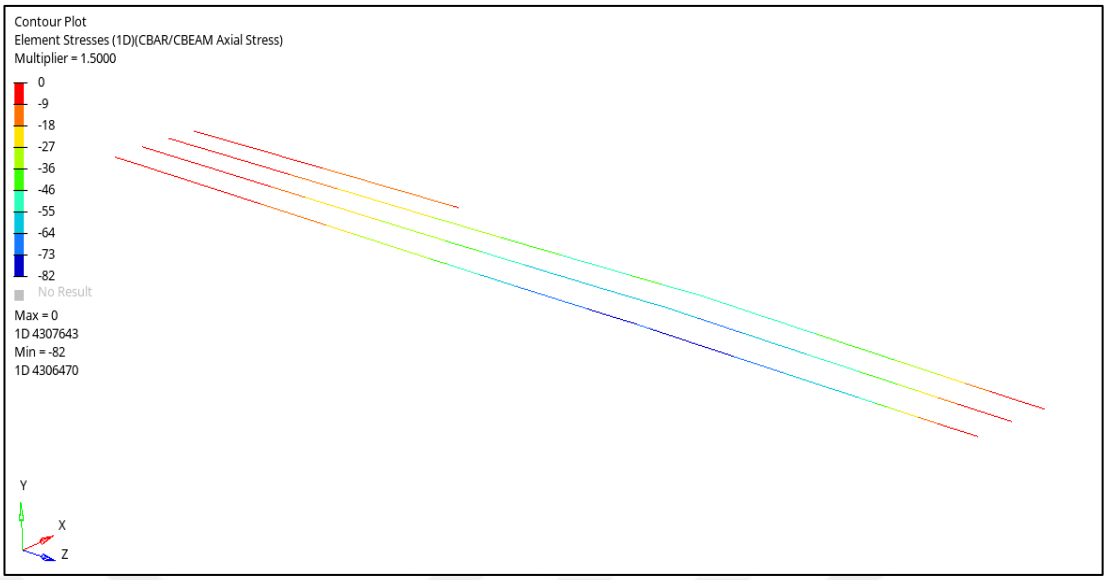

Figure 4.17 Topology Optimization Model Stringers Stress Results

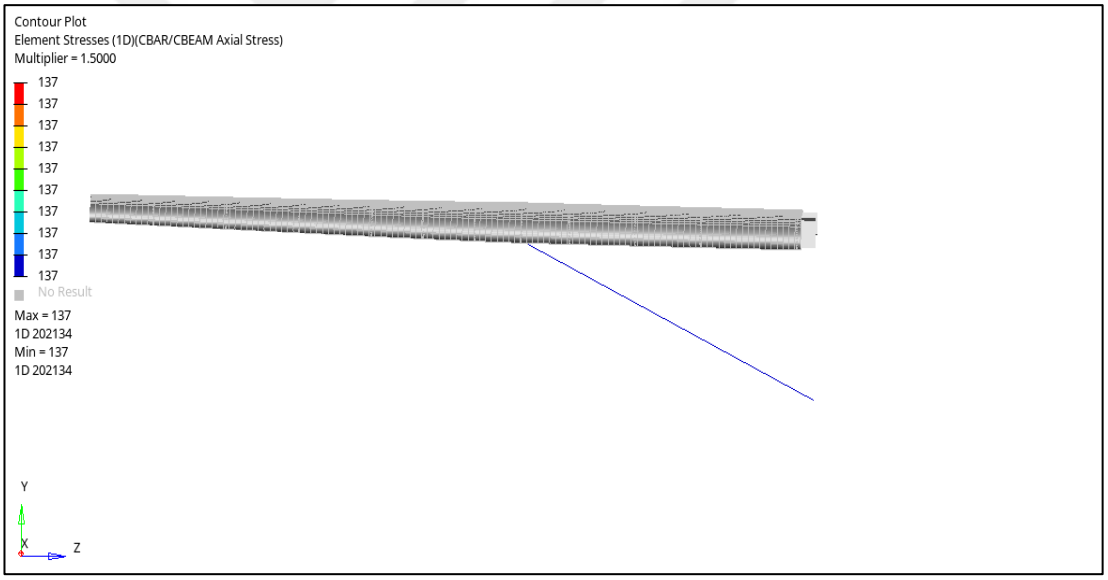

Figure 4.18 Topology Optimization Model Strut Stress Results

After the stress values are obtained, the safety factors of the structure should be greater than 1. The safety factors of the structures in the optimized model are shown in Table 4.3.

Table 4.3 Wing Model Maximum Stress Results and Minimum Reserve Factors

Structure	Maximum Stress (MPa)	Min Reserve Factor
Upper Skin	212	2.02
Lower Skin	203	2.10
Spars	408	1.05
Ribs	407	1.05
Stringer	82	5.21
Strut	137	3.12

After showing that the stress values are in the safe zone, buckling criteria should be checked. While the buckling critical area is normally on the skin panel, free edge areas were formed by opening the cut outs. For this reason, the most critical location in terms of buckling is the web part of the main spar and the other critical point is the web part of the rib, which is closest to the strut. Figure 4.19 shows the most critical buckling location of spar and ribs in Figure 4.20.

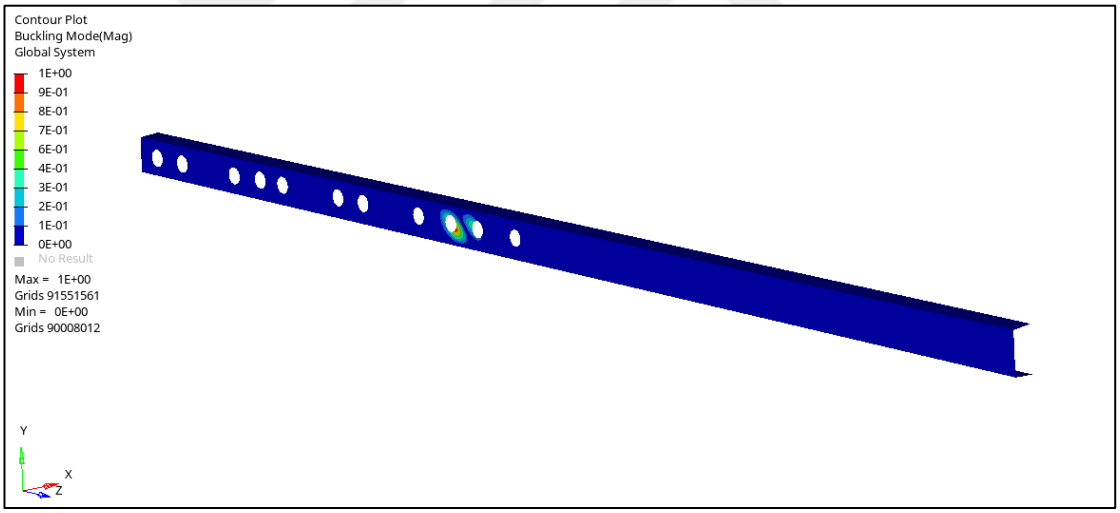

Figure 4.19 Topology Optimization Model Main Spar Buckling Region

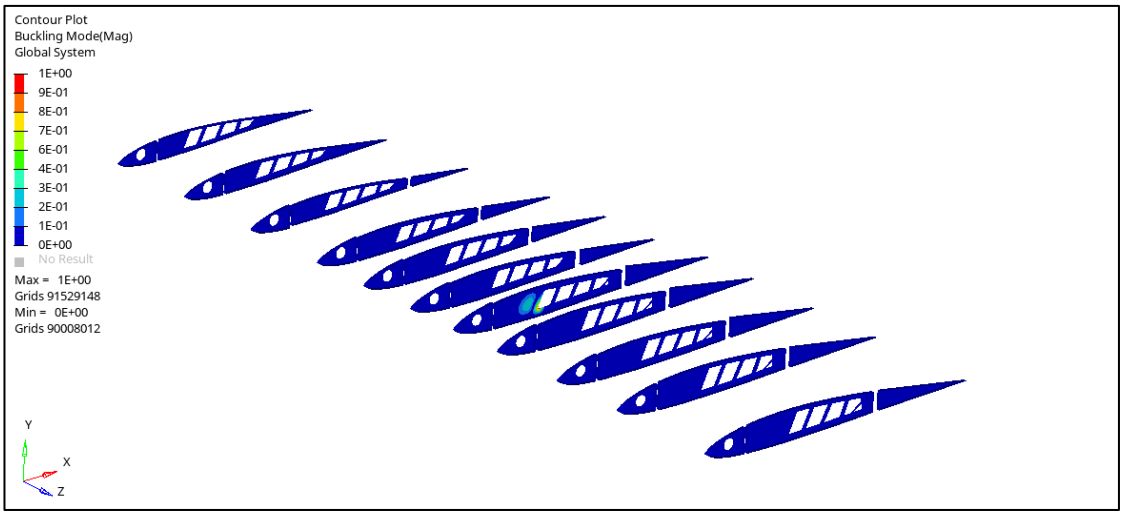

Figure 4.20 Topology Optimization Model Main Ribs Buckling Region

Frequency changes as a result of topology optimization were examined. The greatest change was observed in the first torsion mode, as the greatest weight reduction was in the ribs. Table 4.4 compares the first and second bending and first torsion models.

Table 4.4 Before and After Topology Optimization Frequency Comparison

Mode Type	Before Optimization	After Optimization	Difference (%)
First Bending	13.9	13.9	**0**
First Torsion	32.7	32.1	**1.86**
Second Bending	33.3	33.2	**0.30**

The 10 most critical buckling safety factors in the whole model are shown in Table 4.5. According to the first model, critical locations have changed, and spar and rib webs have also become critical. But all components are in the structurally safe zone.

Table 4.5 Wing Model First 10 Buckling Modes Reserve Factor

Buckling Mode	Reserve Factor
1	**1.01**
2	1.05
3	1.07
4	1.08
5	1.09
6	1.09
7	1.10
8	1.11
9	1.12
10	1.15

After it is seen that the model is safe according to the expected criteria, the weight comparison of the structure should be made. The design area is the web of rib and main spar. Internal structure is all rib and spar web and caps. Results are shown in Table 4.6

Table 4.6 First and After Optimization Weight of the Wing Structures

Structures	First Weight (kg)	After Optimization Weight (kg)	Weight Reduction (%)
Skins	30.6	30.6	0
Total Spars	11.72	11.47	2.13
Total Ribs	5.86	4.81	17.91
Strut	2.91	2.91	0
Stringers	1.3	1.3	0
Fastener	1.48	1.48	0
Total Internal Structure	17.58	16.28	**7.39**
Design Space	4.303	2.856	**33.6**

When the weight values are examined after the topology optimization, it is seen that the highest weight reduction is on the ribs. The part that should be evaluated as a percentage is the amount of weight reduction on the internal structure in terms of structural analysis. The internal structure includes spar and ribs. When the initial and final status are examined, a weight reduction of 7.39 percent has occurred.

CHAPTER 5

CONCLUSION AND DISCUSSION

In this study, topology optimization was applied to the wing model of Cessna 172 Skyhawk. Before applying the topology optimization, it is necessary to complete certain stages. First, in the study, weights should be calculated using the initial weight approximation methods to compare the initial weight of a structure with the final weight. Within the scope of the study, 2 different weight calculation methods were used. Geometrical data of the aircraft are needed in the formulations of these methods. To calculate the wing structure, first, data such as wing area, taper ratio and maximum speed should be known. Some of these data were obtained from Cessna's reference document, while others were calculated with the help of analytical methods. The first method is Raymer's weight calculation method. This method was obtained statistically for aircraft in the general aviation category. Written as a general formulation. Therefore, a weight was calculated that deviates 15.6 percent from the Cessna's wing component. As the second and main method of the study, Roskam's weight calculation method was used with a deviation of about 0.26 percent from the actual data. The weight obtained by the Roskam method was used in the study.

After the initial weight of the structure is found, the aerodynamic loads applied to this structure must be calculated. The aerodynamic loads acting on the wing are lift, drag and pitching moment. The force that most affects the wing structure is the lift loading. In the study, the magnitude of the lift and how it is distributed along the wing were calculated. The maximum lift load of Cessna 172 is 3.8 gravitational force. A 3.8 g lift load means generating a lift load of 3.8 times the weight of the aircraft. It is assumed that all of this load is carried by the wings. The distribution of the lift load is calculated by assuming an elliptical distribution. Calculations for drag and pitching moment were made by calculating the lift load. While finding these forces, angle of attack vs drag coefficient and angle of attack vs pitching moment coefficient graphics of the airfoil were used. A flight loading was obtained by finding the highest values of lift, drag and pitching moment according to the maximum speed and angle of attack limitations of

the aircraft. Forces were applied at 7 different stations on the spanwise. The application point of these forces chordwise on the model was accepted as 25 percent of the chord.

After the critical aerodynamic loading has been obtained, the preparation phase of the finite element model of the Cessna 172 Skyhawk's wing model has started. Altair Hypermesh 2019 was used while modelling. For the static solution of the model, the Optistruct 2019 solver was used. A model of the wing structure close to the real one was created. The aim at this stage is to show that the wing structure has a structurally safe model that is close to its actual weight before optimization. While creating the finite element model of the wing, the locations and thicknesses of the components such as spar, rib and stringer in its internal structure were determined. The structures are modelled using fastener modelling technique to better reflect reality. That is, spar, rib and skin panels are connected to each other with rivets. For the created finite element model to be valid, static and free to free modal finite element validation methods were used. After the results of the checks were verified and the model was proven to work correctly, its structural strength was checked. Displacement, stress, buckling and fastener checks were made in order for the created model to be considered as structurally safe. It has been shown that the wing structure is in the safe zone within 4 different criteria. The most important point is that while the structure is statically stable, it is very close to its actual weight. The actual weight of the Cessna 172 Skyhawk is 53.71 kg. The weight of the model created with the help of finite elements is 53.86 kg. The margin of error between the two data is 0.29 percent. In Table 5.1, the weight comparison of the actual weight and the model created before optimization is made.

Table 5.1 Real and FEM Wing Weight Comparison

Structures	Weight(kg)	Error Rate (%)
Real Wing Weight	53.71	
FEM Wing Weight	53.87	**0.29**

After the main model was created, the topology optimization phase was started. Altair Optistruct 2019 was used for topology optimization. At this stage, SIMP was used as the method. In this methodology, the goal is to provide lightening by removing the

material with low contribution of stiffness from the structure. Before the optimization of the wing area is applied, the design spaces are determined. The web part of the ribs and main spar was chosen as the design space. The main reason is that cut outs are not allowed in the fuel, fastener, and control surface areas. In the study, 2 different topology optimizations were applied to ribs and spars. Optimization was made over 3D modelling for ribs and 2D modelling for spars. In 3D topology optimization, this method is used in ribs because it is possible to determine the extrusion direction of the material and the ribs constitute the largest design area of the work. Since spars will be applied to a smaller area than ribs, circular cut out zones have been determined by applying 2D topology optimization to make it easier in terms of production. First, topology optimization was applied to the ribs. To apply 3D topology optimization to the ribs, the rib with the most critical stress and fastener loading was selected. The optimization pattern obtained from this rib was applied to all ribs. The main purpose of this is to ensure that all ribs come out of a single mold instead of making production difficult by obtaining a different pattern for each rib. While applying topology optimization for the most critical rib, volume and stress constraints are given as constraints. Objectively, it is aimed to maximize the stiffness. The pattern obtained from the topology optimization was applied to all ribs in the main model. After the ribs, 2D topology optimization was applied to the web part of the main spar. Constraints and objectives in ribs were applied to the spars as well. Circular holes were opened by determining the cut-out regions according to the element density map obtained in the 2D structure. After the patterns obtained from the topology optimization were applied to the structure, the safety checks of the model were made. Displacement, stress and buckling criteria were checked from the checks made on the main model. The structure has been shown to be statically safe.

The weight change of the topology optimized structure compared to the first structure is given in Table 5.2 below. At this point, the weight reduction of ribs and spars themselves is shown. A weight reduction of 17.91 percent in ribs and 2.13 percent in spars was achieved. In addition, weight reduction in the total internal structure is given. The sum of the ribs and spars was determined as the internal structure. The weight reduction in the internal structure is 7.39 percent. However, the areas of topology are limited. The design area is the web of rib and main spar. The weight of the main spar

and ribs web before and after optimization, which are the areas where topology can be made, is also shown. The weight reduction in the internal structure is 33.6 percent. This value more clearly shows the weight reduction obtained from this study.

Table 5.2 Weight Comparison of Wing Structures Before and After Topology Optimization

Structures	**Weight Before Optimization (kg)**	**Weight After Optimization (kg)**	**Weight Reduction Percentage (%)**
Total Ribs	5.86	4.81	17.91
Total Spars	11.72	11.47	2.13
Total Internal Structures	17.58	16.28	**7.39**
Design Area	4.303	2.856	**33.6**

In future works, weight reduction in wing has been achieved in this study. However, there are some points that limit topology optimization in this weight reduction. One of the biggest constraints of topology optimization is production. In the study, a single optimization pattern was created for all ribs, and it was tried to be easier in terms of production. If a different pattern was created for each structure and the results were compared, greater reductions in the structure could be obtained. While applying the optimization result to the model, another adverse effect is that the structure obtained from the finite element model cannot be produced directly, it should be arranged in a way suitable for production and the parameters of the program should be well managed. In addition, the component with the largest weight in the scope of the study is the skin panel. The material of this skin panel is aluminum. A lighter structure could have been achieved if the skin panel, the thickness of which was almost minimal in terms of production, was produced from composite material. Another method is to optimize the positions of the structures within the wing box. If the positions of ribs and spars are changed and brought to the most suitable position, lightening can be achieved in the structure.

Other analyzes that should be performed in future studies are fatigue and aeroelastic analyzes. The study was carried out within the scope of static analysis. At this point, fatigue analyses should be made, and it should be shown that the life of the aircraft is above a certain hour. At the same time, the modal analysis was carried out simply in the study. To prevent the wing structure from being exposed to effects such as flutter, it is necessary to control the stiffness of the structure and perform aeroelastic analyzes.

REFERENCES

[1] Robert M. Taylor, The Role of Optimization In Component Structural Design: Application to the F-35 Joint Strike Fighter, 25th International Congress of The Aeronautical Sciences, Texas 2006.

[2] Lars K., Alastair T., Gerrit R. Application of Topology, Sizing and Shape Optimization Methods to Optimal Design of Aircraft Components, Airbus UK, Bristol 2011.

[3] Kate S., Cessna CJ series hits 2,000 deliveries, Flight International, p 24., London 20-26 June 2017.

[4] Cessna 172, (15.03.2023), Retrieved from Cessna 172 - Vikipedi (wikipedia.org), 2022.

[5] Federal Aviation Administration, Pilot's Handbook of Aeronautical Knowledge, FAA-H-8083-25B, U.S. 2016.

[6] Daniel P. Raymer, Aircraft Design: A Conceptual Approach 6th Edition, AIAA, ISBN 978-1-6241-0490-9, 1097 pages, California 2018.

[7] Flight Courses Private Pilot Theory, 1.02.01 Fuselage and Mainplanes.,14.02.2023 (n.d.). retrieved from https://flight-courses.com.

[8] John D. Anderson Jr., Fundamentals of Aerodynamics, McGraw-Hill Series, ISBN 978-0-07-339810-5, 1131 pages, NY 2011.

[9] Mohammad H. Sadraey, Aircraft Design A Systems Engineering Approach, John Wiley & Sons Ltd, ISBN 978-1-1199-5340-1, 799 pages New Hampshire, USA 2013.

[10] NACA 2412 Airfoil, (19.04.2023), Retrieved from http://airfoiltools.com/airfoil.

[11] John D. Anderson Jr., Aircraft Performance And Design, McGraw-Hill Series, ISBN 0-07-001971-1, 599 pages, USA 1999.

[12] Clancy, Laurence J., Aerodynamics, Pitman, ISBN 978-0-273-01120-0, 610 pages , London 1978.

[13] John McIver B., Skyhawk II / 100 Performance Assessment, 14.03.2023, Retrieved from http://www.temporal.com.au, 23rd January 2003.

[14] Bryce L. Horvath, Douglas P. Wells, Comparison of Aircraft Conceptual Design Weight Estimation Methods to the Flight Optimization System, Florida 2018.

[15] Dr. Jan Roskam, Part V: Component Weight Estimation, ISBN 978-1-884885-50-1, 227 pages, USA 2018.

[16] Cessna Aircraft Company, Skyhawk Model 172R Specification and Description, Kansas March 2011.

[17] R. Sedaghati, S.A. Mostafa, S. Ramin, A. Mohammed, The Development of A Preliminary Structural Design Optimization Method of An Aircraft Wing-Box Skin-Stringer Panels, Elsevier, Canada 2010.

[18] Bendsøe MP., Kikuchi N., Generating Optimal Topologies In Structural Design Using Homogenization, Computer Methods in Applied Mechanics and Engineering, 197-224, North Holland 1988.

[19] Taylor R., Thomas J., MacKaron N., Riley S., Lajczok M., Detail Part Optimization on the F-35 Joint Strike Fighter. Proceedings 47th AIAA/ASME/ASCE/AHS/ASC Structures, Structural Dynamics and Materials Conference, Rhode Island, 2006.

[20] Grihon S., Krog L., Bassir D., Numerical Optimization applied to structure sizing at AIRBUS: A multi-step process, Int. J. Simul. Multidisci. Des. Optim. 3, 432-442, 2009.

[21] Bendsøe MP., Sigmund O., Topology Optimization: Theory, Methods and Applications, Springer, ISBN 978-3-642-07698-5, 380 pages, NY 2004.

[22] Z. Ji-Hong, Z. Wei-Hong, X. Liang, Topology Optimization in Aircraft and Aerospace Structures Design, Arch Computat Method Eng, 595-622, Barcelona 2015.

[23] Bendsøe MP., Optimal Shape Design as A Material Distribution Problem, Springer, Structural Optimization 1, 193-202, Denmark 1989.

[24] G.I.N. Rozvany, Aims, Scope, Methods, History and Unified Terminology of Computer-Aided Topology Optimization In Structural Mechanics, Springer, Struct Multidisc Optim 21, 90–108, Budapest 2001.

[25] Bendsøe MP., Sigmund O., Material Interpolation Schemes In Topology Optimization, Springer, Archive of Applied Mechanics 69, 635-654, Denmark 1999.

[26] Y.M. Xie, G.P. Steven, A Simple Evolutionary Procedure For Structural Optimization, Elsevier, Computers and Structures Vol. 49, 885-896, Great Britain 1994.

[27] Y.M. Xie, G.P. Steven, Evolutionary Structural Optimization, Springer, ISBN 13 :978-1-4471-1250-1, pages 199, Berlin 1997.

[28] X. Huang, Y.M. Xie, A Further Review of ESO Type Methods For Topology Optimization, Springer, Struct Multidisc Optim, 41:671-683, 2010.

[29] N. P. Van Dijk, K. Maute, M. Langelaar, F. Van Keulen, Level-Set Methods for Structural Topology Optimization: A Review, Springer, Struct Multidisc Optim, Berlin 2013.

[30] G. I. N. Rozvany, A Critical Review of Established Methods of Structural Topology Optimization, Springer, Struct Multidisc Optim 37:217–237, 2008.

[31] Cessna 172 Speeds, 12.02.2023, Retrieved from https://www.beverlyflightcenter.com/zoadutin/2017/05/172SPEEDmph.pdf.

[32] Goebel Fasteners, Blind Rivet Catalog, 03.01.2023, retrieved from https://www.goebelfasteners.com/

[33] Micheal C. Niu, Airframe Stress Analysis and Sizing, ISBN 962-7128-08-2, USA 1997.

[34] Micheal C. Niu, Airframe Structural Design, ISBN 962-7128-04-X, California 1988.

[35] Gudmundsson S., General Aviation Aircraft Design, Elsevier, ISBN 978-0-12-818465-3, 2022.

[36] Dominique M., Practical Finite Element Analysis For Mechanical Engineering, ISBN 978-1-9990475-0-4, Canada 2020.

[37] Altair, Practical Aspects of Structural Optimization with Altair Optistruct, 16.03.2023, retrieved from https://www.altair.com/.

[38] L. Binkai, G. Yu, X. Hao, G. Yukui, L. Enquan, A Two-Dimensional Model for Pin Load Distribution and Failure Analysis of Composite Bolted Joint, June 2021.

[39] Airbus Specification, 51-47-00-Description-Fastener Pitch and Edge Distance Data , May 2020.

[40] Federal Aviation Administration, Metallic Materials Properties Development and Standardization (MMPDS), Virginia January 2003.

[41] Cessna Aircraft Company, Cessna 172 Skyhawk Pilot’s Operating Handbook, Kansas 1977.

[42] Zhi S., Ronghua C., Tianchen C., Chang L., An Optimization Approach for Stiffener Layout of Composite Stiffened Panels Based on Moving Morphable Components (MMCs), ISSN 1860-2134, 2019.

[43] B. Phacharaporn, S. Vis, Design of a Wing Structure for a Single Turboprop Normal Category Aircraft, International Journal of Aviation Science and Technology, Volume 3, 45-57, 2022.

APPENDICES

APPENDIX A: CODE FOR FASTENER MODELLING IN HYPERMESH

This code is written in tcl base and is for modeling fasteners in the structure.

```
#STAGE 1
set fastener_diameter 4.8
set fastener_to_fastener_gap 4.5
set free_edge_gap [expr $fastener_to_fastener_gap/2]
set row_number "Single"
set distance_1 [expr $fastener_diameter*$free_edge_gap]
set distance_2 [expr ($fastener_diameter*$free_edge_gap +
$fastener_diameter*$fastener_to_fastener_gap)]
*createmarkpanel lines 1
set marked_lines [hm_getmark lines 1]
set vector_directions [hm_getdirectionpanel panel]
set vector_direction [lindex $vector_directions 0]
foreach marked_line $marked_lines {
        *createmark lines 1 $marked_line
        *duplicatemark lines 1 1
        *createmarklast lines 1
        set marked_line_translate [hm_getmark lines 1]
        *createmark lines 1 $marked_line_translate
        *createvector 1 [lindex $vector_direction 0] [lindex $vector_direction 1] [lindex
$vector_direction 2]
        *translatemark lines 1 1 $distance_1
        *clearmarkall 1
        set start_point [hm_getlinestartpoint $marked_line_translate]
        set end_point [hm_getlineendpoint $marked_line_translate]
        *createnode [lindex $start_point 0] [lindex $start_point 1] [lindex $start_point 2] 0 0 0
        *createmarklast nodes 1
        set node_1 [hm_getmark nodes 1]
        *clearmarkall 1
        *createnode [lindex $end_point 0] [lindex $end_point 1] [lindex $end_point 2] 0 0 0
        *createmarklast nodes 1
        set node_2 [hm_getmark nodes 1]
        *clearmarkall 1
        *createmark nodes 1 $node_1
        *createvector 1 [expr [lindex $end_point 0]-[lindex $start_point 0] ] [expr [lindex $end_point
1]-[lindex $start_point 1] ] [expr [lindex $end_point 2]-[lindex $start_point 2] ]
        *translatemark nodes 1 1 [expr $fastener_diameter*2+1]
        *clearmarkall 1
        *createmark nodes 1 $node_2
        *createvector 1 [expr [lindex $start_point 0]-[lindex $end_point 0] ] [expr [lindex
$start_point 1]-[lindex $end_point 1] ] [expr [lindex $start_point 2]-[lindex $end_point 2] ]
        *translatemark nodes 1 1 [expr $fastener_diameter*2+1]
        *clearmarkall 1
        # Node_Distance
        *createmark nodes 1 $node_1
        *createmark nodes 2 $node_2
        set shortest_distance [expr [hm_linelength $marked_line_translate]-2*($fastener_diameter*2
+ 1)]
        *clearmarkall 1
```

```
	*clearmarkall 2
	set fastener_number_real [expr
$shortest_distance/($fastener_diameter*$fastener_to_fastener_gap)]
	set fastener_number [expr int ($fastener_number_real)]
	*createmark nodes 1 $node_1 $node_2
	*createlist lines 1 $marked_line_translate
	*createlist nodes 1
	*markprojectnormallytoline nodes 1 1 1
	*clearmarkall 1
	*clearmarkall 2

	if {$fastener_number > 1} {
		*createlist nodes 2 $node_1 $node_2
		*createarray 1 [expr $fastener_number]
		*nodecreatebetweennodes lines $marked_line_translate 2 1 1 0 0 0
		*createmarklast nodes 1
		set node_check_fast_to_fast [hm_getmark nodes 1]
		*createmark nodes 1 $node_1
		regsub $node_1 $node_check_fast_to_fast "" node_check_fast_to_fast
		*createmark nodes 2 {*}$node_check_fast_to_fast
		set shortest_distance_checker [expr abs ([lindex [hm_measureshortestdistance nodes
1 0 nodes 2 0 0] 3])]
		*clearmarkall 1
		*clearmarkall 2
		set check_6D [expr $fastener_diameter*6]

			if {$shortest_distance_checker>$check_6D} {
			puts "1 Fastner is increased"
			set fastener_number [expr $fastener_number+1]
			*createmark nodes 1 $node_1
			*createmark nodes 1 {*}$node_check_fast_to_fast
			*nodemarkcleartempmark 1
			*clearmark nodes 1
			*createlist nodes 2 $node_1 $node_2
			*createarray 1 [expr $fastener_number]
			*nodecreatebetweennodes lines $marked_line_translate 2 1 1 0 0 0

			}
		} elseif {$fastener_number == 0} {

		*createlist nodes 2 $node_1 $node_2
		*createnodesbetweennodelist 2 1 0 0
		*createmark nodes 1 $node_1 $node_2
		*nodemarkcleartempmark 1

		}
	*createmark lines 1 $marked_line_translate
	*deletemark lines 1
	*clearmarkall 1

	if {$row_number=="Double"} {

	*createmark lines 1 $marked_line
	*duplicatemark lines 1 1
	*createmarklast lines 1
	set marked_line_translate_2 [hm_getmark lines 1]
	*createmark lines 1 $marked_line_translate_2
```

```
	*createvector 1 [lindex $vector_direction 0] [lindex $vector_direction 1] [lindex
$vector_direction 2]
	*translatemark lines 1 1 $distance_2
	*clearmarkall 1
	set start_point [hm_getlinestartpoint $marked_line_translate_2]
	set end_point [hm_getlineendpoint $marked_line_translate_2]
	*createnode [lindex $start_point 0] [lindex $start_point 1] [lindex $start_point 2] 0 0 0
	*createmarklast nodes 1
	set node_1 [hm_getmark nodes 1]
	*clearmarkall 1
	*createnode [lindex $end_point 0] [lindex $end_point 1] [lindex $end_point 2] 0 0 0
	*createmarklast nodes 1
	set node_2 [hm_getmark nodes 1]
	*clearmarkall 1
	*createmark nodes 1 $node_1
	*createvector 1 [expr [lindex $end_point 0]-[lindex $start_point 0] ] [expr [lindex $end_point
	1]-[lindex $start_point 1] ] [expr [lindex $end_point 2]-[lindex $start_point 2] ]
	*translatemark nodes 1 1 [expr $fastener_diameter*2+1]
	*clearmarkall 1
	*createmark nodes 1 $node_2
	*createvector 1 [expr [lindex $start_point 0]-[lindex $end_point 0] ] [expr [lindex
$start_point 1]-[lindex $end_point 1] ] [expr [lindex $start_point 2]-[lindex $end_point 2] ]
	*translatemark nodes 1 1 [expr $fastener_diameter*2+1]
	*clearmarkall 1
	#Node_Distance
	*createmark nodes 1 $node_1
	*createmark nodes 2 $node_2
	set shortest_distance [expr [hm_linelength $marked_line_translate]-2*($fastener_diameter*2
+ 1)]
	*clearmarkall 1
	*clearmarkall 2
	set fastener_number_real [expr
$shortest_distance/($fastener_diameter*$fastener_to_fastener_gap)]
	set fastener_number [expr int ($fastener_number_real)]
	*createmark nodes 1 $node_1 $node_2
	*createlist lines 1 $marked_line_translate_2
	*createlist nodes 1
	*markprojectnormallytoline nodes 1 1 1
	*clearmarkall 1
	*clearmarkall 2

	if {$fastener_number > 1} {
		*createlist nodes 2 $node_1 $node_2
		*createarray 1 [expr $fastener_number]
		*nodecreatebetweennodes lines $marked_line_translate 2 1 1 0 0 0
		*createmarklast nodes 1
		set node_check_fast_to_fast [hm_getmark nodes 1]
		*createmark nodes 1 $node_1
		regsub $node_1 $node_check_fast_to_fast "" node_check_fast_to_fast
		*createmark nodes 2 {*}$node_check_fast_to_fast
		set shortest_distance_checker [expr abs ([lindex [hm_measureshortestdistance nodes
1 0 nodes 2 0 0] 3])]
		*clearmarkall 1
		*clearmarkall 2
		set check_6D [expr $fastener_diameter*6]

		if {$shortest_distance_checker>$check_6D} {
		puts "1 Fastner is increased"
```

```
                set fastener_number [expr $fastener_number+1]
                *createmark nodes 1 $node_1
                *createmark nodes 1 {*}$node_check_fast_to_fast
                *nodemarkcleartempmark 1
                *clearmark nodes 1
                *createlist nodes 2 $node_1 $node_2
                *createarray 1 [expr $fastener_number]
                *nodecreatebetweennodes lines $marked_line_translate 2 1 1 0 0 0

                }
                } elseif {$fastener_number == 0} {

                        *createlist nodes 2 $node_1 $node_2
                        *createnodesbetweennodelist 2 1 0 0
                        *createmark nodes 1 $node_1 $node_2
                        *nodemarkcleartempmark 1

                }
                *createmark lines 1 $marked_line_translate_2
                *deletemark lines 1
        *clearmarkall 1
        }
        }

#STAGE 2 / Fastener_Bush_Line
*createmarkpanel nodes 1
set caps_fastener [hm_getmark nodes 1]
*createmarkpanel surfs 1
set skin_panel [hm_getmark surfs 1]

foreach one_cap_node $caps_fastener {

*createmark nodes 1 $one_cap_node
set checkher_id_2 [hm_getmark nodes 1]
set checker_2 [llength $checkher_id_2]
*clearmarkall 1
*createmark nodes 1 [expr $one_cap_node + 1000000]
set checker_id [hm_getmark nodes 1]
set checker [llength $checker_id]
*clearmarkall 1

        if {$checker_2==1 && $checker==1 } {
        *createmark nodes 1 [expr $one_cap_node + 1000000]
        *nodemarkcleartempmark 1
        *createmark nodes 1 $one_cap_node
        *duplicatemark nodes 1 28
        *createmarklast nodes 1
        set duplicate_node [hm_getmark nodes 1]
        *clearmarkall 1
        *createmark nodes 1 $duplicate_node
        *renumbersolverid nodes 1 [expr $one_cap_node + 1000000] 1 0 0 0 0 0
        set project_node [expr $one_cap_node + 1000000]
        *createmark nodes 1 $one_cap_node
        *createmark surfs 1 {*}$skin_panel
        set closest_skin_panel [lindex [hm_measureshortestdistance surfs 1 0 nodes 1 0 0 ] 4 ]
        *clearmarkall 1
        *clearmarkall 2
        *createmark nodes 1 $projected_node
```

```
            *markprojectnormallytosurface nodes 1 $closest_skin_panel
            *clearmarkall 1
            *clearmarkall 2

            } elseif {$checker_2==1 && $checker==0} {

            *createmark nodes 1 $one_cap_node
            *duplicatemark nodes 1 28
            *createmarklast nodes 1
            set duplicate_node [hm_getmark nodes 1]
            *clearmarkall 1
            *createmark nodes 1 $duplicate_node
            *renumbersolverid nodes 1 [expr $one_cap_node + 1000000] 1 0 0 0 0 0
            set project_node [expr $one_cap_node + 1000000]
            *createmark nodes 1 $one_cap_node
            *createmark surfs 1 {*}$skin_panel
            set closest_skin_panel [lindex [hm_measureshortestdistance surfs 1 0 nodes 1 0 0 ] 4 ]
            *clearmarkall 1
            *clearmarkall 2
            *createmark nodes 1 $projected_node
            *markprojectnormallytosurface nodes 1 $closest_skin_panel
            *clearmarkall 1
            *clearmarkall 2

            } elseif {$checker_2==0} {

            puts "just skip"


            }
}

            #Line_Creation

            foreach one_cap_node $caps_fastener {

if {[catch {*createlist nodes 1 $one_cap_node [expr $one_cap_node + 1000000]}] || [catch
{*linecreatefromnodes 1 0 150 5 179}] } {
                        continue
                        } else {
                        puts "go"

                        }

}
```

APPENDIX B: MODAL ANALYSIS RESULT BEFORE-AFTER OPTIMIZATION

BEFORE TOPOLOGY OPTIMIZATION

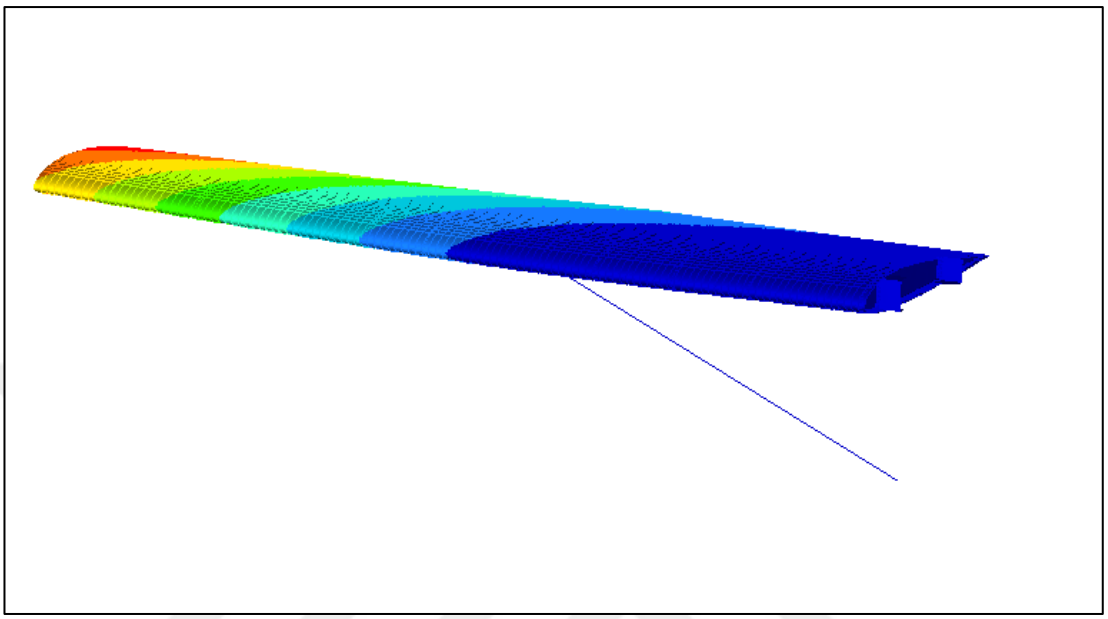

Figure Appendices B.1 First Bending Mode

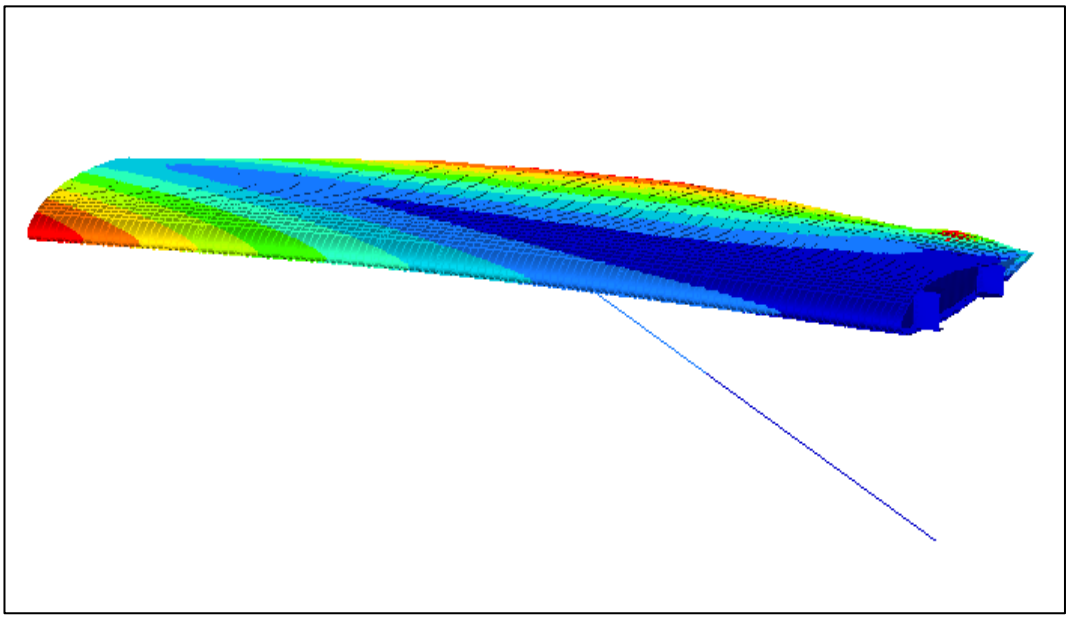

Figure Appendices B.2 First Torsion Mode

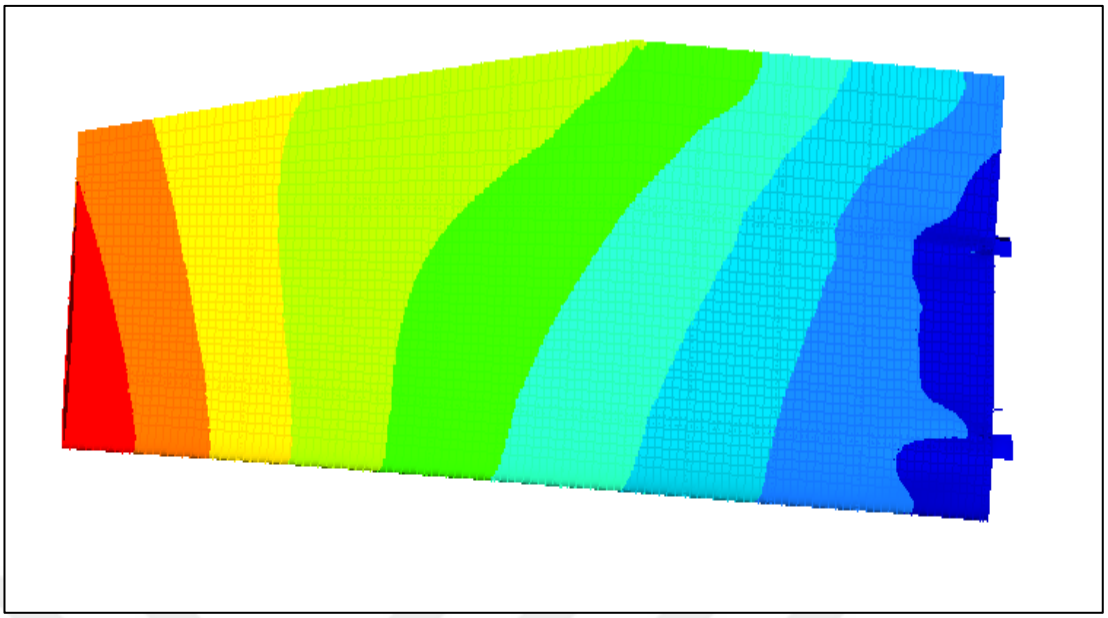

Figure Appendices B.3 Second Bending Mode

Table Appendices B.1 Wing Model before Optimization First 15 Buckling Modes Reserve Factor

Mode	Frequency	Types
1	1.39E+01	First Bending
2	3.27E+01	First Torsion
3	3.33E+01	Second Bending
4	4.05E+01	
5	5.45E+01	
6	5.91E+01	
7	6.36E+01	
8	6.63E+01	
9	6.93E+01	
10	7.01E+01	
11	7.22E+01	
12	7.45E+01	
13	7.59E+01	
14	7.94E+01	
15	8.63E+01	

AFTER TOPOLOGY OPTIMIZATION

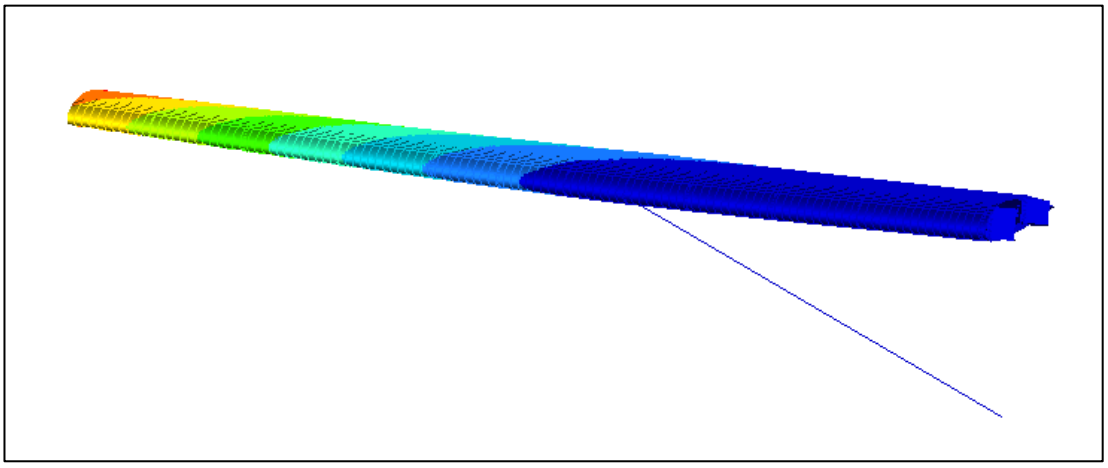

Figure Appendices B.4 First Bending Mode

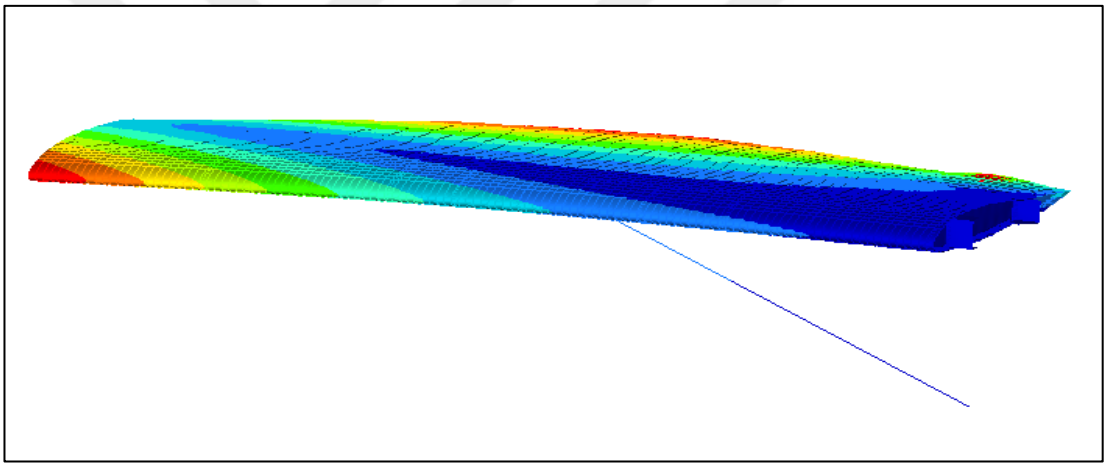

Figure Appendices B.5 First Torsion Mode

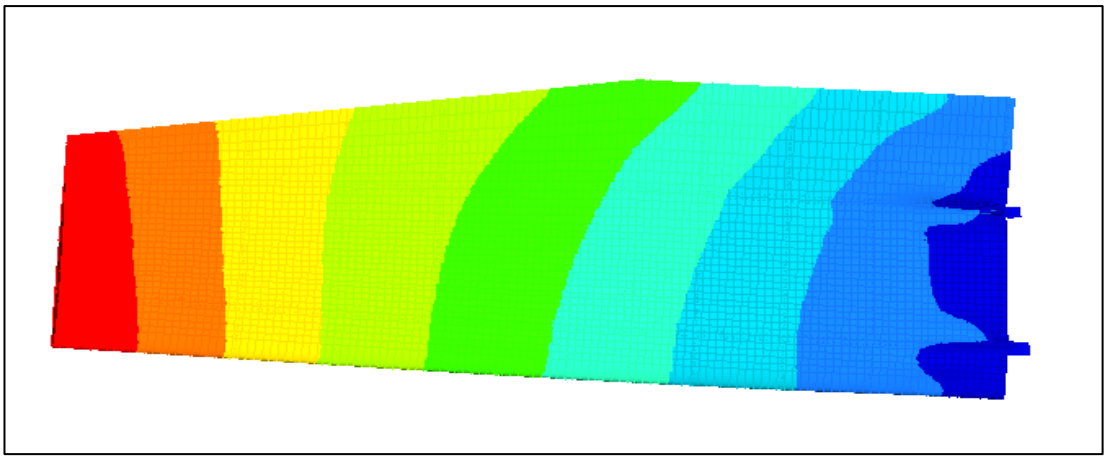

Figure Appendices B.6 Second Bending Mode

Table Appendices B.2 Wing Model After Optimization First 15 Buckling Modes Reserve Factor

Mode	Frequency	Types
1	1.39E+01	First Bending
2	3.21E+01	First Torsion
3	3.32E+01	Second Bending
4	3.88E+01	
5	5.34E+01	
6	5.85E+01	
7	6.18E+01	
8	6.42E+01	
9	6.83E+01	
10	6.84E+01	
11	7.05E+01	
12	7.33E+01	
13	7.35E+01	
14	7.79E+01	
15	8.48E+01	

CURRICULUM VITAE

PERSONAL INFORMATION

Name Surname **:** Hasan Hüseyin ONAY
Date of Birth **:**
Phone **:**
E-mail

EDUCATION

High School : Yıldırım Beyazıt Anatolian High School (82/100) : Ankara Yıldırım Beyazıt University / Mechanical Engineering (3.59/4)-2015-2020

Bachelor

Master Degree : Ankara Yıldırım Beyazıt University / Aerospace Engineering-2020- Continued

WORK EXPERIENCE

Candidate Engineer / Quality Control Engineer
Turkish Aerospace Industries/Ankara
2018-2019

Candidate Engineer / Assembly Engineer
Turkish Aerospace Industries/Ankara
2019-2020

Structural Analysis Engineer
Turkish Aerospace Industries/Ankara
2021-Continued

PRESENT ORGANIZED SOURCES / PRESENTATION

Weight Reduction In Aircraft With Topology Optimization / 2. International Mediterranean Scientific Research and Innovation Congress

June 2023
ANKARA

Department of Aerospace Engineering

Hasan Hüseyin ONAY

